جمهورية العراق

وزارة التعليم العالي والبحث العلمي

التحليل اللاخطي للأعتاب الخرسانية المنحنية أفقياً والمستندة على أُسس مرنة

رسالة

مقدمة الى كلية الهندسة في جامعة بابل

كجزء من متطلبات نيل درجة ماجستير علوم

في الهندسة المدنية

(هندسة إنشاءات)

مسلم عبد الأمير خضير التميمي

بكلوريوس هندسة مدنية

تشرين الأول، **2005**

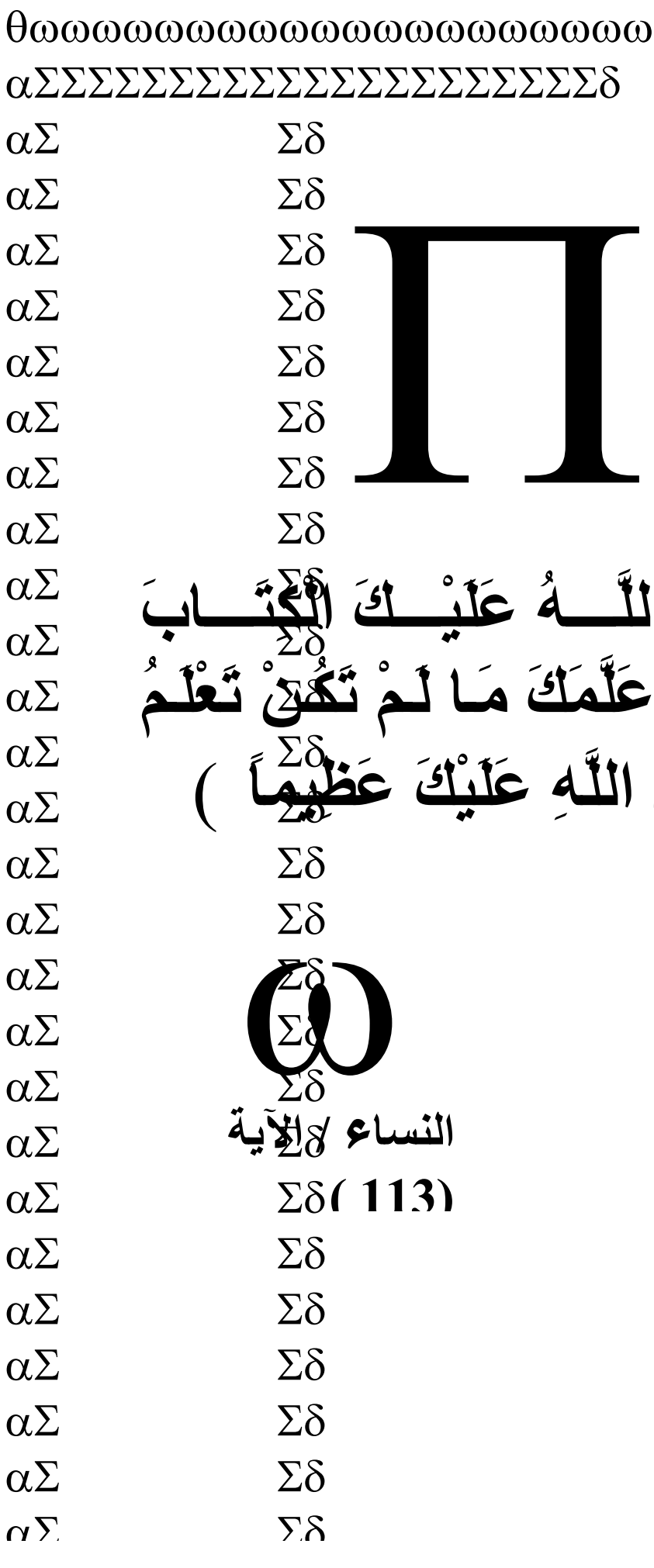

(وَأَنـــزَلَ اللَّـــهُ عَلَيْـــكَ الْكِتَـــابَ وَالْحِكْمَةَ وَعَلَّمَكَ مَـا لَـمْ تَكُنْ تَعْلَـمُ وَكَانَ فَضْلُ اللَّهِ عَلَيْكَ عَظِيماً)

النساء /الآية (113)

الاهداء

لو أنكرت الثمرةُ الورقة .....
فلقد أنكرت أصلها .....وظلمت بختها

فعرفاناً بالجميل:
للورقةِ والغصن.....أمي وأبي
للجذع والجذر.....الأسلام المحمدي
للماءِ و الهواءِ.....أساتذتي

منكم تعلمتُ.....أنْ أُطأطأُ رأسي تواضعاً،
وأنْ أرفعهُ باحثاً
متسائلاً !!

جُلّ أحترامي...وتقديري.....والسلام.

مسلم عبد الأمير خضير التميمي

الخُـــــلاصة

يتناول هذا البحث تحليل الأعتاب المنحنية المصنوعة من الكونكريت المسلح والمستندة على أسس مرنة باستعمال طريقة العناصر المحددة. تم أخذ اللاخطية لتصرف المادة بنظر الاعتبار للعتب الخرساني المنحني. عنصر طابوقي ذي عشرين عقدة وستين درجة حرية تم توظيفه لتمثيل الخرسانة. مثلت قضبان حديد التسليح كعناصر محورية مطمورة ضمن العناصر الطابوقية.

مثلت التربة برد فعل عمودي ورد فعل أفقي. مثلت المركبة العمودية بنموذج ونكلر (Winkler Model)، و نموذج كوندنر(Kondner Model)، و نموذج متعدد الحدود(Polynomial Model)، بينما مثلت المركبة الأفقية بنموذج ونكلر(Winkler Model) .

أظهرت المقارنة بين نتائج العناصر المحددة والنتائج العملية المتوفرة توافقاً جيداً.

نظمت دراسات نظرية لاختبار تأثير بعض المتغيرات المحددة(نسبة نصف القطر إلى طول الفضاء(R/L)، النهايات الحدية، نسبة الإجهاد المتحرر كعرض الشق، الفقدان في الإجهاد في لحظة حصول التشقق، نوع التربة، قضبان حديد التسليح) على تصرف منحني الحمل-الهبوط للأعتاب الخرسانية المنحنية والمستندة على أسس مرنة. من النتائج المستحصلة من الأمثلة المأخوذة، وجد أنه يمكن زيادة الحمل الأقصى للعتب الخرساني المنحني والمستند على أساس مرن بزياد نسبة نصف القطر إلى طول الفضاء(R/L)(عندما تزداد نسبة(R/L) من 1 الى 5 الحمل الأقصى يزداد بنسبة 40% تقريباً)، تمتلك قضبان حديد التسليح القصي تأثيراً واضحاً على تقصان الحمل الأقصى, وجد أن الحمل الأقصى ينقص بمقدار % 51 عند إزالة قضبان حديد التسليح القصي.

List of Contents

CHAPTER FOUR: MODELING of MATERIAL PROPERTIES

CHAPTER FIVE: NUMERICAL APPLICATIONS AND PARAMETRIC STUDY

CHAPTER ONE
INTRODUCTION

1.1 General

In the past, horizontally curved beams have been used primarily in such exotic instances as the round corners of a building, circular balconies, and beams in circular structures.

Recently, horizontally curved beams are extensively used in the construction of modern highway intersections and elevated freeways in addition to their normal used in circular structures such as bridges and concrete tanks (Fig. (1.1)). Such beams, when loaded transverse to their planes, are subjected to torsion, bending, and shear. Therefore, special feature of the analysis and design of such beams is the necessity to include torsional effects. In a reinforced concrete structures, cracks form even at service load. Such cracking causes local reduction in torsional and flexural stiffnesses resulting in redistribution of internal forces.

Torsion is almost invariably a secondary effect in reinforced concrete building and the subject has not received the same attention as bending, transverse shear, or diagonal tension.

Concrete members are directly subjected to torsional stresses in the following cases:

1.Curved beams in horizontal plane.

2.Beams supporting a cantilever balcony.

3.Screw piles.

In addition to these cases there are other cases where it appears at first that torsion does not occur, but closer examination shows that torsion does exist. For example:

1.Beams and slabs with alternate panel loading.

2.Exterior floor beams.

3.Framed structures. [4]

Generally speaking, we may find members subjected to torsion in every modern structural form Fig.(1.1).

a- Water Tank

b- Curved Bridge

c- Reinforced Concrete Curved Beam on Elastic Foundation

Figure(1.1): Applications of Reinforced Concrete Curved Beam

1.2 Reinforced Concrete Curved Beams in Plan:

Beams curved in plan are often used to support the circular walls of reinforced concrete water tanks, curved balconies and ring beam of domes and shells. The curved beams are generally supported on columns spaced at regular intervals. Since the loads and reactions do not lie along the axes at any point of beam, torsional moment developed at certain cross section of a curved beam. However in the case of circular beams supported by symmetrically placed columns, the vertical reactions are provided by the columns and due to the symmetry, the torsional moments at the center of the curved beam between any two consecutive supports will be zero. Also the maximum negative bending moment develops at the support sections and positive maximum bending moment at sections between the supports[48]. Maximum torsional moments will develop at sections nearer the supports and where the bending moment is zero. In other words, the maximum torque occurs at points of contraflexure. Also the shear forces will be maximum at the support sections.

Hence the support sections have to be designed for maximum negative bending moment and shear and sections where the torque is maximum has to be designed for maximum torsional moment and the corresponding shear force at the section. [48]

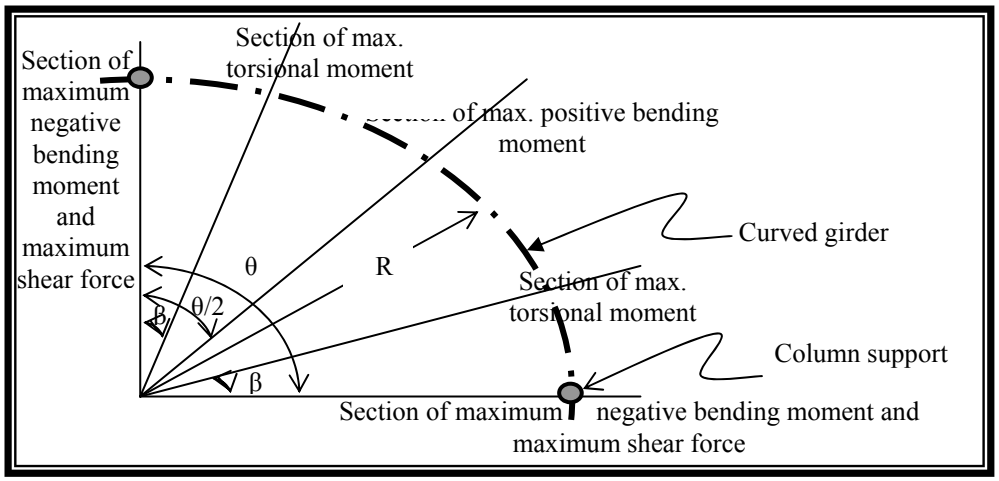

Figure (1.2): Position of Maximum Moment in Curved Girders[48].

1.3 NonLinear Behavior of Soil

Most of the phenomena in the solid mechanics are non-linear. In many applications, however, it is practical and convenient to use linear formulations of problems to obtain engineering solutions. On the other hand, some problems definitely require non-linear analysis if realistic results are to be obtained.

The stress-strain relation of any type of soil depends on a number of different factors including density, water content, structure of the soil, drainage conditions, strain conditions (i.e. plane strain, triaxial), duration of loading, stress history and confining pressures. (39)

It is commonly found(15) that the stress-strain curve for all soils is nonlinear except in a very narrow region near the origin. **Kondner** (31) proposed that the stress-strain curve, which is shown in Fig. (1.3), could be represented by a hyperbolic equation of the form: -

$$\sigma_1 - \sigma_3 = \frac{\in}{a + b \in} \qquad \ldots (1.1)$$

where

σ_1 and σ_3 are the major principal stresses.

$\in$ is the axial strain and

(a) and (***b***) are constants which can be determined experimentally.

There are also various elastic foundation models are explained in Chapter Three.

▲ $Asymptote = (\sigma_1 - \sigma_3)_{ult} = \frac{1}{b}$

1.4 Objective and Scope

This thesis deals with reinforced concrete curved horizontal beams resting on elastic foundations. Most of the applications on this study are circular water tanks and nuclear plants, and ring foundation of domes and shells.

The main aim of this work is to include all types of stresses and strains to present a better understanding for behavior of reinforced concrete curved beam in plane and to predict the ultimate load that causes the failure for the curved beam resting on elastic foundations. To achieve this aim a theoretical work using a materially nonlinearity finite element analysis is carried out to study the behavior of reinforced concrete curved beam using a brick element to represent the concrete.

1.5 Thesis Layout

This thesis consists of six chapters. Chapter one introduces and explains briefly the problem in hand, the aim of the study and the subjects included in other chapters. Chapter two is devoted to the review of literature. Outlines of some previous research works on curved beam in plane are presented.

Chapter three contains a finite element method and the formulation of the governing equilibrium equations. The adopted quadratic brick element, the steel representation and integration rules used in evaluating the element stiffness matrix are also described. The incremental-iterative Newton-Raphson method and the nonlinear solution techniques used for solving the set of nonlinear equations are also presented. Also the various elastic foundation models are explained in this chapter. The outline of computer program is also presented in this chapter.

In Chapter four, material modeling concerning the plastic model used for concrete in compression is described. A smeared crack model that is used to model the concrete in tension, and the elastic-linear work hardening model used to simulate the reinforcement are also given. In Chapter five, several numerical examples are presented and verified by the previous analytical and experimental studies. Chapter six gives the conclusions and recmmendations for future studies.

CHAPTER TWO
Review of Literature

2.1 General

Reinforced concrete beams curved in plane occur frequently as members in buildings, bridges, and other structures. Methods for the determination of ultimate loads for straight beams have been the subject of many studies and are well established. Ultimate loads for reinforced concrete curved beams have not been studied in any detail although steel bents and beams curved in plane were the subject of a pioneering study by Johansen [32] and have also been studied by other research workers. In this chapter a literature survey is divided into two major scopes:

1. Experimental studies.
2. Theoretical studies.

2.2 Experimental Studies

In 1974, **Jordaan et al.**[34] investigated four concrete curved beams and the results were compared with those predicated by a plastic analysis based on a yield criterion which defines the behavior of the cross-section under the combined action of bending and torsion only, i.e. shear is neglected. Four reinforced concrete curved beams were tested. Each beam having a (152 mm*310 mm)cross-section, radius (2200 mm), and a subtended central angle of (86°). The differences between those beams are state of loading and type the boundary condition. The instrumentation enable measurement of applied loads, deflections, angles of twist and steel strains. Loads were applied by hydraulic jacks and were measured by load cells. Fig. (2.1) shows the system of forces

applied on the torsion arms of the heads and the straight end portions of the curved beams.

For this test, the following conclusions were drawn:

1. The plastic theory used gives satisfactory prediction of the mode of failure, i.e., the location and type of plastic hinges.
2. The predicted value of ultimate load was conservative for modes of failure containing pure bending and combined bending-torsion hinges in which bending predominates. The predicted value was slightly higher than the experimental ultimate load for modes of failure containing free hinges.
3. Small changes in geometry due to large deformations during loading can have a significant effect on the value of the collapse load for curved beams failing in a mode that contains free hinges.

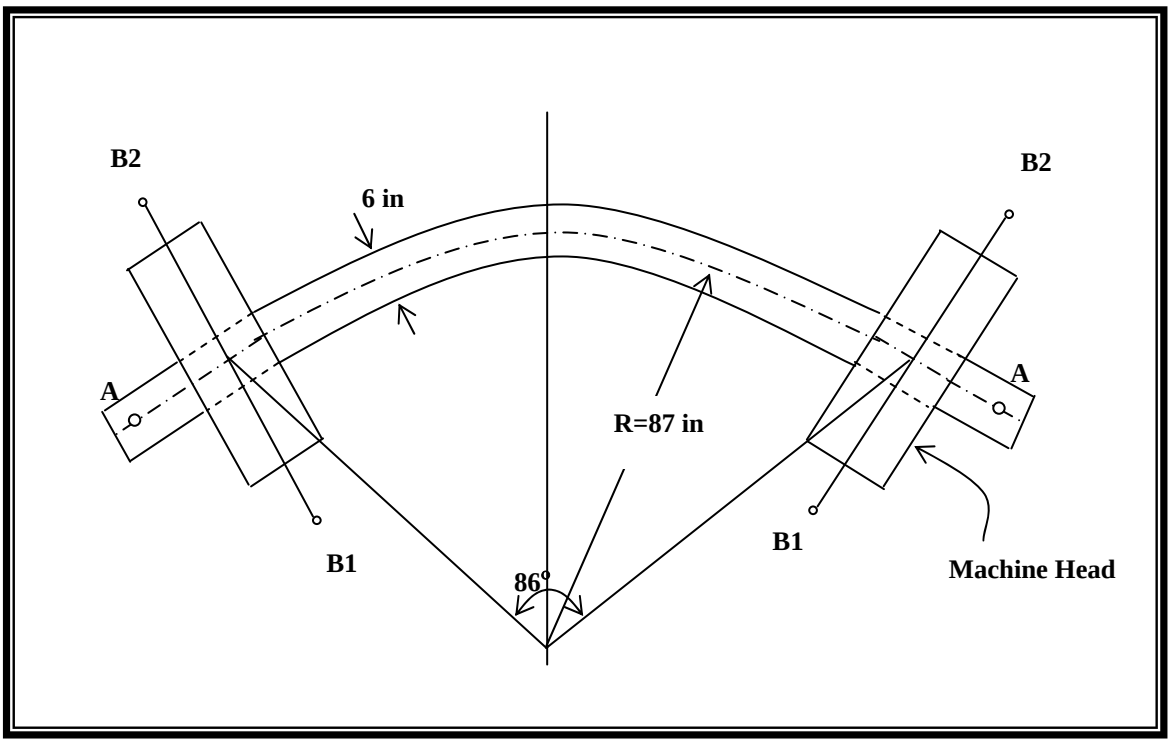

Figure(2.1): Geometry of Test Specimens[34] .

The logical extension of previous work was to include the effects of shear in the analysis of reinforced and prestressed concrete; therefore, in 1977 **Badawy et al.**[10] formulated two yield criteria to represent the behavior of a reinforced concrete section under the combined action of bending, torsion and shear, and the analysis was modified to include the effect of shear . They tested seven straight and eight curved beams, and the results were compared with the modified analysis. Seven straight beams were tested under different combinations of bending, torsion and shear. In this test on curved beams, the plastic hinge locations and consequently the modes of failure were recognized from the crack patterns, the deformed shape of the beam and the measured reinforcement strains. The workers observed the plastic hinges either torsion-shear hinges, flexural hinges, or bending-torsion-shear hinges. Analysis of the test results and comparison with the results predicated by the plastic theory indicates the following conclusions:

1. The methods of plastic analysis can be applied to reinforced concrete curved beams.
2. An analysis using the first criterion gives a good predication of the ultimate load, mode of failure and the internal forces. Whereas an analysis using the second criterion establishes a lower bound for the ultimate load and the internal forces. The dimensionless equations for these two surfaces are :

   $$m^2 + t^2/(1-v^2) = 1 \qquad \text{.....(2-1)}$$

   for the first yield criterion and

   $$m^2 + t^2/(1-v)^2 = 1 \qquad \text{.....(2-2)}$$

   for the second yield criterion where :

   $m=M/M_p$, $t=T/T_p$, $v=V/V_p$; M, T, and V are the bending moment, torsion and shear respectively; and M_p, T_p, and V_p are the corresponding plastic capacities of the cross-section in pure bending, torsion, and shear.

3. Two types of redistribution of internal forces occur in a curved beam, one due to cracking and the other due to plastic hinge formation.
4. The effect of modes of failure is accurately predicted by the analysis.

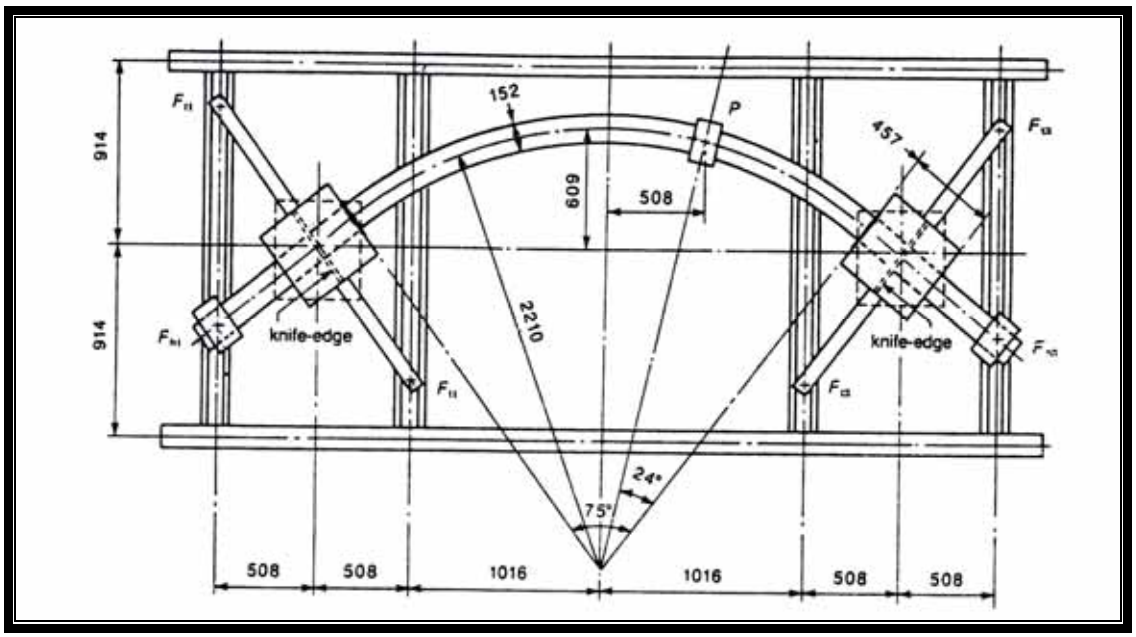

Figure(2.2): Geometry of Test Specimens[10] .

Hsu et al.[27] in 1978 carried out experimental studies on reinforced concrete horizontally curved beams. Seven reinforced concrete horizontally curved beams have been tested. Each beam had a cross-section of (152.4 mm*304.8 mm), a radius of (2.74 m), and a subtending angle of (90°). Each beam was designed to be fixed at both ends and subjected to a concentrated load at midspan. The main aim of that study was to investigate the torsional and flexural moment redistribution after cracking and to suggest an appropriate design method based on this post-cracking behavior. From this they concluded:

1. The conventional design of reinforced concrete horizontally curved beams is to calculate the flexural moments, torsion moments and the shear forces by an elastic analysis using uncracked section.

2. Since moment redistribution occurred after cracking, design of curved beams using cracked section is recommended, particularly near the supports where torsional moment changes rapidly during the length.
3. Torsional moments in a horizontal curved beam are primary moment required by equilibrium. They can not be reduced or neglected.

Abul Mansur and **Vijaya Rangan**[1] (1981) examined three different methods for the design of reinforced concrete curved beams. Three fixed-ended beams designed by these three methods were tested under a point load to study the behavior, strength, and mode of collapse. The suitability of the design methods is discussed from these viewpoints as well as from economy of reinforcing steel. The design methods investigated are: (1) a collapse load method proposed by Badawy et al.[10] ,(2) the classical elastic methods based on uncracked section, and (3) a limit design method proposed by Abul Mansur and Vijaya Rangan. From this test, the following conclusions were drawn:

1. Redistribution of internal forces in a reinforced concrete beam occurs at two stages: one after cracking, and the other after formation of some of the plastic hinges.
2. The collapse load method proposed by Badawy et al. is satisfactory within the scope of the tests, but it requires significantly more steel (especially hoops) than the conventional elastic design and the limit design method.
3. Both conventional elastic method and limit design method give satisfactory designs for reinforced concrete curved beams.
4. For the specimens designed by the conventional elastic method and the limit design method, the elastic analysis based on uncracked sections gives a close estimate of the values of internal forces up to the service load level. But near the ultimate load, the elastic analysis based on cracked sections is more appropriate.

Concerning steel beams curved in plane, both theoretical and experimental studies have been carried out in the past to investigate the behavior of curved I- or box-girder bridges. The Structural Stability Research Conuncil-Task Group 14 ("Horizontally curved" 1991) identified that research on the behavior of curved beams in the inelastic range, including material and geometric nonlinearities, is needed for both I-girder and box-girder bridges since most of the experimental research in the past was restricted to specimens in the elastic range.

Heins and **Spates**[53] (1970) carried out laboratory tests on a curved I-girder subjected to a combination of concentrated loads and torsional moments. The model constructed by them was embedded in concrete blocks to provide a fixed support. However, the models were loaded in the elastic range. The girder tested was 8.3 m long with 15.4 m horizontal radius.

Evans and **Al-Rifaie**[53] (1975) successfully employed both sand and araldite and steel box girder models to establish the accuracy of the finite element method in analyzing box girders curved in plan. Eighteen models of different curvatures were tested: each under different loading conditions. To study the elastic behavior of box girders curved in plan, specimens were selected to cover a wide range of horizontal curvature, including the curvature with R/L of 0.75 which was much greater than that normally encountered in practice.

Another series of experimental investigations to study the effect of curvature on the ultimate load behavior of laterally unsupported curved I-beams was reported by **Fukumoto et al.** [53] (1981). They tested six simply supported curved I-beams of practical size under a concentrated load at the midspan. Longitudinal residual stresses and initial out-of-straightness were measured for

all curved beam specimens with curvature R/L ranging from 12.5 to 125. During experiments the beams were restrained at their supports against twist, but not against warping. Intermediate lateral restraint was not considered in the tests reported so far.

2-3 Theoretical Studies

In 1932, **Osterbloom** [43] in a paper published by the American Concrete Institute, stated; "One may assume the simple case of complete fixity at the supports and, also, a uniform loading, and, thereby, covers the major part of the problem actually occurring in practice.". He developed an equation for the bending moment at the center of a uniformly loaded circular beam, and expressions for the bending and torsion at the supports. He developed a table for the moment factors for the bending and torsion for circular beams of several lengths. The value of stiffness ratio (K) used for rectangular sections was as follows:

$$K = \mathbf{0.65}(\mathbf{1} + \frac{d^2}{b^2}) \qquad \text{.....(2-3)}$$

where $K = \frac{EI}{GJ}$ and ,

d is depth of the section.

b is width of the section.

EI is flexural rigidity.

GJ is torsional rigidity.

The above formula is based on the assumption that the ratio of the modulus of elasticity (E) to the modulus of rigidity (G) is equal to (2.35), and Sant Venant's approximate formula:

$$J = \frac{A^2}{\mathbf{40}IP} \qquad \text{.....(2-4)}$$

where:

IP is polar moment of inertia.

A is the area of the section.

J is the stiffness rigidity factor.

In 1937, a paper was published by **Moorman** [41] for solving curved beams loaded with concentrated loads, using a semi-graphical method. The method is applicable to beams of any curvature, circular, parabolic, elliptic, ect.; it gives accurate results only when the beam is symmetrically loaded.

The method of analysis presented by **Baker** [47] in 1942 is probably the most general method for analyzing circular beams fixed at the ends, loaded with uniformly distributed loads and concentrated loads.

Voluntinei's[56] paper in 1950 was a contribution to the general approach to the analysis of curved beams on several supports. He derived expressions for stiffness factors and carry-over factors for beams subjected to torsion. **Voluntinei's** major contribution was to extend the principle of moment distribution to members resisting combined bending and torsion.

In 1962, **Al-Hassaini**[4] studied a reinforced concrete beams curved in horizontal plane. An elastic theory was used in that study. The main aim of that study was to reduce the amount of labor involved in the computations accompanying the frames containing curved horizontal beams. This is accomplished by offering a comprehensive derivation of the equations for cantilever and fixed end beams, with concentrated and uniformly distributed loads, and for various subtending angle. He derived in that study a general

expression for the bending moment, torsion and shear at the fixed end and midspan of the beam.

In 1977, **Wang** and **Stephen**[57] investigated the effects of Winkler-Pasternak foundations of natural frequencies of a single straight finite Timoshenko beam with different restraints.

Panayotouakos and **Theocaris**[44] in 1979 presented the problem of the linear static analysis of a circular beam on an elastic foundation in the most general case of response and loading. They developed a system of six coupled linear differential equations of first order in which the influences of torsional reaction of the soil and of the shearing deformation are taken into consideration.

Kassam[35] in 1986 studied the effect of foundation parameters and a follower force applied at the cantilever free end, on natural frequencies and vibration stability of a cantilever beam resting on viscoelastic foundation.

Ahmad and **Jaafar**[3] in (1992) studied the effects of Winkler-Pasternak foundations on natural frequencies of finite curved beams. The governing system of partial differential equations for transverse vibrations was first presented with inextensible properties of the curved beam being assumed. He obtained the general solutions of these equations and he derived the dynamic stiffness matrix.

Considerable attention has been given to the linear elastic analysis of a circular beam on an elastic foundation under static loading by many investigators. The method of harmonic analysis is applied by **Bechert** [13] and **Voltera** [54,55] to obtain an approximate solution to the aforementioned problem.

Also of interest are the investigations of **Oravas**[42] and **Petersen**[45] , both of whom achieved close to the solutions of the differential equations describing the equilibrium of the foregoing beam, but in special cases of loading. Moreover, in Refs.[13,54,55,42,45] the influence of torsional reaction of the soil is taken into account.

Shanmugam et al. [53] in (1995), studied a steel I-beams curved in plan. He tested two sets of I-beams (one comprising rolled sections and the other built-up sections) experimentally and theoretically by using the elastoplastic finite element analysis; he discretized the curved beam into a mesh consisting of triangular and quadrilateral shell elements. Figure (2-3) shows a typical finite element mesh. Also he studied the effects of residual stresses and radius of curvature to span-length ratio (R/L) on ultimate strength. From that study he concluded that, with various values of horizontal radius of curvature, it is shown the ultimate capacity decreases significantly with a decrease in the R/L ratio.

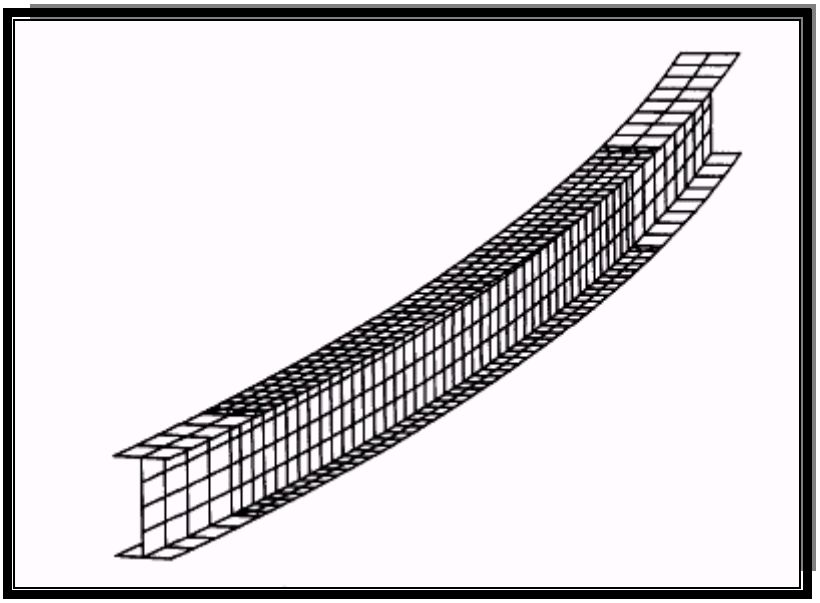

Figure (2-3): Typical Finite Element Mesh[53].

Al-khafaji, 2002[5] presented a theoretical study for the nonlinear analysis of plane steel structures with prismatic or non prismatic members and resting on linear or nonlinear elastic foundation under static loads including the post-buckling behavior. He used polynomial model and hyperbolic stress-strain model to represent the normal reaction for soil as nonlinear elastic behavior of foundation. He used the beam-column approach in analyzing.

In the present study, the theoretical basis for the reinforced concrete horizontally curved beams resting on linear or nonlinear elastic foundations under static loads, will be presented by using finite element method.

CHAPTER THREE
FINITE ELEMENT FORMULATION

3.1 General:

Finite element analyses are performed to gain a better understanding of the behavior and characteristics of reinforced concrete structures under a variety of loading and boundary conditions. While simplified analyses that use either beam elements or two-dimensional finite elements are quite useful, only three-dimensional analyses can fully represent all the aspects of the response of concrete structures[37].

Three-dimensional analyses of reinforced concrete structures require the availability of three-dimensional concrete laws that can describe the main features of the nonlinear concrete response under triaxial states of stress, such as compression crushing, tensile cracking, increased strength and ductility under large confining stresses, etc. All these phenomena are of primary importance for the accurate description of the physical behavior of reinforced concrete structures, such as reinforced concrete columns with different shear reinforcement subjected to large lateral deformations.

In some special situations, only a three-dimensional analysis can provide certain response information of interest to the designer that the other methods cannot provide. The implementation of concrete laws in a finite element environment adds to the complexity of the task, because of discretization errors and because concrete is a highly discontinuous, non-homogeneous material, while the finite element discretization tends to treat it as a continuous medium. In particular, cracking is a discontinuous phenomenon that is typically treated with two major approaches; discrete and smeared crack. The concept of the discrete crack approach is well matched with the nature of the physical cracks; however, the crack regions have to be predefined or remeshing is required. The

smeared crack approach better fits the finite element philosophy, but it may lead to overestimation of the shear strength of structural members[37]. In turn, smeared cracks can be fixed or rotating. As for the steel reinforcement in reinforced concrete structural members, it is modeled by either discrete bar elements, it is embedded in solid finite elements, or it is smeared over the volume of the finite element. According to Darwin[22], the different modeling schemes for the steel reinforcement do not have a significant impact on the results.

3.2 Finite Element Formulation

In structural analysis, the finite element method represents a general method of analysis. In this method, the continuum of infinite degrees of freedom is replaced by a mathematical model that is an assembly of subdivision of finite number of degree of freedom called finite element. The finite element is consisting of a finite number of joints called nodes. Those elements are interconnected at the nodes. The external loading is also transformed into equivalent forces applied at the nodes. The behavior of the assembly of these elements is obtaining by relating their response to that of the nodes.

Referring to Fig. (3.1), the deformation of a solid body corresponding to six stress components are six independent stresses components; these are the three

normal strain components:

εx , εy , εz

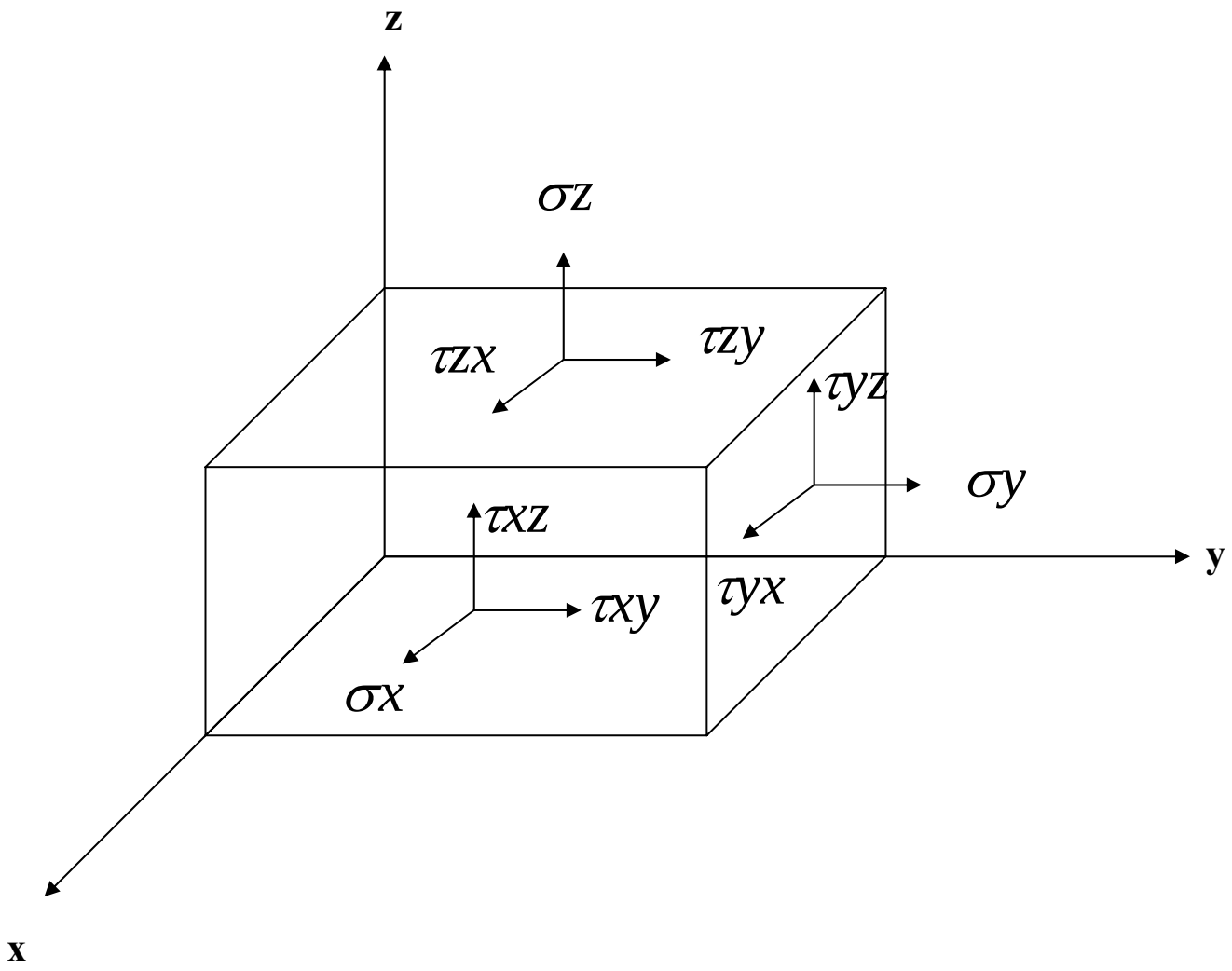

Figure (3.1): Designation of Stress Components.[19]

And the three shearing strain components strain components are: γxy , γyz , γxz

or in vector form:

$$\varepsilon = \{\varepsilon x\ \varepsilon y\ \varepsilon z\ \gamma xy\ \ \gamma yz\ \ \gamma xz\ \} \qquad \text{.....(3.1)}$$

The relationship between linear strains and displacements can be expressed as follows:

$$\{\varepsilon\} = \begin{Bmatrix} \varepsilon_x \\ \varepsilon_y \\ \varepsilon_z \\ \gamma_{xy} \\ \gamma_{yz} \\ \gamma_{zx} \end{Bmatrix} = \begin{Bmatrix} \frac{\partial u}{\partial x} \\ \frac{\partial v}{\partial y} \\ \frac{\partial w}{\partial z} \\ \frac{\partial u}{\partial y} + \frac{\partial v}{\partial x} \\ \frac{\partial v}{\partial z} + \frac{\partial w}{\partial y} \\ \frac{\partial w}{\partial x} + \frac{\partial u}{\partial z} \end{Bmatrix} \qquad \text{.....(3.2)}$$

The general stress-strain relationship is usually written in the form:

$$\{\sigma\} = [D].\{\varepsilon\} \qquad \text{.....(3.3)}$$

The vector of stresses, $\{\sigma\}$ is given by:

$$\{\sigma\} = \{\sigma x \sigma y \sigma z \tau xy \tau yz \tau xz\} \qquad \text{.....(3.4)}$$

and $[D]$, is the elasticity matrix.

In the deriving of the basic equations of the finite elements technique a work done by the internal forces during any kinematically admissible virtual displacement displacement approach is used. It states that a deformable body is in equilibrium if the total work done by all the external forces plus the total internal work is zero leading to[(2)]:

$$\delta W_{\text{int}} - \delta W_{ext} = 0 \qquad \text{.....(3.5)}$$

Where:

$$\delta W_{int} = \int_v \{\partial \varepsilon\}^T \{\sigma\} dv \quad \text{(work of the internal forces)} \quad \ldots\ldots\ldots\ldots\ldots(3.6)$$

$$\delta W_{ext} = \{a\}^T . \{F_G\} \quad \text{(work of the external forces)} \quad \ldots\ldots\ldots\ldots\ldots(3.7)$$

Where:

$\{a\}^T$ is an arbitrary vector of virtual displacement, and

$\{F_G\}$ is the global force vector.

Substitution of equation (3.3) into (3.6) yields:

$$\delta W_{int} = \int_v \{\partial \varepsilon\}^T . [D] \{\varepsilon\} . dv . \qquad \ldots\ldots\ldots\ldots\ldots..(3.8)$$

by making use of (3.7) and (3.8), equation (3.5) may be expressed as:

$$\int_v \{\partial \varepsilon\}^T . [D] \{\varepsilon\} . dv . - \{a\}^T . \{F_G\} = \{0\} \qquad \ldots\ldots\ldots\ldots\ldots.(3.9)$$

which is the general equilibrium equation for linear or nonlinear systems.

In the finite elements analysis, the general three dimensional body is approximated as an assemblage of an arbitrary number of finite elements (n). Consider a finite element (e) of the discrete model and let the displacement vector at any point within the element (u^e), be interpolated as:

$$u^e = N.a^e \qquad \ldots\ldots\ldots\ldots\ldots..(3.10)$$

where, N is a matrix containing the interpolation which relates the displacement (u^e) to the nodal displacement (a^e). The corresponding strains (ε^e) are obtained by the differentiation of the displacements such that:

$$\varepsilon^e = A.u^e \qquad \text{.....(3.11)}$$

where, A is a matrix which contains the differential operators.

Substitution of equation (3.10) into (3.11) yields:

$$\varepsilon^e = B.a^e \qquad \text{.....(3.12)}$$

where, B is the strain displacement matrix given by:

$$B=A \,.\, N \qquad \text{.....(3.13)}$$

3.3 Finite Element Idealization:

The idealization by three-dimensional finite elements has been used in this study. Concrete is simulated by hexahedral brick elements and the reinforcement bars have been modeled as one-dimensional embedded elements built into the three-dimensional concrete elements.

3.3.1 Concrete Idealization

In the finite element method, the construction of the stiffness matrix of the brick element has been facilitated by three advances in the finite element technology: natural coordinates, isoparametric definition and numerical integration[9].

These advances revolutionized the finite element field in mid-1960's, mainly, when the 8-node linear and the 20-node quadratic brick elements were used in representing the three dimensional solid bodies

The quadratic 20-node brick element shown in Fig. (3.2) is adopted to represent concrete in the present study. This type of element is popular due to its superior performance [2]. A major advantage of the quadratic 20-node brick element over the 8-node brick element, when studying complex cases, is that a less number of elements can be used, as well as it may have curved sides and therefore provides a better fit to curved sides of an actual structure[21].

This element has been successfully used in three-dimensional nonlinear analysis of reinforced concrete members by many researchers[2,8,28].

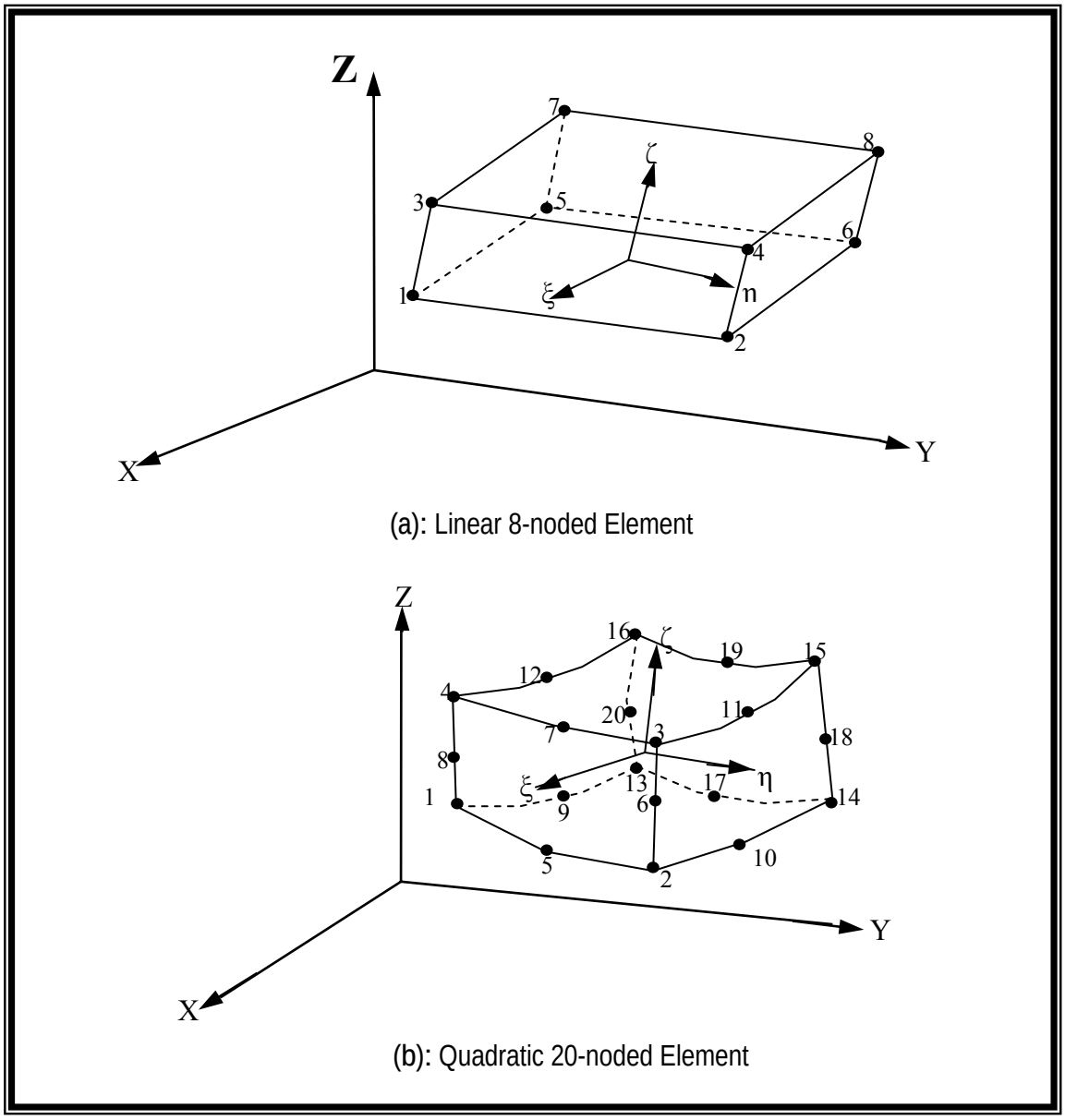

Figure (3.2): Linear and Quadratic Isoparamatric Solid Element.[9]

3.3.2 Shape Functions:

The main concept here is to define the displacement field within its boundary in terms of displacement values at the nodes. It is convenient to express the shape functions in terms of the non-dimensional co-ordinate element (ξ,η,ζ) which varies from -1 to +1 over the element for standard local co-ordinate, Figure (3.3)

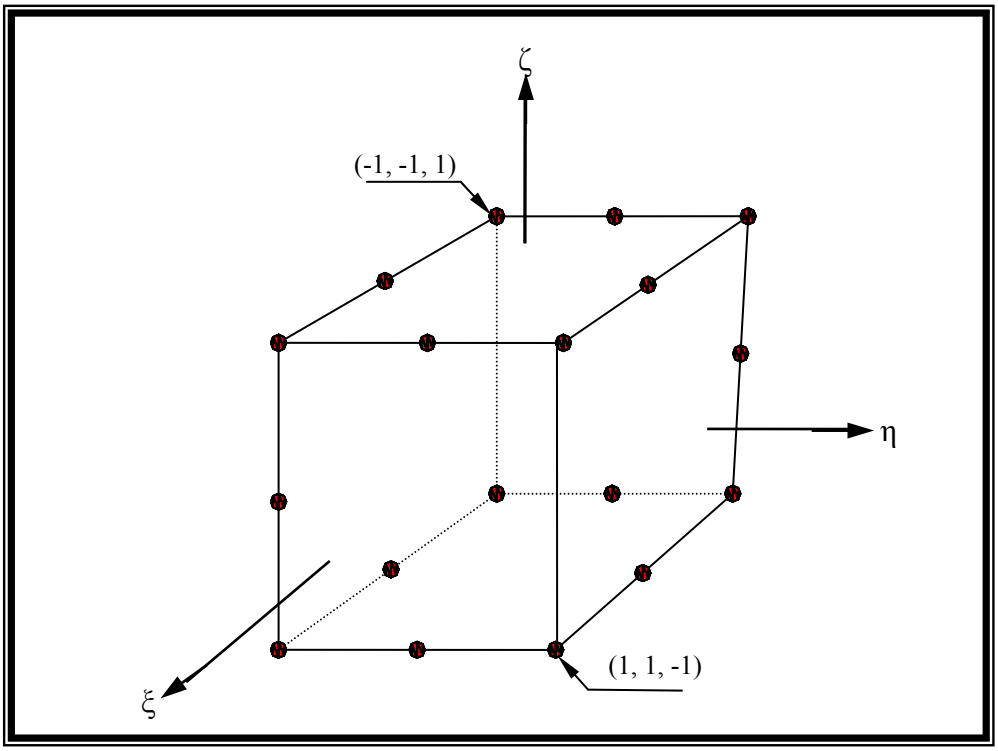

Figure (3.3): Local Coordinates System.[9]

Displacement components at a particular point p(ξ,η,ζ) are defined using the nodal values at each of the twenty nodes and the quadratic shape functions such that:

$$\left.\begin{aligned} u(\xi,\eta,\zeta) &= \sum_{i=1}^{n} Ni\ (\xi,\eta,\zeta)ui \\ v(\xi,\eta,\zeta) &= \sum_{i=1}^{n} Ni\ (\xi,\eta,\zeta)vi \\ w(\xi,\eta,\zeta) &= \sum_{i=1}^{n} Ni(\xi,\eta,\zeta)wi \end{aligned}\right\} \qquad \text{.....(3.14)}$$

where N_i (ξ, η, ζ) is the shape function at the i-th node and u_i, v_i and w_i are the corresponding nodal displacements. The shape functions of the quadratic 20-node brick element are shown in Table (3.1)[28]

Table (3.1): Shape Functions of the Quadratic 20-Node Brick Element [21]

Location	ξ	η	ζ	Ni (ξ, η, ζ)
Corner nodes	± 1	± 1	± 1	$(1+\xi\,\xi_i)(1+\eta\,\eta_i)(1+\zeta\zeta_i)\,(\xi\,\xi_i+\eta\,\eta_i+\zeta\,\zeta_i-2)/8$
Mid-side nodes	0	± 1	± 1	$(1-\xi^2)(1+\eta\,\eta_i)(1+\zeta\,\zeta_i)/4$
Mid-side nodes	± 1	0	± 1	$(1-\eta^2)(1+\xi\,\xi_i)(1+\zeta\,\zeta_i)/4$
Mid-side nodes	± 1	± 1	0	$(1-\zeta^2)(1+\xi\,\xi_i)(1+\eta\,\eta_i)/4$

In the isoparametric group of elements, the shape functions are also used to define the geometry of the element. Therefore, the Cartesian co-ordinate values of any point $p(\xi,\eta,\zeta)$ within the element may be defined as:

$$\left.\begin{aligned} x(\xi,\eta,\zeta) &= \sum_{i=1}^{20} Ni\,(\xi,\eta,\zeta)\,xi \\ y(\xi,\eta,\zeta) &= \sum_{i=1}^{20} Ni\,(\xi,\eta,\zeta)\,y_i \\ z(\xi,\eta,\zeta) &= \sum_{i=1}^{20} Ni\,(\xi,\eta,\zeta)\,zi \end{aligned}\right\} \qquad \ldots\ldots\ldots\ldots\ldots\ldots (3.15)$$

where x_i , y_i and z_i are the global coordinates of the node i .

3.3.3 Stress and Strain Fields

Since the geometrical nonlinearities are not considered in the present work, displacement gradients remain small throughout the loading process and hence the engineering components of strain can be expressed in terms of the first partial derivatives of the displacement components. Therefore, the linearized strain-displacement relationships may be written as follows[(2)]:

$$\{\varepsilon\} = \begin{Bmatrix} \varepsilon_x \\ \varepsilon_y \\ \varepsilon_z \\ \gamma_{xy} \\ \gamma_{yz} \\ \gamma_{zx} \end{Bmatrix} = \begin{Bmatrix} \frac{\partial u}{\partial x} \\ \frac{\partial v}{\partial y} \\ \frac{\partial w}{\partial z} \\ \frac{\partial u}{\partial y} + \frac{\partial v}{\partial x} \\ \frac{\partial v}{\partial z} + \frac{\partial w}{\partial y} \\ \frac{\partial w}{\partial x} + \frac{\partial u}{\partial z} \end{Bmatrix} = \sum_{i=1}^{20} \underbrace{\begin{bmatrix} \frac{\partial Ni}{\partial x} & 0 & 0 \\ 0 & \frac{\partial Ni}{\partial y} & 0 \\ 0 & 0 & \frac{\partial Ni}{\partial z} \\ \frac{\partial Ni}{\partial y} & \frac{\partial Ni}{\partial x} & 0 \\ 0 & \frac{\partial Ni}{\partial z} & \frac{\partial Ni}{\partial y} \\ \frac{\partial Ni}{\partial x} & 0 & \frac{\partial Ni}{\partial z} \end{bmatrix}}_{[B]} \cdot \underbrace{\begin{Bmatrix} u_i \\ v_i \\ w_i \end{Bmatrix}}_{\{a\}^e} \qquad \ldots(3.16)$$

Since the shape functions N_i are functions of the local coordinates rather than Cartesian coordinates, a relationship needs to be established between the derivatives in the two coordinates systems. By using the chain rule, the partial differential relation can be expressed in matrix form as[2]:

$$\begin{bmatrix} \frac{\partial Ni}{\partial \xi} \\ \frac{\partial Ni}{\partial \eta} \\ \frac{\partial Ni}{\partial \zeta} \end{bmatrix} = \underbrace{\begin{bmatrix} \frac{\partial x}{\partial \xi} & \frac{\partial y}{\partial \xi} & \frac{\partial z}{\partial \xi} \\ \frac{\partial x}{\partial \eta} & \frac{\partial y}{\partial \eta} & \frac{\partial z}{\partial \eta} \\ \frac{\partial x}{\partial \zeta} & \frac{\partial y}{\partial \zeta} & \frac{\partial z}{\partial \zeta} \end{bmatrix}}_{[J]} \cdot \begin{bmatrix} \frac{\partial Ni}{\partial x} \\ \frac{\partial Ni}{\partial y} \\ \frac{\partial Ni}{\partial z} \end{bmatrix} \qquad \ldots. (3.17)$$

where [J] is the Jacobian matrix and the elements of this matrix can be obtained by differentiation of equation (3.15).

The Jacobian matrix can be expressed as[2] :

$$[J] = \begin{bmatrix} \sum \frac{\partial Ni}{\partial \xi} x_i & \sum \frac{\partial Ni}{\partial \xi} y_i & \sum \frac{\partial Ni}{\partial \xi} z_i \\ \sum \frac{\partial Ni}{\partial \eta} x_i & \sum \frac{\partial Ni}{\partial \eta} y_i & \sum \frac{\partial Ni}{\partial \eta} z_i \\ \sum \frac{\partial Ni}{\partial \zeta} x_i & \sum \frac{\partial Ni}{\partial \zeta} y_i & \sum \frac{\partial Ni}{\partial \zeta} z_i \end{bmatrix} \quad \ldots. (3.18)$$

Then, the derivatives of the shape function with respect to Cartesian coordinates can be obtain as[2] :

$$\begin{bmatrix} \frac{\partial Ni}{\partial x} \\ \frac{\partial Ni}{\partial y} \\ \frac{\partial Ni}{\partial z} \end{bmatrix} = [J]^{-1} \cdot \begin{bmatrix} \frac{\partial Ni}{\partial \xi} \\ \frac{\partial Ni}{\partial \eta} \\ \frac{\partial Ni}{\partial \zeta} \end{bmatrix} \quad \ldots. (3.19)$$

where $[J]^{-1}$ is the inverse of Jacobian matrix given by:

$$[J]^{-1} = \begin{bmatrix} \frac{\partial \xi}{\partial x} & \frac{\partial \eta}{\partial x} & \frac{\partial \zeta}{\partial x} \\ \frac{\partial \xi}{\partial y} & \frac{\partial \eta}{\partial y} & \frac{\partial \zeta}{\partial y} \\ \frac{\partial \xi}{\partial z} & \frac{\partial \eta}{\partial z} & \frac{\partial \zeta}{\partial z} \end{bmatrix} \quad \ldots. (3.20)$$

As $[J].[J]^{-1} = [J]^{-1}.[J] = [I]$ (unit matrix)

The vector of stresses is given by:

$$\{\sigma\} = \begin{Bmatrix} \sigma_x \\ \sigma_y \\ \sigma_z \\ \tau_{xy} \\ \tau_{yz} \\ \tau_{zx} \end{Bmatrix} \qquad \ldots.(3.21)$$

and the stress-strain relationship is represented as:

$$\{\sigma\} = [D].\{\varepsilon\} \qquad \ldots. (3.22)$$

where [D] is the elasticity matrix.

3.3.4 Evaluation of Element Stiffness Matrix:

In order to establish the governing equations of static equilibrium, which will lead to the derivation of the stiffness matrix, the principle of virtual displacements for a deformable body is used. It is simply to state that a deformable body is in equilibrium if the total work done by all the external forces plus the total work done by all the internal forces during any kinematically admissible virtual displacement is zero[28] or in other words, strain energy is equal to loss of potential work by external forces:

$$\delta W_{int} - \delta W_{ext} = 0 \qquad \ldots. (3.23)$$

The external work can be expressed as the work done in moving the body forces $\boldsymbol{b}$ and surface traction t_s through the virtual displacement $\{\partial U\}$, as:

$$\delta W_{ext} = \int_V \{\partial u\}^T \{b\}\, dv + \int_S \{\partial U\}^T \{t_S\} ds \qquad \ldots. (3.24)$$

where v is the volume of the body and s is that part of the surface of the body where external tractions are prescribed.

The change in the strain energy. or internal work, due to a set of virtual strains, $\{\partial\varepsilon\}$, corresponding to the virtual displacement $\{\partial U\}$ is:

$$\delta W_{int} = \int_v \{\partial\varepsilon\}^T \{\sigma\} dv \qquad \text{..... (3.25)}$$

by substituting equations (3.22) into equation (3.25) then

$$\delta W_{int} = \int_v \{\partial\varepsilon\}^T [D]\{\varepsilon\} dv \qquad \text{..... (3.26)}$$

by substituting equations (3.24) and (3.26) into equation (3.23), then:

$$\int_V \{\partial\varepsilon\}^T [D]\{\varepsilon\} dv - \int_V \{\partial u\}^T \{b\} dv - \int_S \{\partial u\}^T \{t_S\} ds = 0 \qquad \text{..... (3.27)}$$

This expression represents the equation of static equilibrium for a general body.

The basic concept of finite element analysis is to discretize the continuum into arbitrary numbers of small elements connected together at their common nodes. For a finite element, e, of the discrete model, the displacement vector at any point is:

$$\{U\} = [N]\{a\}^e \qquad \text{.....(3.28)}$$

where [N] is a matrix containing the interpolation functions which relate the displacement $\{U\}^e$, to the nodal displacements $\{a\}^e$.

By differentiation of the displacements, the corresponding strains, $\{\varepsilon\}^e$, are obtained such that:

$$\{\varepsilon\}^e = [A]\{U\}^e \qquad \text{....(3.29)}$$

where [A] is the matrix, which contains the differential operators. Substituting of equation (3.28) into equation (3.29) yields:

$$\{\varepsilon\}^e=[A][N]\ \{a\}^e \qquad \ldots.(3.30)$$

or

$$\{\varepsilon\}^e=[B]\{a\}^e \qquad \ldots..(3.31)$$

where [B] is the strain displacement matrix, which represents the values of the strain at any point within the element, due to unit values of nodal displacements. In the discrete model, the equations of equilibrium of the continuum may be written as the sum of integration over the volume and surface area for all the finite elements. Therefore, by making use of equations (3.28) and (3.31), equation (3.27) becomes:

$$\partial\{a\}^T\left\{\sum_{n}\int_V[B]^T[D][B]\,dv^e\{a\}^e-\sum_{n}\int_V[N]^T\{R\}^e\,dv^e-\sum_{n}\int_S[N]^T\{T_S\}^e\,ds^e\right\}=\{0\} \qquad \ldots..(3.32)$$

Since the relationship must be valid for any set of virtual displacements, and since $\partial\{a_e\}^T$ is arbitrary or $\partial\{a_e\}^T$ not equal 0, then equation (3.32) is written in brief from one element ***e*** as:

$$\{f\}^e=[k]^e.\{a\}^e \qquad \ldots.(3.33)$$

where [k] is the structural stiffness matrix of the assemblage of the elements and given by:

$$[k]=\sum_{n}\int_V[k]^e \qquad \ldots.(3.34)$$

and {a} is the corresponding element assemblage nodal displacement vector, and {f} is the element assemblage of external nodal force vector given by:

$$\{f\}=\sum_{n}\int_{ve}[N]^T\{b\}^e\,dv^e+\sum_{n}\int_{se}[N]^T\{T_S\}^e\,ds^e \qquad \ldots.(3.35)$$

For an element of volume ***v***, the stiffness matrix is presented implicitly in equation (3.34) as:

$$[K]^e = \int_{v^e} [B]^T .[D].[B]\, dv^e \qquad \ldots.(3.36)$$

For three-dimension elements, the differential volume dv^e may be written as:

$$dv^e = dxdydz \qquad \ldots.(3.37)$$

Equation (3.37) can be transformed into the natural coordinates as:

$$dv^e = |J| d\xi d\eta d\zeta \qquad \ldots.(3.38)$$

where $|J|$ is the determinant of the Jacobian matrix. The limits of integration in the natural coordinates become –1 an +1 and the element stiffness matrix can therefore be written as:

$$[K]^e = \int_{-1}^{+1}\int_{-1}^{+1}\int_{-1}^{+1} [B]^T [D][B]|J| d\xi d\eta d\zeta \qquad \ldots.(3.39)$$

In general it is not possible to evaluate the element stiffness matrix explicitly. Thus, numerical integration has to be used.

3.3.5 Reinforcement Idealization

In developing a finite element model for reinforced concrete members, at least three alternative representations of reinforcement have been used:

a) Smeared Representation

For a smeared representation, Fig. (3.4a), reinforcement bars are assumed to be distributed through over the concrete element in any specified direction. A composite concrete-reinforcement constitutive relation is used in this case[19]. To derive such relation, perfect bond between the concrete and the steel bars must be assumed.

b) Discrete Representation

A discrete representation by using one-dimensional elements to idealize the reinforcement has been widely used, Fig. (3.4b). Axial force members, or bar links, may be implemented and assumed to be pin connected with two – degrees of freedom at each nodal points. Beam elements may also be used, and assumed to resist axial force, shear, and bending, with three degrees of freedom assigned at each node. In either cases, the one-dimensional reinforcement elements are easily superimposed on the multi-dimensional finite element mesh representing the concrete. A significant advantage of the discrete representation in addition to its simplicity is that it can account for possible displacement of the reinforcement with respect to the surrounding concrete[21,19].

c) Embedded Representation

The embedded representation, Fig. (3.3c), may be used in connection with higher order isoparametric concrete elements. The reinforcing bar is considered to be an axial member built into the isoparametric concrete element such that its displacements are consistent with those of the element. Perfect bond between the steel and the concrete has been assumed in this case. A major advantage of this approach is that the steel bars can be placed in their correct positions without imposing any restrictions on mesh choice and hence the finite element analysis can be carried out with a smaller number of brick elements compared to the discrete representation of reinforcement. Therefore, the embedded representation is adopted in the present work[9].

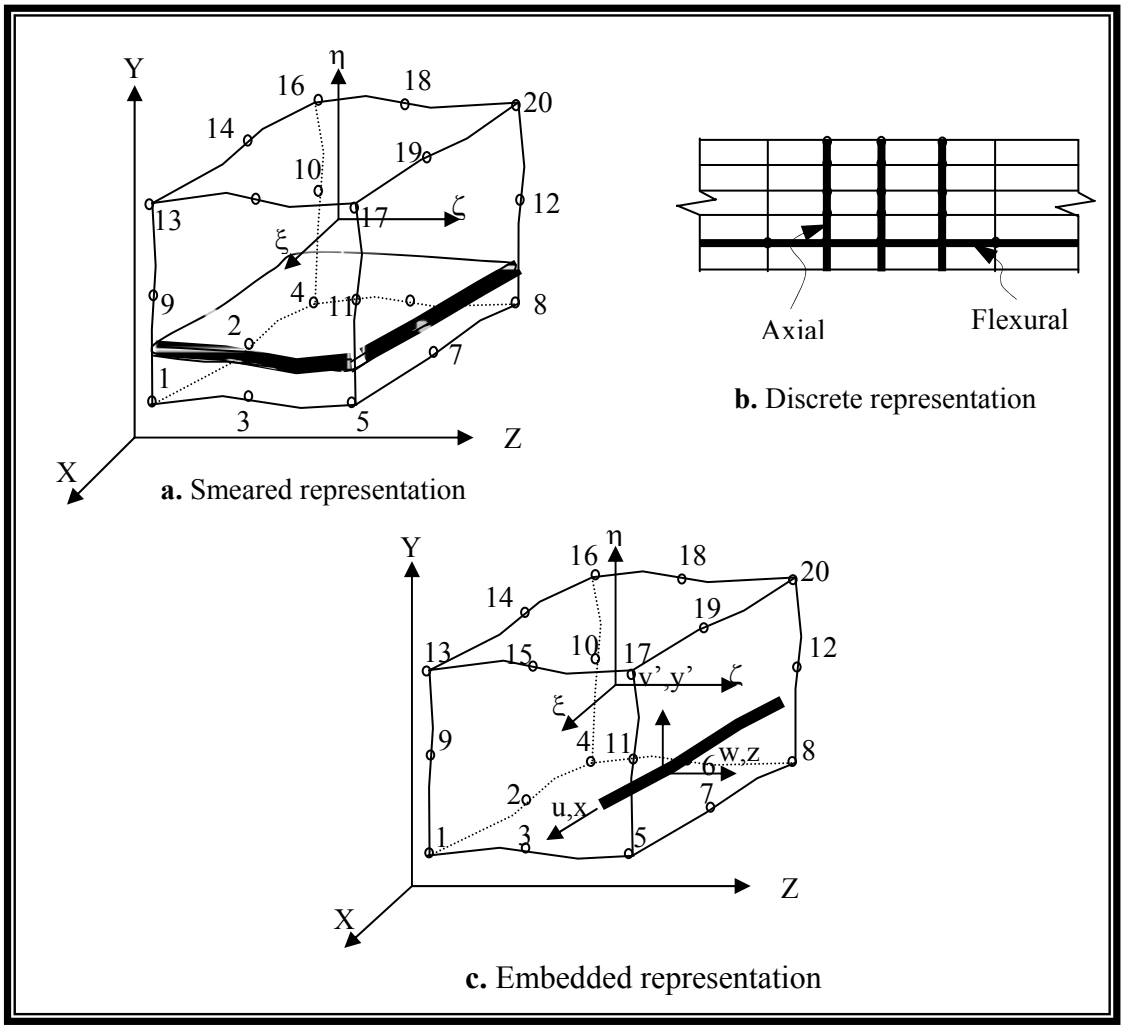

Figure (3.4): Alternative Representations of Steel Reinforcement.[9]

For particular types of problems, a combination of representations may be used. As an example, discrete beam elements may be used for the main reinforcement in beams while axial bar elements are used for stirrups[8]. Or a smeared model can be used for the steel throughout the surface of the curved shell and discrete bar or beam elements for special reinforcement along the edge[8]. For a bar lying inside a hexahedral brick element and parallel to the local coordinate axis ξ, with $\eta = \eta_c$ and $\zeta = \zeta_c$, the displacement representations are[2]:

$$\left.\begin{aligned} u &= \sum_{i=1}^{n} N_i(\xi) u_i \\ v &= \sum_{i=1}^{n} N_i(\xi) v_i \\ w &= \sum_{i=1}^{n} N_i(\xi) w_i \end{aligned}\right\} \quad \text{....(3.40)}$$

The strain-displacement relationship can be expressed in the local coordinate system as [8]:

$$\varepsilon' = \sum_{i=1}^{n} \left[\frac{1}{h^2} \begin{bmatrix} c_1 & c_2 & c_3 \\ c_2 & c_4 & c_5 \\ c_3 & c_5 & c_6 \end{bmatrix} \begin{bmatrix} \frac{\partial N_i}{\partial x} \\ \frac{\partial N_i}{\partial y} \\ \frac{\partial N_i}{\partial z} \end{bmatrix} \right] \begin{bmatrix} u_i \\ v_i \\ w_i \end{bmatrix} \quad \text{....(3.41)}$$

where:

$$C_1 = (\partial x/\partial \xi)^2, C_2 = (\partial x/\partial \xi)(\partial y/\partial \xi), C3 = (\partial x/\partial \xi)(\partial z/\partial \xi)$$
$$C_4 = (\partial y/\partial \xi)^2, C_5 = (\partial y/\partial \xi)(\partial z/\partial \xi), C_6 = (\partial z/\partial \xi)^2$$

and

$$h = \sqrt{C_1^2 + C_4^2 + C_6^2} \quad \text{....(3.42)}$$

Eq. (3.41) is expressed in a compact form as[8]:

$$\{\varepsilon'\} = [B'] \{a\}^e \quad \text{....(3.43)}$$

where [B′] is the strain-displacement matrix of the bar element. Then the stiffness matrix of an axially loaded bar element may be expressed as[2]:

$$[K']^e = [B']^T [D'] [B'] dv^e \quad \text{.... (3.44)}$$

The constitutive matrix [D′] represents the modulus of elasticity of the steel bar for the case of one-dimensional bar element lying in the direction parallel to the natural coordinate lineξ, and the volume differential dv^e can be written as[8]:

$$dv^e = As.dx' = As.h.d\xi \quad ....(3.45)$$

where *As* is the cross-sectional area of the bar. By substitution of Eq. (3.45) into Eq.(3.44), the stiffness matrix of the embedded bar can be expressed as[28]:

$$[K']^e = As \int_{-1}^{+1} [B]^T [D'] [B'].h.d\xi \quad ....(3.46)$$

3.3.6 SOIL-Structure Interaction Analysis

Evaluating the response of soil media to the applied external loads can be made from knowledge of the complete stress strain characteristics of soil. The stress-strain relations are the mathematical distribution of the mechanical properties of the soil (the soil constitutive equation) [26]. A complete stress-strain relationship for the soil will furnish, at the least in the theory, the stresses and strains in a soil media at any particular time under any given load conditions. It seems unlikely that generalized stress-strain relations can be developed to fulfill the requirements of every type of soil behavior, especially in relation to the analysis of the interaction between the soil and the foundation. There are many empirical, semi empirical, graphical, and theoretical approaches depending on many unrealistic assumptions for the soil behavior, while other approaches depend mainly on representation of practical problems by oversimplified model from which the required solutions may be obtained.[6]

There are several parameters that go in the definition of soil structure interaction. Some of these parameters are the importance only in special

problems, while other basic parameters are important in all soil structure interaction problems. These basic parameters are [52]:

1- The stiffness of both soil and structure.

2-The nonlinear stress behavior and dependency of the modulus of elasticity and Poisson's ratio of both soil and structure.

3-The nonlinear behavior of soil-structure interface, and

4-Time.

In this section, a brief exposition of some idealized models is presented and employed in the governing equations for reinforced concrete curved beams on elastic foundations.

3.3.7 Elastic Foundation Properties

The constant of proportionality between the applied normal or shear stress at a point on the surface of soil and the corresponding surface displacement is the modulus of subgrade reaction for soil mass, or soil configuration at that point. The modulus of subgrade reaction gives the relationship between the soil pressure and the resulting deflection[5].

The subgrade reaction model of soil behavior was originally proposed by Winkler in (1867), characterizing the soil as a series of unconnected linearly elastic springs. The deflection at any point (or any spring) occurs only where loading exists at that point. The obvious disadvantage of this soil model is the lack of continuity. Real soil is at least to some extent continuous. A further disadvantage is that the spring modulus of the model (modulus of subgrade reaction) is dependent on the size of foundation. In spite of these drawbacks, the subgrade reaction approach has been widely employed in foundation practice because it provides a relatively simple means of analysis and enables factors, such as nonlinear, variation of soil stiffness with depth and layering of the soil profile to be taken into account.

In order to characterize the behavior of a soil mass as being equivalent to a Winkler medium, the following conditions should be satisfied[5]:

1.The surface displacement at each point of the soil medium should be proportional to the applied normal stress. Plate bearing tests give approximate linearity especially when the loads are small.
2.The surface displacement of the soil medium outside the loaded region should be zero irrespective of the location or magnitude of the applied load. Real soil (and other solid granular materials) do not fulfill this condition. The error is usually small in most computations.

Soil configuration can be presented by using two kinds of subgrade reaction moduli along the foundation length, the normal and tangential. The normal subgrade reaction modulus (K_n) is defined as the load required to act normally on a unit area of the elastic foundation to produce a unit of normal displacement. The tangential subgrade reaction modulus (K_t) is defined as the load required to act tangentially on a unit area of elastic foundation to produce a unit of horizontal displacement[5].

3.3.8 Elastic Models of Soil Behavior

The theory of elasticity was used by several investigators to solve soil-structure interaction problems[51]. The soil is treated as a semi-infinite homogenous, isotropic and elastic material possessing full continuity and characterized by a Young's modulus (E) and Poisson's ratio (ν).

Results obtained by this approach are not completely correct except for special cases, because of the fact that the soil is neither linear nor homogenous in general. More acceptable results are obtained by considering an inelastic behavior of soils (nonlinearity, nonhomogeneity and anisotropy).

3.3.8.1 Compression Resistance Models

A compressional resistance is the transverse reaction of the medium to the overlying foundation. The following models are presented[36]:

3.3.8.1.1 Winkler Model

This model assumes that the base is consisting of closely spaced, independent linear spring. Consequently, the contact pressure at any point on the soil-structure contact is proportional to the deflection at that point and is independent of deflection at other points (Fig.(3.5)). This model is a one-parameter model. The pressure beneath the foundation is given by:

$$p(x,y) = k_z w(x,y) \qquad \text{.....(3.47)}$$

where k_z is termed the modulus of subgrade reaction with units of stress per unit deflection.

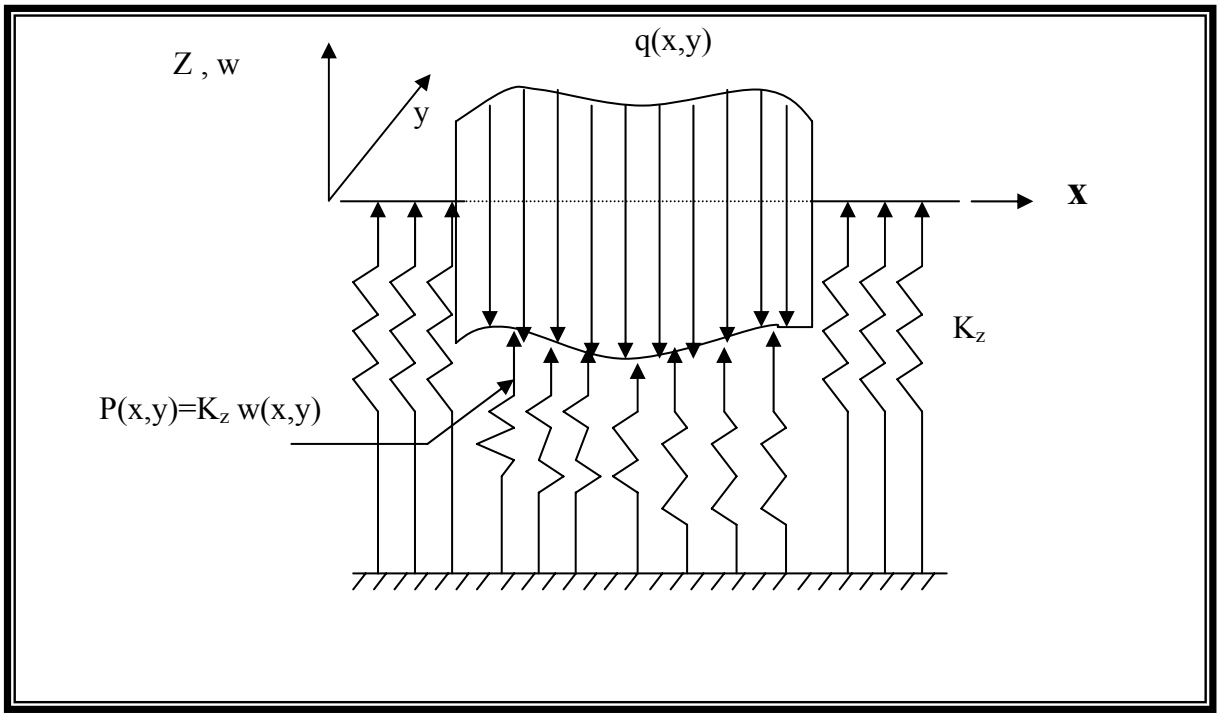

Figure (3.5): Surface Displacements of Winkler Model to a Non-uniform Load.[6]

3.3.8.2 Two-Parameter Elastic Model

Winkler one-parameter model neglects any transverse shearing stress between adjacent points in soil, and accounts for nonlinearity or inelasticity of soil. In an attempt to find a physical close and mathematically simple representation for soil-structure interaction model, many models of two parameters are developed. The term "two-parameter" signifies the fact that the model is defined by two independent elastic constants. The development of these two-parameter soil models has been approached along two distinct lines. The first proceeds from the discontinuous Winkler model and eliminates its discontinuous behavior by providing interaction between individual spring elements. Such physical model of soil behavior have been proposed by Filonenko-Borodich (1940), Heteny (1946), Pasternak (1954) and others where interaction between the spring elements is provided by either elastic membranes, elastic beams or elastic layers capable of purely shearing deformation. The second approach starts from the elastic continuum model and introduces constraints or simplifying assumptions with respect to the distribution of displacements and stresses. The soil models proposed by Reissner (1958) and Vlasov and Leontiev (1966) take into consideration such simplifications[36].

(a) Filonenko-Borodich Model

This model acquires continuity between the spring elements by connecting the ends of the springs by a stretched elastic membrane subjected to constant tension T as in Fig.(3.6). The contact normal pressure is given by[6]:

$$P(x,y) = k_z.w(x,y) - T\nabla^2 w(x,y) \qquad \text{.....(3.48)}$$

where $T\nabla^2 w$ is part of pressure by the assumed membrane. The two elastic constants necessary to characterize the soil model are k_z and T.

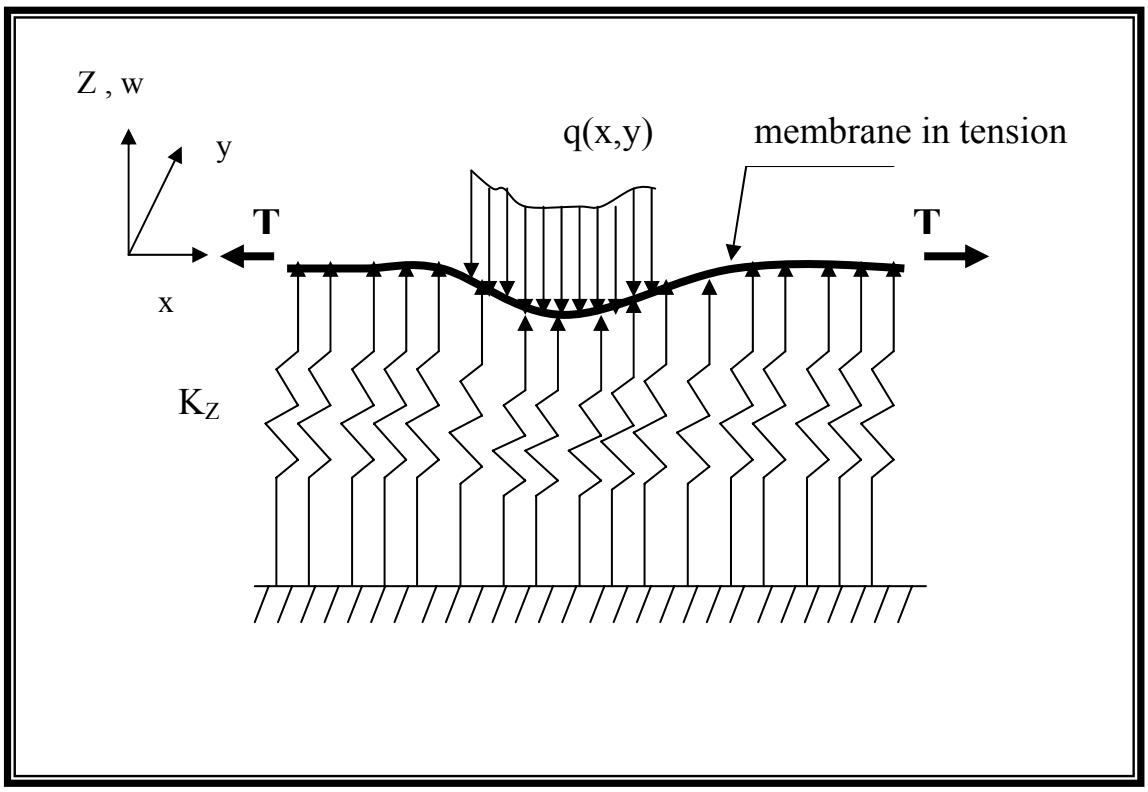

Figure (3.6): Surface Displacement of Filonenko-Borodich Model. [6]

b) Pasternak Model

The Pasternak two-parameter model assume that there is shear interaction between the spring elements. This shear interaction may be accomplished by connecting the ends of springs to an incompressible layer which deforms in transverse shear only (Fig.(3.7)). The contact normal pressure is given by[6] :

$$P(X,Y) = K_Z w(x,y) - G_P \nabla^2 w(x,y) \qquad \text{.....(3.49)}$$

where G_P is the shear modulus for the shear layer and $G_P \nabla^2 w$ is the pressure taken by the shear in the layer.

It can be seen that equation (3.49) is identical to equation (3.48) if T is replaced by G_P . Thus, the surface deflection profiles by this model will be similar to those by Filonenko-Borodich model.[6]

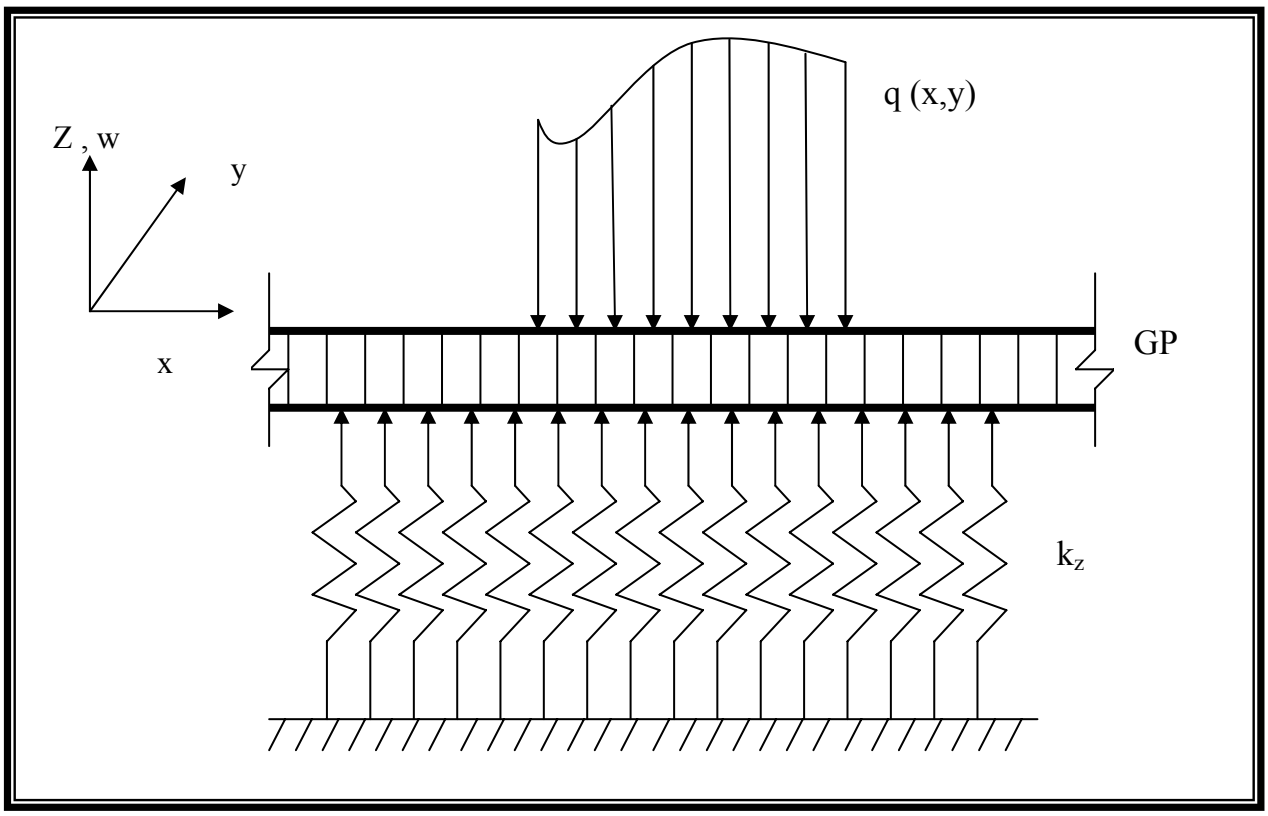

Figure (3.7): Pasternak Model. [6]

c)Heteny Model

The interaction between the independent spring elements is accomplished by connecting the springs by an elastic thin plate. The response function of this model is given by[6]:

$$P(x,y) = K_z w(x,y) - D_f \nabla^4 w(x,y) \qquad \text{.....(3.50)}$$

where D_f represents the flexural rigidity of the foundation plate that connects the springs and $D_f \nabla^4 w$ is the pressure taken by the assumed plate[6].

.

d) The Elastic Continuum Model

Soil media have been idealized as three dimensional continuous elastic solids or elastic continua. The initial impetus for the continuum representation of soil media stems from the work of Boussinesq (1885), who analyzed the problem of a semi-infinite homogenous isotropic linear elastic solid subjected to a concentrated load. After this, many solutions are formed for various types of loads. Some of these solutions take into consideration nonlinearity, nonhomogeneity, inelasticity and anisotropy of soils. The considered soil parameters are moduli of elasticity and Poisson's ratios. Reissner (1958) , Vlasov and Leonetiev (1966) models are examples for two-parameter elastic continuum models. A detailed exposition for such models is presented in [Ref. 36].

3.3.8.2 Frictional Resistance Models

The application of loads on plate resting on elastic foundations produces deformations (movements) in the contact face of the plates; these movement cause shearing or friction force dependent on the soil, the plate, and the applied loads.

There are several assumptions for the interface condition between a foundation and underlying soil medium. These range from completely smooth to completely adhering interfaces with either Winkler, Coulomb friction or finite (constant value) friction.

3.3.8.2.1 Winkler Model

According to the definition of compressional Winker model in section(3.3.8.1.1), the frictional resistance could be modeled on the same manner.(6)

$$F_x(x,y) = K_x.u(x,y) \qquad \ldots (3.51)$$

$$F_y(x,y) = K_y.v(x,y) \qquad \ldots (3.52)$$

where F_x and F_y are the friction force per unit area in x and y-direction, K_x and K_y are the modulus of subgrade reaction in x and y-direction respectively, with a unit of stress per unit of displacement, and $u_{(z=-h/2)}$ or $v_{(z=-h/2)}$ is the horizontal displacement in x or y-direction (Fig.(3.8)).

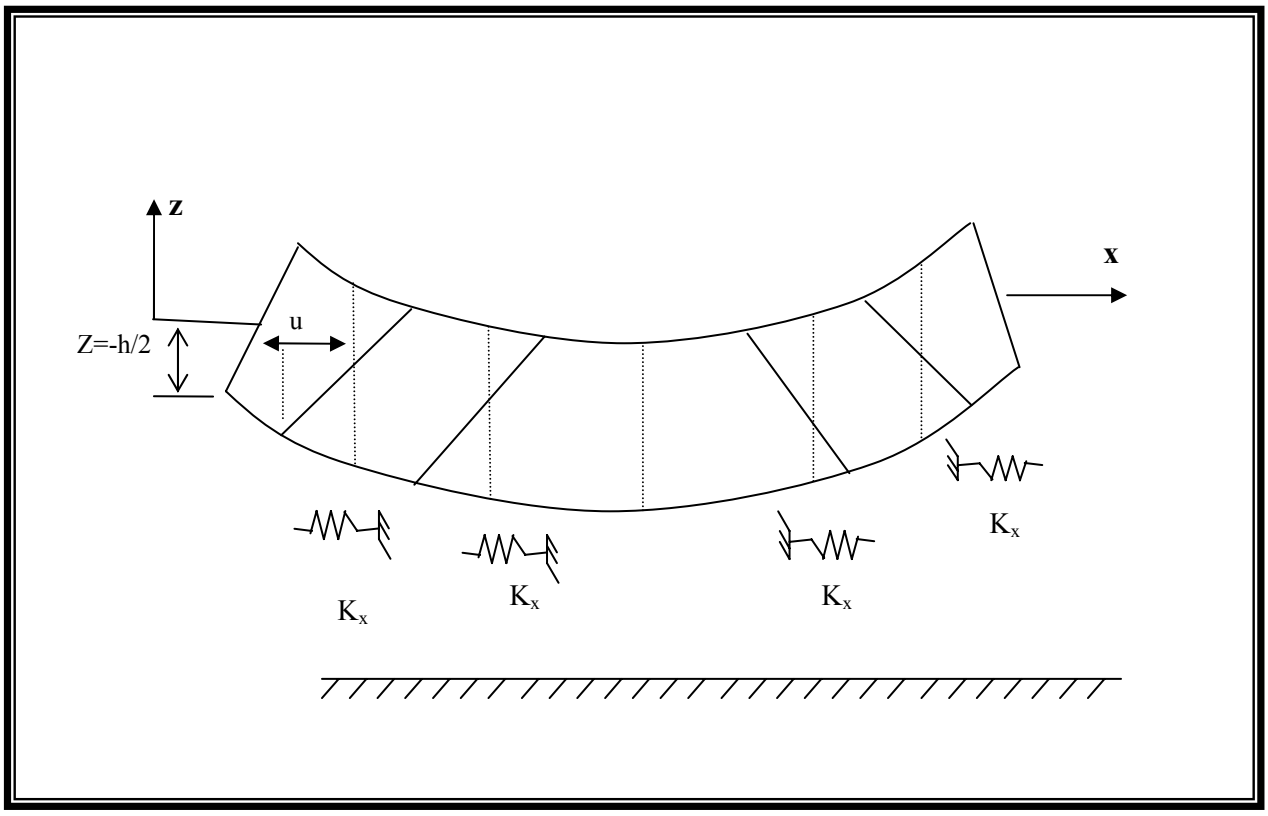

Figure (3.8): Winkler Friction Model. [5]

3.3.8.2.2 Coulomb Model

Coulomb friction (or sliding friction between two surfaces in contact) is independent on the value of horizontal displacement (or sliding) but it is directly proportional to the normal reaction. Accordingly, the friction forces F_x or F_y could be related to transverse displacement w as follows[6]:

$$F_x = K_z.w.\tan(\delta_x) \quad \ldots(3.53)$$

$$F_y = K_z.w.\tan(\delta_y) \quad \ldots(3.54)$$

where $K_z.w$ is the normal reaction of Winkler model, and δ_x or δ_y is the angle of friction between the soil and the foundation in x or y-direction respectively (Fig.(3.9)).

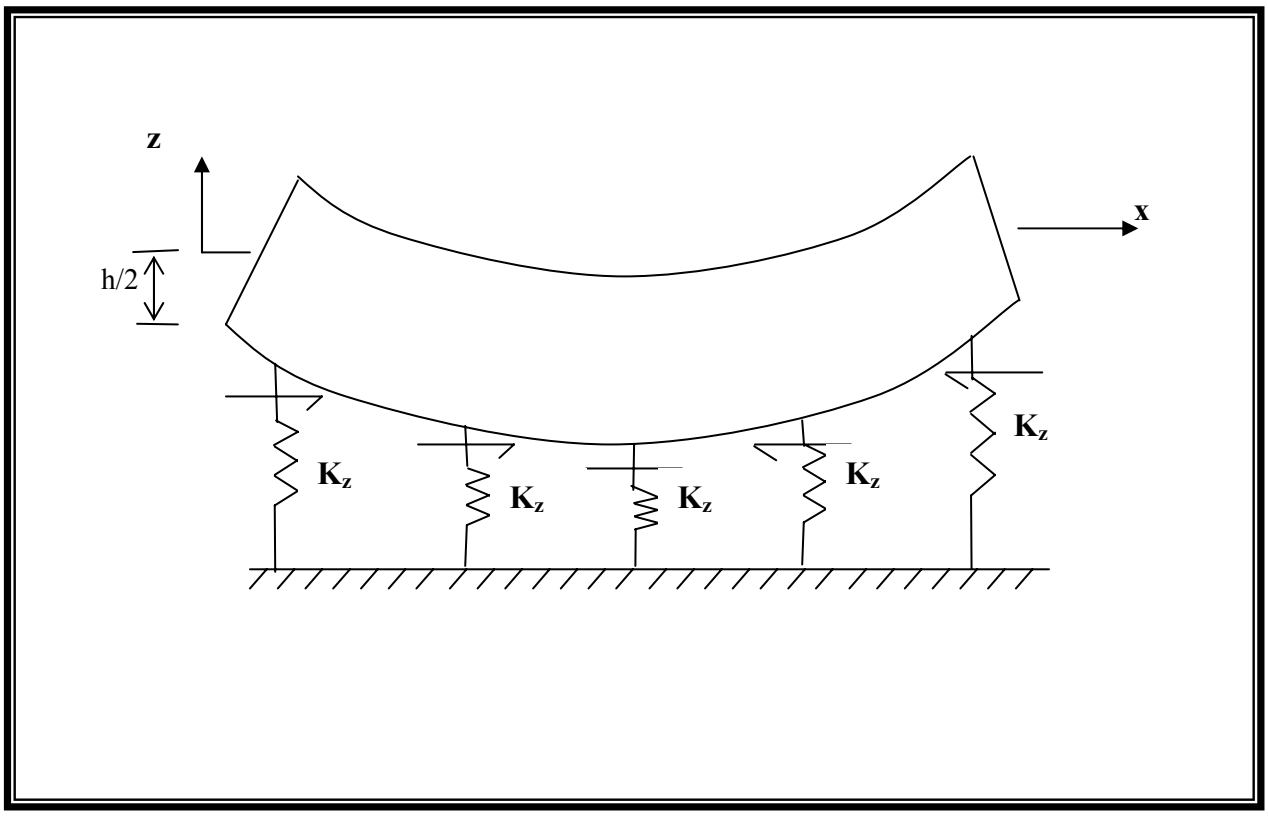

Figure (3.9): Coulomb Friction Model .[6]

3.3.8.2.3 Constant Frictional Model

When plates are resting on cohesive soils ($\phi = 0$), the soil will adhere to the bottom faces and the friction will be constant and equal to the cohesion of the soil. Thus,

$$F_x = C_x\{\xi\} \qquad \text{.....(3.55)}$$

$$F_y = C_y\{\xi\} \qquad \text{.....(3.56)}$$

where C_x or C_y is the cohesion of soil in x and y-direction respectively and $\{\xi\}$ is local coordinate. This type of friction is not considered in the application of this study.

3.3.9 NonLinear Behavior of Soil

Before the development of electronic computers, it was not feasible to perform analysis of loads in soil masses for other than the assumed linear elastic soil behavior.

Now, due to the availability of high-speed computer and powerful numerical analytical techniques, it is possible to approximate nonlinear, elastic soil behavior in analysis. In order to perform non- linear analysis of soil, however, it is necessary to be able to describe the load-deflection behavior of the soil in quantitative terms and to develop techniques for incorporating this behavior in the analysis.

3.3.9.1 Soil Characterization

The stress-strain of any type of soil depends on a number of different factors including density, water content, structure, drainage condition, strain conditions (i.e. plane strain, triaxial), duration of loading, stress history and confining pressure [39].

In many cases it may be possible to take account of these factors by selecting soil specimens and testing condition which simulates the corresponding field conditions. When this can be done accurately, it would be expected that the strains resulting from given stress changes in laboratory would be representative for the same stress changes. Among many theories established for studying different materials properties, the following theories are widely used in studying soil characteristics especially stress-strain relation under different stress changes:

1.Classical linear elastic theory.

2.Plasticity theory.

3.Elasto-plastic theory.

4.Visco-elastic theory.

5.Nonlinear elasticity theory.

It is commonly found that the soil behavior over a wide range of stress is non-linear, inelastic, and dependent upon the magnitude of the confining pressures employed in the tests.

3.3.9.2 Modeling of Stress-Strain Curve of Soils

The stress-strain curve for all soils is non-linear except in a very narrow region near the origin[15]. In this section, two models can be used to model the stress-strain response of soils: -

1-Hyperbolic stress-strain model.

2-Polynomial model.

3.3.9.2.1 Hyperbolic Stress-Strain Model

In this model, the stress -strain curve could be represented by a hyperbolic curve. **Kondener** [31] proposed a hyperbolic equation of the form:

$$\sigma_1 - \sigma_3 = \frac{\epsilon}{a + b\,\epsilon} \qquad \text{... (3.57)}$$

where:

σ_1 and σ_3 are the major principal stresses.

ϵ is the axial strain, and

(***a***) and (***b***) are constants whose values may be determined experimentally.

The ultimate value of the principal stresses difference $(\sigma_1 - \sigma_3)_{ult.}$ can be obtained by taking the limit of Eq. (3.57) as $(\in)$ becomes very large, or

$$(\sigma_1 - \sigma_3)_{ult.} = \lim_{\in \to \infty} (\sigma_1 - \sigma_3) = \frac{1}{b} \qquad \text{... (3.58)}$$

Differentiating Eq. (3.58) with respect to the strain and evaluating the derivative at $(\in)$ equal to zero yields:

$$\left(\frac{d(\sigma_1 - \sigma_3)}{d \in} \right)_{\in=0} = \frac{1}{a} \qquad \text{…(3.59)}$$

Thus, both of these constants ***a*** and ***b*** have a visualized physical meaning, referring to Fig. (3.10), (***a***) is the reciprocal of the initial tangent modulus, ***Ei*** ,and **(*b*)** are the reciprocal of the asymptotic value of stress difference which the stress-strain curve approaches at infinite strain $(\sigma_1 - \sigma_3)_{ult.}$

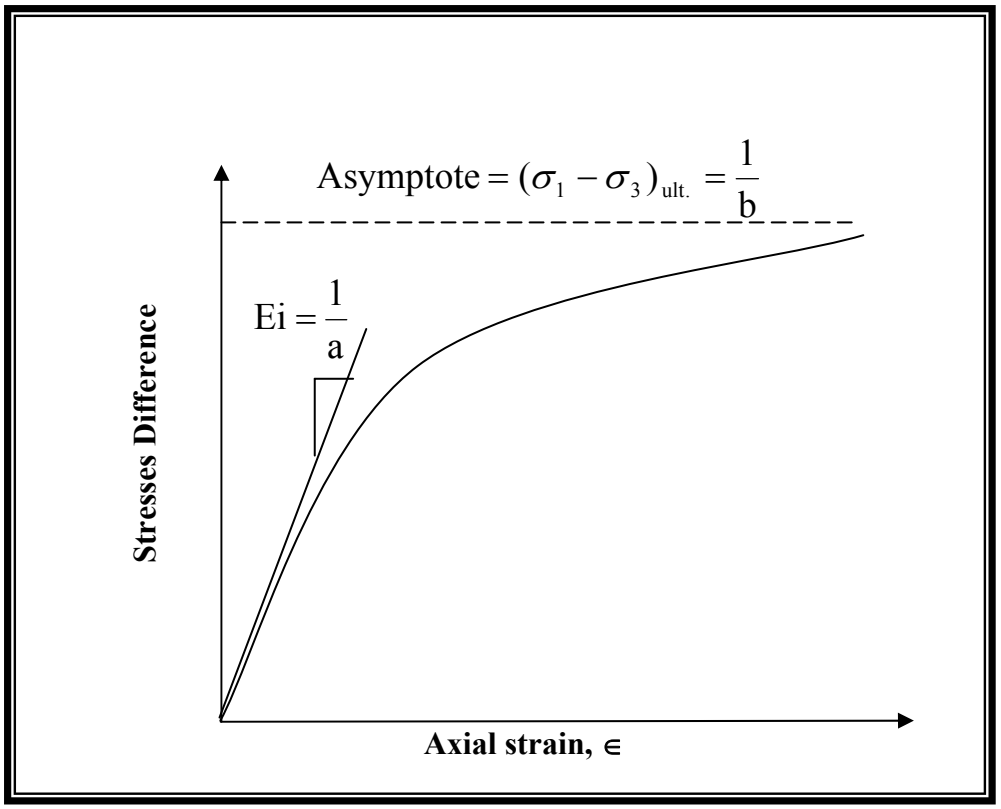

Figure (3.10): Proposed Hyperbolic Stress-Strain Curve of Soil .[31]

In order to develop a realistic model in soil mechanics, such a model must use a combination of:

1.Observations of the material behavior, and
2.Laboratory experiments that will measure the physical parameters needed to transfer the model into usable mathematical equations.

Since the behavior of the soil under compressive loading is nonlinear as verified by the results of plate-load test and considering the load-settlement curve a plate-load test in the field, the plate element resting on soil response can approximately be modeled using the two-constant hyperbolic stress-strain equation which now takes the following form:

$$\mathbf{P} = \frac{\delta}{\mathbf{a} + \mathbf{b}\delta} \qquad \ldots(3.60)$$

Eq.(3.60) was used firstly by **AL-Rubai**[7]**,** to represent the nonlinear behavior of the soil.

Fig. (3.11a) shows the hyperbolic load-settlement curve of plate-load test.

Differentiating Eq. (3.60) with respect to the settlement (δ) yields:

$$K_n = \frac{a}{(a + b\delta)^2} \qquad \ldots (3.61)$$

where:

P : is the lateral load on beam-column element which is concentrated at the node.

δ : is the lateral displacement of the node .

$\mathbf{K}_n$: is the normal subgrade reaction of soil.

(***a***) and (***b***) are the physical parameters required for the hyperbolic equation which can be obtained from the load-settlement curve of the plate-load test.

The value of the coefficients (***a***) and (***b***) may be determined most readily if the load-settlement data are plotted on transformed axes as shown in Fig. (3.11b) when Eq. (3.60) is written in the following form:

$$\frac{\delta}{p} = a + b\delta \qquad \ldots(3.62)$$

where, (a) and (b) are the intercept and the slope of the resulting straight line shown in Fig.(3.11 b), respectively.

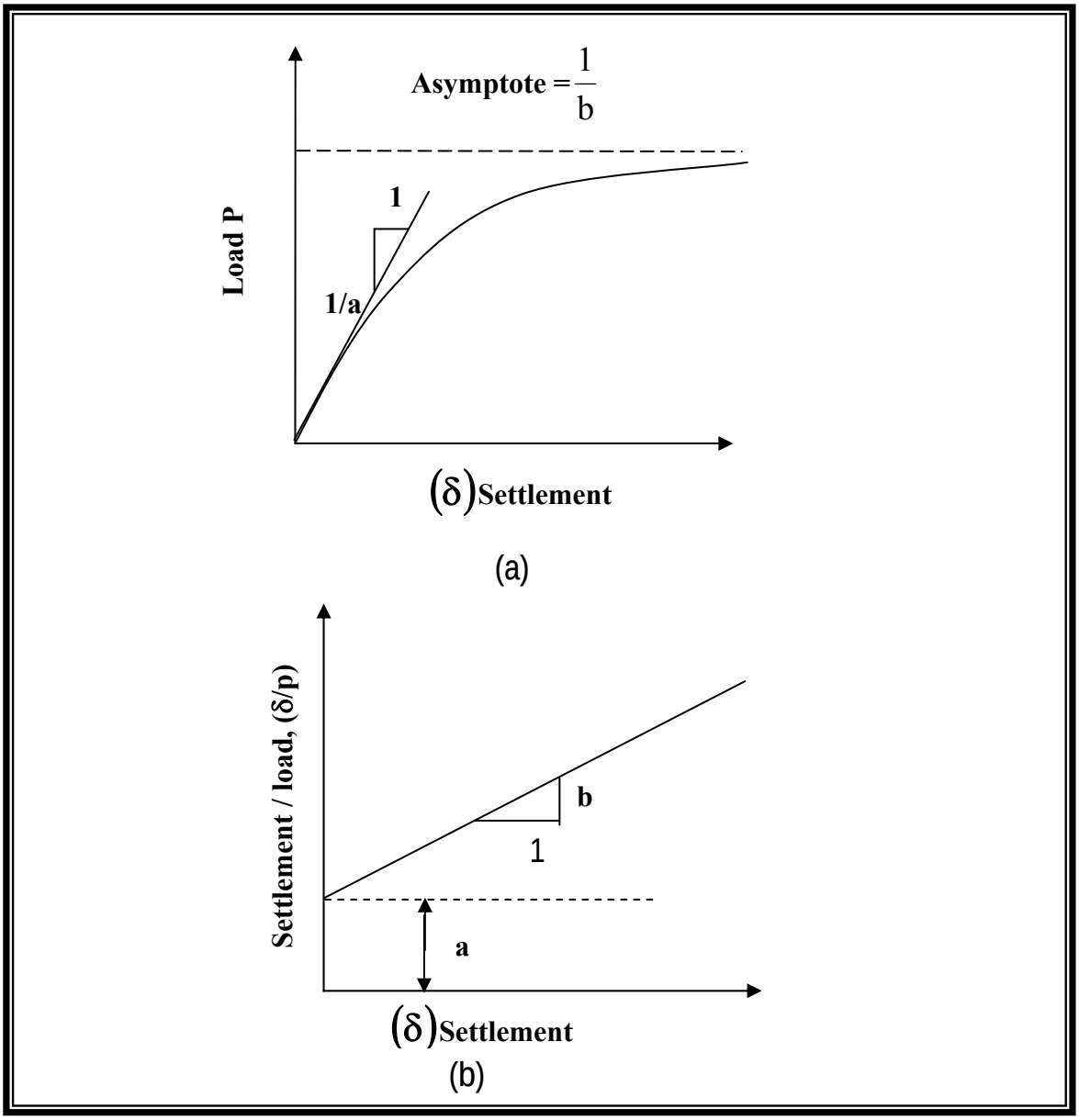

Figure (3.11): (a) Hyperbolic Load -Settlement Curve.
(b) Transformed Hyperbolic Load-Settlement Curve.[5]

3.3.9.2.2 Polynomial Model

In this model, the non linear behavior of the soil can be represented by a polynomial Equation which takes the following form:

$$P = a_0 + a_1\delta + a_2\delta^2 + a_3\delta^3 + a_4\delta^4 + ... \quad ... (3.63)$$

where

$\mathbf{a_0, a_1, a_2, a_3}$ and $\mathbf{a_4}$ are the coefficients required for the polynomial Equation.

The values of the coefficients $\mathbf{a_1, a_2, a_3 .....}$ may be determined by making curve fitting for the experimental load-settlement data.

Differentiating Eq. (3.63) with respect to settlement (δ) yields:

$$K_n = a_1 + 2a_2\delta + 3a_3\delta^2 + 4a_4\delta^3 + ... \quad ...(3.64)$$

where:

δ : is the lateral displacement of the node.

K_n : is the normal subgrade reaction of soil.

3.3.10 Elastic Foundation Models Adopted in This Work:

In this study, the elastic foundation is represented by linear elastic models and nonlinear elastic models. In linear elastic models the Winkler model is used for representing the compressional and frictional resistances of elastic foundation. In the nonlinear elastic model, the polynomail, Kondener models are used for representing compressional resistance and the Winkler model was used for representing the frictional resistance. Therefore, the stiffness matrix is:

$$[K]_f = \begin{bmatrix} [R_w] & 0 & 0 & 0 & 0 & 0 & 0 & 0 & 0 & . & 0 \\ 0 & [R_w] & 0 & 0 & 0 & 0 & 0 & 0 & 0 & . & 0 \\ 0 & 0 & [R_w] & 0 & 0 & 0 & 0 & 0 & 0 & . & 0 \\ 0 & 0 & 0 & [R_w] & 0 & 0 & 0 & 0 & 0 & . & 0 \\ 0 & 0 & 0 & 0 & [R_w] & 0 & 0 & 0 & 0 & . & 0 \\ 0 & 0 & 0 & 0 & 0 & [R_w] & 0 & 0 & 0 & . & 0 \\ 0 & 0 & 0 & 0 & 0 & 0 & [R_w] & 0 & 0 & . & 0 \\ 0 & 0 & 0 & 0 & 0 & 0 & 0 & [R_w] & 0 & . & 0 \\ 0 & 0 & 0 & 0 & 0 & 0 & 0 & 0 & 0 & . & 0 \\ . & . & . & . & . & . & . & . & . & . & . \\ 0 & 0 & 0 & 0 & 0 & 0 & 0 & 0 & 0 & 0 & 0 \end{bmatrix}_{20*20} \quad \text{.....(3.65)}$$

where:

$$[R_w] = \begin{bmatrix} K_{f1} & 0 & 0 \\ 0 & K_{f2} & 0 \\ 0 & 0 & K_{f3} \end{bmatrix} \quad \text{....(3.66)}$$

The stiffness of foundation distributed on the node of element is like the distribution of pressure load on the bottom surface of the element (ζ=-1), thus at node k

$$K_{f1} = \int_{-1}^{+1}\int_{-1}^{+1} k_x.N(\xi,\eta,-1).|J(\xi,\eta,\zeta)|.d\xi.d\eta \quad \text{....(3.67)}$$

$$K_{f2} = \int_{-1}^{+1}\int_{-1}^{+1} k_y.N(\xi,\eta,-1).|J(\xi,\eta,\zeta)|.d\xi.d\eta \quad \text{....(3.68)}$$

$$K_{f2} = \int_{-1}^{+1}\int_{-1}^{+1} k_z.N(\xi,\eta,-1).|J(\xi,\eta,\zeta)|.d\xi.d\eta \quad \text{....(3.69)}$$

where k_x, k_y, and k_z are the subgrade coefficients in the local coordinate x,y, and z, $N^k(\xi,\eta)$ is the shape function at node k and $|\boldsymbol{J(\xi,\eta,\zeta)}|$ is the determinate of Jacobian matrix.

The total stiffness of curved beam on elastic foundation will be:

$$[K]_{tcbf} = [K]^e + [K]_f \qquad \ldots.(3.70)$$

3.4 Numerical Integration

The element stiffness matrix in equation (3.39)can not be solved analytically. An alternative technique of numerical integration is required.

There are a number of techniques available for numerically evaluation of integrals. Usually the Gauss-Legendre quadrature numerical integration technique is ysed to perform the integration required to set up the stiffness matrix.

For three-dimensional situation, the enquired integral of equation (3.39) can be expressed as[9]:

$$I = \int_{-1}^{+1}\int_{-1}^{+1}\int_{-1}^{+1} F(\xi,\eta,\zeta)\,d\xi\,d\eta\,d\zeta \qquad \ldots.(3.71)$$

which may be rewritten numerically as:

$$I = \sum_{i=1}^{ni}\sum_{j=1}^{nj}\sum_{k=1}^{nk} Wi.Wj.Wk\,F(\xi_i,\eta_j,\zeta_k) \qquad \ldots.(3.72)$$

where ***ni, nj, nk*** are the number of Gaussian points in the ξ_i,η_j,ζ_k direction respectively. The function $F(\xi_i,\eta_j,\zeta_k)$ represents the matrix multiplication ($[B]^T.[D].[B].det\,[J]$) at sampling points ξ_i,η_j,ζ_k.

In a similar manner, the integral of the stiffness matrix of the embedded reinforcement can be written as:

$$I = \sum_{i=1}^{ni} Wi\,F(\xi_i) \qquad \ldots.(3.73)$$

It is necessary to choose a suitable integration rule that is both accurate the computationally efficient since a large amount of computational time is required for three-dimensional finite element problems when compared with two-dimensional problems. Several types of integration rules can be used such as the eight (2 *x* 2 *x* 2), and the twenty-seven (3 *x* 3 *x* 3), Gaussian rules are used to integrate the stiffness matrix of eight-node linear and twenty-node quadratic brick element respectively. Also, there is the fifteen-node Gauss type integration rule that evaluates the integration for the twenty-node quadratic brick element [Irons (1971)].

The integration rules, which exist in this program, are the 27 (3 *x* 3 *x* 3) Gauss quadrature, 15A, 15B and 14 points type integration rule. The weights and abscissa of the sampling points are listed in Appendix (A) .The relative distribution of the Gaussion points over the element is given in Fig. (3.12).

In the present study, 15 Gauss points are used for the numerical integration, because the reduced integration rules were found to be accurate and computationally efficient than other types of integration rules.[16]

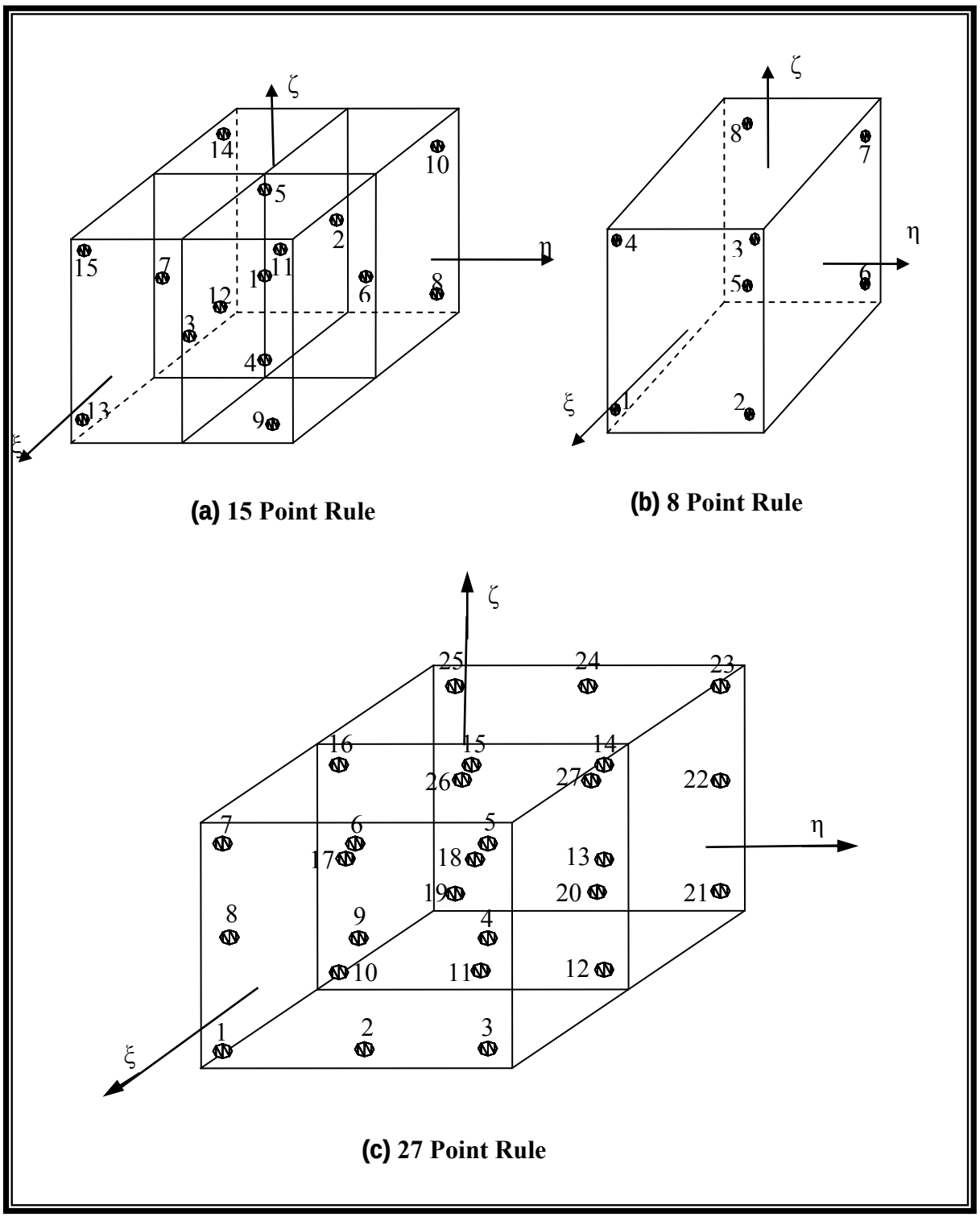

Figure (3.12): Distribution of Sampling Points over the Element in 8,15 and 27- Gaussian Point Integration Rules.[9]

3.5 Nonlinear Solution Technique

The load-deformation response of concrete exhibits a nonlinear behavior. This behavior may be attributed to material nonlinearity, geometric nonlinearity, or combination of the two categories. While no structure is free from material nonlinearity, the geometrical nonlinearity is related to the large deformations. In many finite element applications to reinforced concrete members, the geometrical nonlinearity is neglected as a result of the early onset of the material nonlinearities.

The material nonlinear behavior, including sudden changes in the element due to cracking and crushing of concrete and yielding of reinforcement, represents the main source of nonlinearity.

For the solution of a nonlinear structural problem, the state of equilibrium of the structural system corresponding to the applied load must be satisfied. In finite element terms these equilibrium equations can be written as:

$$\{P(a)\} - \{f\} = 0 \qquad \text{.....(3.74)}$$

where:

$\{a\}$ is the vector of nodal displacement.

$\{f\}$ is the vector of externally applied nodal loads.

$\{P(a)\}$ is the internal nodal loads vector given by:

$$\{P(a)\} = \int_v [B]^T . \{\sigma\} . dv \qquad \text{.....(3.75)}$$

The equilibrium equation will not be exactly satisfied and a system of residual forces $\{r(a)\}$ will exist such that:

$$\{r(a)\} = \{P(a)\} - \{F\} \neq \{0\} \qquad \text{.....(3.76)}$$

The solution of nonlinear problems by a finite element method usually attempted by one of the three basic solution techniques:

a. Incremental or stepwise procedures.
b. Iterative or Newton methods.
c. Step-iterative or mixed procedure.

3.5.1 Incremental Procedure

The basic of the incremental or stepwise procedure is the subdivision of the load into many small partial load or increments. Usually these load increments are of equal magnitude, but in general they need not to be equal. The load is applied one increment at a time, and during the application of each increment the equations are assumed to be linear, as shown in Figure (3.13).

Essentially, the incremental procedure approximates the nonlinear problem as a series of linear problems, that is the nonlinearity is treated as piecewise linear. Because the purely incremental techniques do not account for the redistribution of forces during the application of loading increments, they suffer from a progressive and uncorrected tendency to drift from the true equilibrium path.

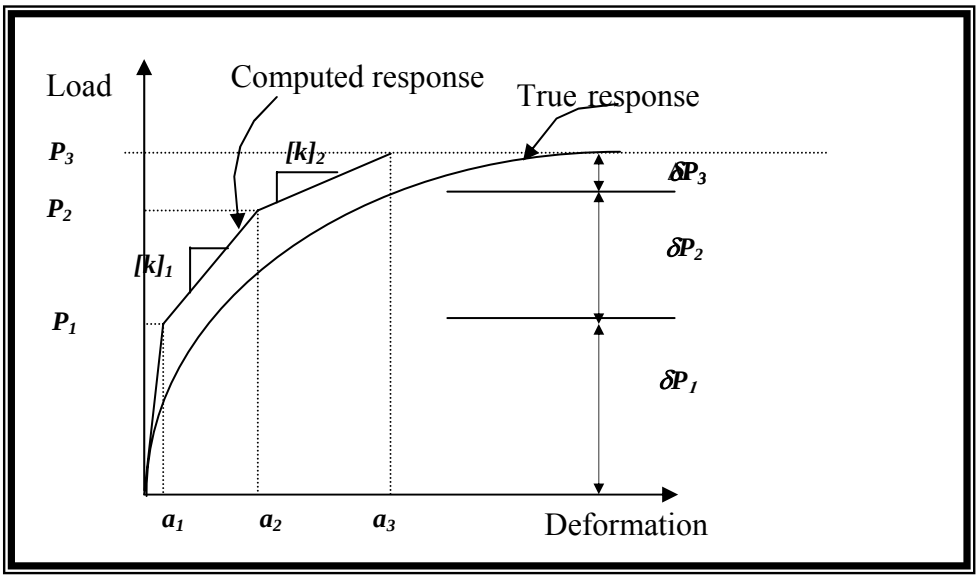

Figure (3.13): Linear Incremental Method.[9]

3.5.2 Iterative Procedure

The iterative procedure is a sequence of calculations in which the body or structure is fully loaded in a single increment. Essentially, the iterative procedure consists of successive correction to the solution until equilibrium under the total is satisfied, as shown in Figure (3.14).

This type of technique is not suitable for tracing the entire nonlinear equilibrium path because it fails to produce information about the intermediate stage of loading.

There are several types of iteration procedures, some of them are:

- Conventional Newton-Raphson method.
- Modified Newton-Raphson method.
- Combined (conventional and modified) Newton-Raphson method.

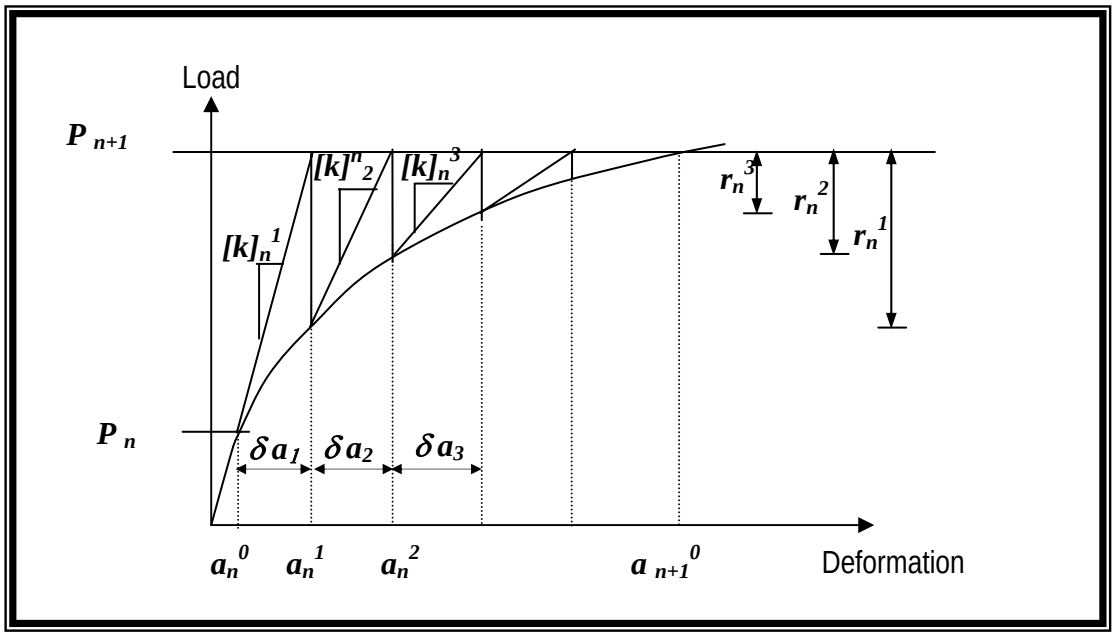

Figure (3.14): Conventional Newton-Raphson Method.[9]

3.5.3 Mixed Procedure

In this type of technique, Fig. (3.15), the load is applied as a series of increments, and at each increment, iterative solution is carried out to find the truest response of the structure. The conventional, modified and combined Newton-Raphson methods may also be used in the iteration process within each step. These methods are briefly discussed in the following sections.

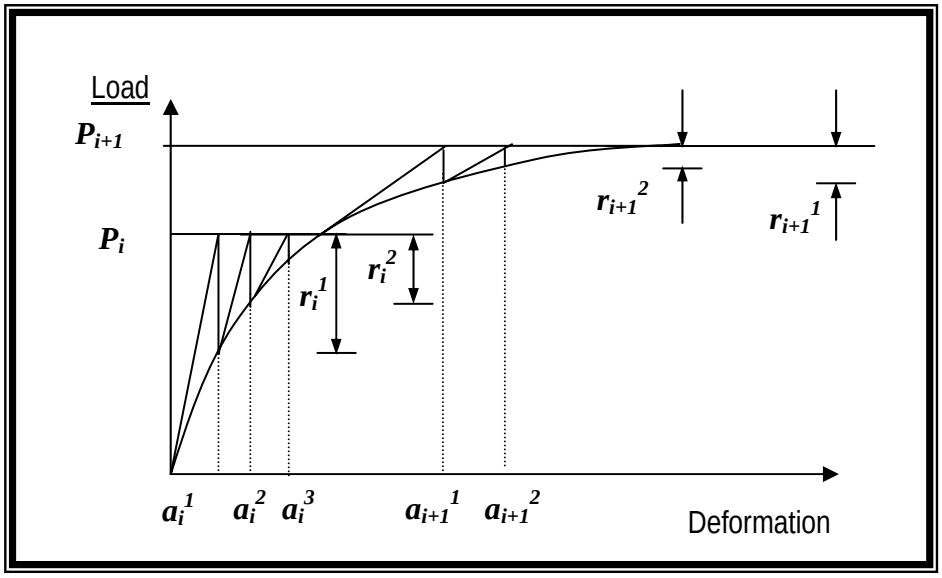

Figure (3.15): Incremental-Iterative Technique.[9]

3.5.3.1 Conventional Newton - Raphson Method

The conventional Newton-Raphson method, Fig. (3.16), is one of the earliest known methods used in solving nonlinear problems. For simplicity, a single degree of freedom system is considered with a load level $\{P\}_0$, with the assumption that the corresponding deformed configuration of the system which may be denoted symbolically by $\{a\}_0$ is known. Then, to determine a new configuration, $\{a\}_1$, corresponding to a load level $\{p\}_1$ where:

$$\{\mathrm{P}\}_1 = \{\mathrm{P}\}_0 + \{\Delta\mathrm{P}\}_1 \qquad \ldots(5.1)$$

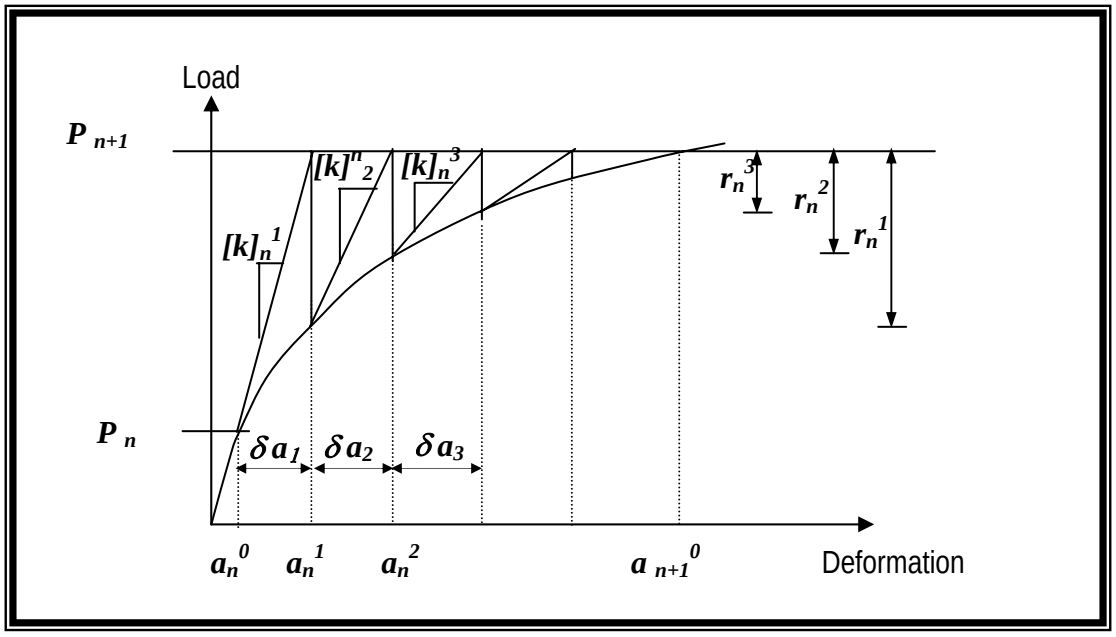

Figure (3.16): Conventional Newton-Raphson Method .[9]

Where $\{\delta \mathrm{P}\}_1$ is the additional applied load is obtained by using a linearized analysis, where the change in configuration $\{\delta a\}_1$ is first computed from:

$$\{\delta \mathrm{P}\}_1 = [\mathrm{k}]_0 \{\delta a\}_1 \qquad \ldots(5.2)$$

In which the tangent stiffness matrix $[k]_0$ is evaluated at the beginning of the load interval, i.e. the load level $\{P\}_0$. The term $\{a\}_1 = \{a\}_0 + \{\delta a\}_1$ represents an approximate configuration which is then corrected by updating new tangent stiffness matrix from the approximate configuration $\{a\}_1$. The internal forces $\{\mathrm{f}\}_1$ corresponding to this configuration can be determined as:

$$\{\mathrm{f}\}_1 = [\mathrm{k}]_1 \{\mathrm{a}\}_1 \qquad \ldots(5.3)$$

Generally for any level of iteration (j):

$$\{\mathrm{a}\}_\mathrm{j} = \{\mathrm{a}\}_{\mathrm{j-1}} + \sum_{\mathrm{m=1}}^{\mathrm{n}} \{\delta a\}_m \qquad \ldots(5.4)$$

where:

$\{a\}_j$ is the vector of displacement after the iteration. Then, the out of balance force vector $\{r\}_j$ can be obtained from:

$$\{r\}_j = \{P\}_f - \{f\}_j \quad \ldots(5.5)$$

The unbalanced joint forces are then treated as load increments and the correction vector $\{\delta a\}_{j+1}$ is then obtained from the incremental relationship:

$$[k]_j \{\delta a\}_{j+1} = \{r\}_j \quad \ldots(5.6)$$

A new approximate configuration is then computed by making use of Eq. (5.6). The process continues until the latest correction vector is sufficiently small.

The conventional Newton-Raphson method requires that the tangent stiffness matrix is to be updated and a new system of equations is solved for each iteration. This is expensive if the problem to be solved is too large. Accordingly various modifications have been proposed.

3.5.3.2 Modified Newton -Raphson Method

In this method, Figure (3.17), the stiffness matrix is updated only once for each increment of loading. As compared with the conventional Newton-Raphson method, the modified Newton-Raphson method is more economical. However, this method requires more steps for convergence, but each step is done quickly by avoiding time consuming repetitions of forming the tangent stiffness matrix. This method is used in the present study.

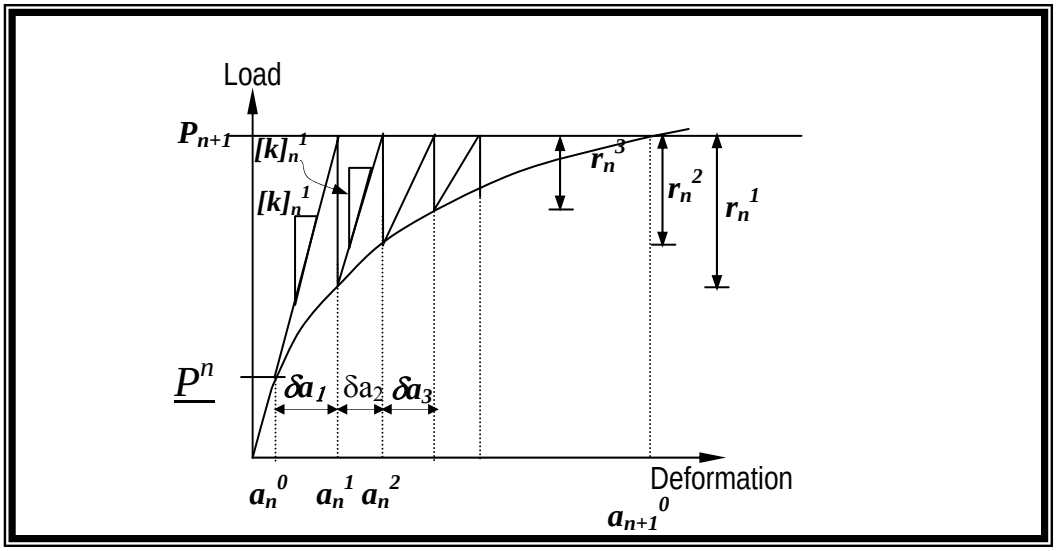

Figure (3.17): Modified Newton-Raphson Method.[9]

3.5.3.3 Combined Newton - Raphson Method

This method, Fig. (3.18), is a modification of the conventional Newton-Raphson method. It involves updating the stiffness matrix after remaining constant for a certain number of iterations. The stiffness matrix can be recalculated at:

The beginning of first iteration of each increment.

- Beginning of second iteration.
- First, eleventh, twenty first, … stiffness matrices over each load increment.
- Second, twelfth, twenty second, … stiffness matrices over each load increment.

The disadvantage of this method is represented in the fact that the convergence is slower than that of the conventional Newton-Raphson method

and requires a great number of iterations to achieve the solution within each load increment.

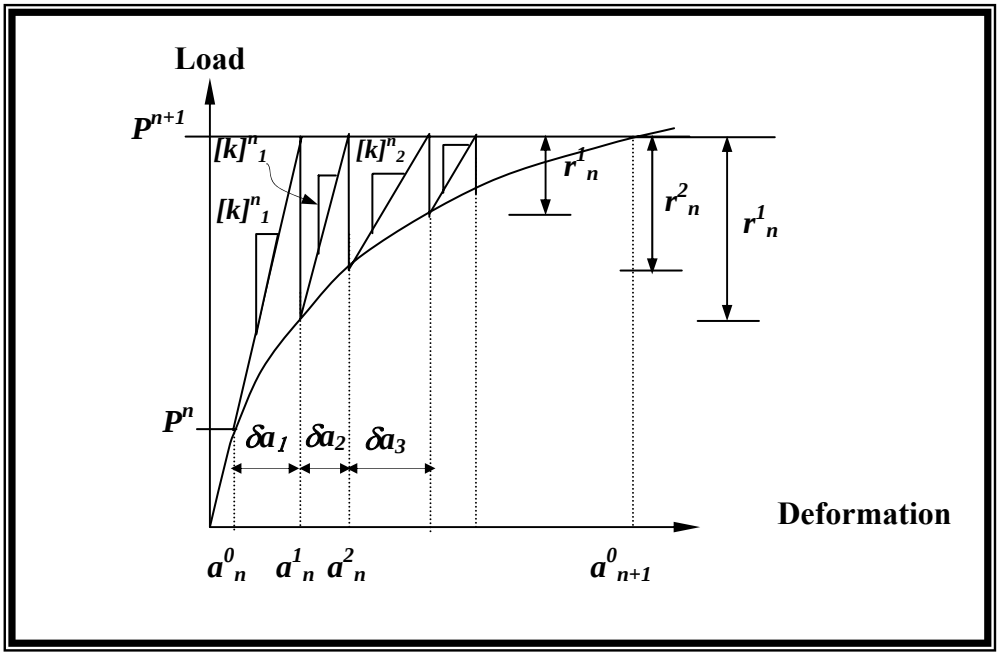

Figure (3.18): Combined Newton-Raphson Method.[9]

3.6 Convergence Criterion

A termination criterion for the iterative process should be used to stop iteration when a sufficient accuracy is achieved, i.e, when no further iterations are necessary. The different useful criteria are the displacement, the force and the work done criteria. Only the force criterion is adopted in the present study. This criterion depends on comparing the internal force vector $\{f\}$ and the applied load vector $\{P\}$. In other words, seeking a vector called "unbalanced force vector" to be small within a prescribed tolerance. The convergence is assumed to occur when the inequality:

$$\left[\frac{\sum_{i=1}^{n}\left(\{P\}_i-\{f\}_i\right)^2}{\sum\left(\{P\}i\right)^2}\right]^{0.5} \le \text{tol.} \qquad \ldots(5.7)$$

is satisfied.

3.7 Analysis Termination Criterion

The nonlinear finite element analysis must be provided with a criterion to detect failure of the solution. In the physical test under load control, the collapse of a structure takes place when no further loading can be sustained. This is usually indicated in the numerical tests by successively increasing iterative displacements and continuous growth in the dissipated energy. Hence, convergence of the iterative procedure can not be achieved and therefore, it is necessary to specify a suitable criterion to terminate the analysis and save wasting computation efforts.

In the present study, the nonlinear analysis is terminated when the stiffness matrix is no longer positive definite, a steel bar has fractured, or excessive concrete crushing at sampling points has taken place.

3.8 Outline of Computer Program

The computer program ***3DCBEFA*** (three-dimensional curved beam on elastic foundation analysis) has been used in the present study. This program is a modified version to the program ***P3DNFEA*** (three-dimensional nonlinear finite element analysis). This latter program was developed by Al-Shaarbaf (Al-Shaarbaf 1990). The program is coded in ***FORTRAN 77*** language. The main objective of the present program ***3DCBEFA*** is to analyze reinforced concrete members resting on soil and subjected to three-dimensional static loading up to failure.

In the present study, the ***Fortran PowerStation 4.0*** compiler produced by Microsoft incorporation was used to operate the program under PC Pentium III with Intel MMX 900 MHZ processor and 128 MB RAM.

CHAPTER FOUR

MODELING Of MATERIAL PROPERTIES

4.1 General

One of the pieces of basic information required in any three-dimensional nonlinear finite element analysis of reinforced concrete structures is the material constitutive model, which describes the current multi-dimensional stress-strain relations governing the behavior of the structure. Since the concrete and the reinforcing steel have very different material properties, the behavior of the composite, reinforced concrete, is usually simulated by considering the constitutive relations of the constituents independently. Full interaction between the two materials has been assumed to exist throughout the present work. This chapter outlines the constitutive models for the concrete and steel used in the present study.

Due to its complex behavior the concrete constitutive model is given special emphasis. The observed behavior of concrete under different loading conditions is outlined in section (4-2). Section(4-3) describes the different components required to model the concrete. A plasticity model for concrete in compression and a smeared crack model for concrete in tension have been adopted in the current study. These models are illustrated in section(4-4) .The model used for the reinforcing steel is presented in section(4-5) .

4.2 The Observed Behavior of Concrete

Concrete is a material with a grossly heterogeneous internal structure . It consists of inert aggregate particles embedded within a binding paste made from particles of cement and water each concrete hardens as a result of chemical reactions between the cement and water to form a solid and durable structural

material. Due to the incomplete hydration, hardening concrete usually contains capillary pores filled with air or water. The presence of capillary pores, internal flaws in the aggregate and bond micro-cracks at interfaces between the cement paste and the aggregate prior to any load application can be viewed as a source of weakness in the structure of concrete[9]. Many of these micro-cracks are caused by segregation, shrinkage and thermal movements in the mortar[19]. The gradual growth of these micro-cracks with further loading contributes to the nonlinear behavior of concrete.

Concrete can behave as either a linear or a nonlinear material depending on the nature and the level of the applied stresses. Stiffness and strength properties of concrete subjected to multiaxial lading conditions differ from those displayed under uniaxial compression. Under a low level of stresses, linear elastic behavior is observed, while concrete exhibits a highly nonlinear response at higher stress level. Many experimental studies of the behavior of concrete under uniaxial and multiaxial loading conditions have been performed.[9]

In the following sections, the responses of concrete under uniaxial and multiaxial loading states are briefly described.

4.2.1 Uniaxial Behavior of Concrete

A typical uniaxial compression stress-strain curve is shown in Fig.(4.1). Up to a stress level of about 30 percent of its uniaxial compressive strength, f_c', concrete behaves as a linear elastic material . This stress level is termed the point of onset of the localized cracking and has been proposed as a limit of elasticity at stresses between $0.3\, f_c'$ - $0.5\, f_c'$; the bond cracks start to extend due to stress concentration at the crack tips and the stress-strain curve starts to show a slight non-linearity in this range of loading. When the stress exceeds $0.5\, f_c'$ some cracks at nearby aggregate surfaces start to bridge in the form of mortar cracks with other cracks continuing to grow slowly. A gradual increase in the curvature

of the stress-strain curve occurs up to about 0.75 f_c'. For compression stresses above this value, the rate of crack propagation increases rapidly and the stress-strain curve bends sharply until the peak stress level is reached. Beyond the peak stress, concrete exhibits a strain-softening response characterized by the descending portion of the curve. This falling part of the stress-strain curve is mainly dependent on testing machine properties .

The initial modulus of elasticity of concrete highly depends on the compressive strength in lieu of actual test data. The initial modulus of elasticity, E, can be calculated approximately from the following empirical formula (ACI Code 318-77):

$$E=33w_c^{1.5} f_c'^{0.5} \qquad \text{.....(4.1)}$$

where w_c is the concrete unit weight in pound per cubic foot and E and f_c' are expressed in pound per square inch.

The poisson's ratio, ν, of concrete has been observed to remain approximately constant and ranges from about 0.15 to 0.22 up to a stress level of 80 percent of f_c' . beyond this level; poisson's ratio increases rapidly and values in excess of 1.0 have been measured by **Darwin**, **Pecknold**, **Maekawa** and **Okamura**.

Under tensile stress, the strength of concrete, f_t, is approximately a tenth of the compressive strength. A typical tensile stress-strain curve is shown in Fig.(4.2). Up to a stress level of 60 percent of f_t the curve is linearly elastic. Beyond this level, the bond micro-cracks starts to grow and the non-linearity of the curve starts to increase as the stress level increases until the peak stress is reached . Following this level, a post softening regime is observed . The elastic modulus in uniaxial tension is slightly greater than in uniaxial compression,

while the poisson's ratio in tension is somewhat smaller than that in compression.

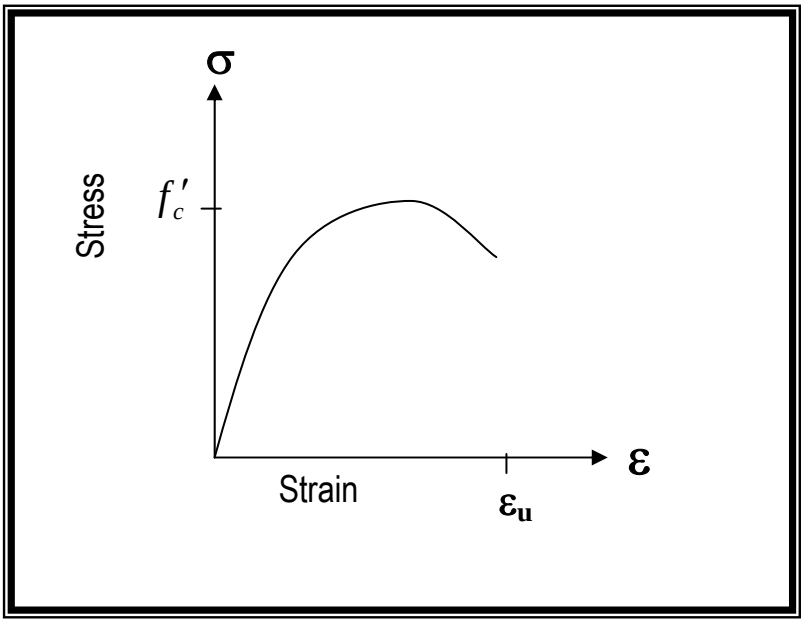

Figure (4.1): Typical Uniaxial Stress-Strain Curve for Concrete in Compression.[9]

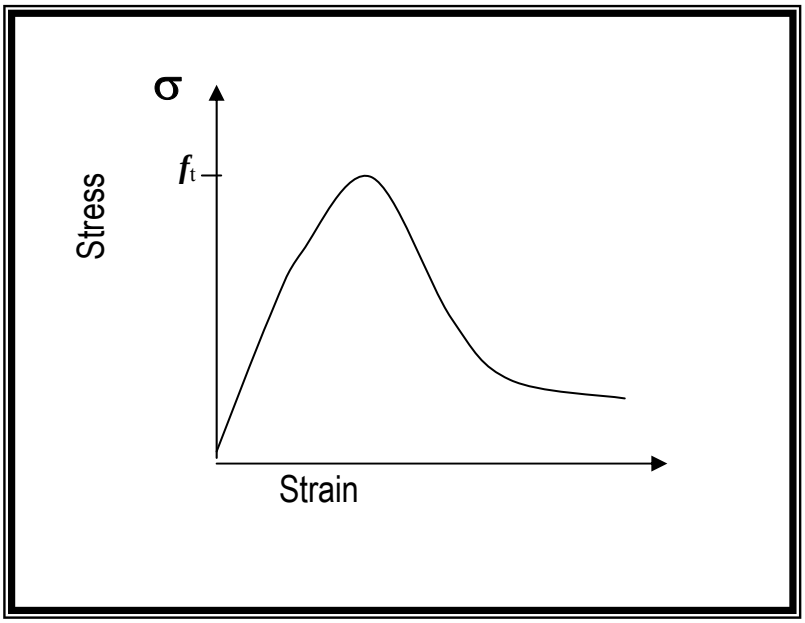

Figure (4.2): Typical Uniaxial Stress-Strain Curve for Concrete in tension. .[9]

4.2.2 Multiaxial Behavior of Concrete

The behavior of concrete under multi-axial stress condition is very complex if it is compared with that under uniaxial stress condition and has not yet been assessed experimentally in a complete manner. Various material models with considerable simplifying assumption have been proposed in literature. A typical biaxial strength envelope is shown in Fig.(4.3) .

It was seen that the maximum compressive strength increases for biaxial compression state. A maximum strength increase of approximately 25 percent is achieved at a stress ratio of (σ_1 / σ_2 =0.5) , and this is reduced to about 16 percent at an equal biaxial compressive state (σ_1 / σ_2 =1). Under biaxial compression-tension state of stress, the compressive strength decreases almost linearly as the applied tensile stress in increased[19]. Under biaxial tension, the strength is almost the same as that of uniaxial tensile strength when subjected to triaxial compressive stresses, concrete exhibits strength, which increases with the increase of confining pressure[9].

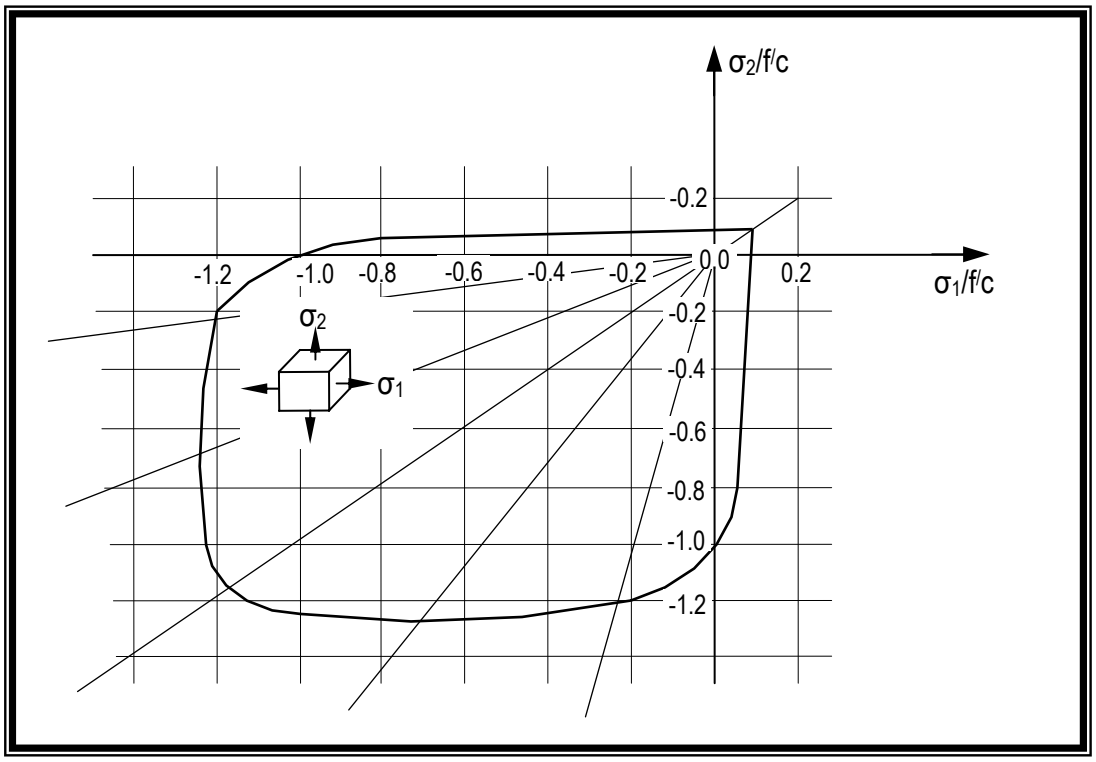

Figure (4.3): Biaxial Strength of Concrete.[9]

Experiments indicate that concrete in triaxial stresses has a fairly consistent failure surface which is a function of the three principal stresses, Fig. (4.4). This failure surface can be represented by three-stress invariants. These invariants are the first invariant of the stress tensor (I), the second and the third invariant of the stress deviatoric tensor (J2) and (J3)[19].

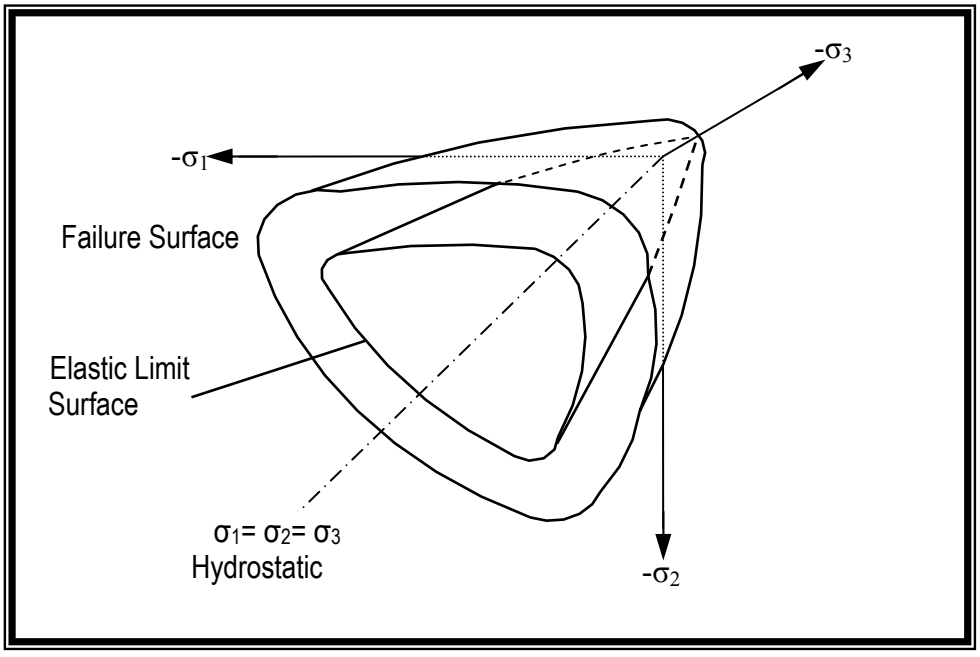

Figure(4.4): Triaxial Strength Envelope of Concrete .[19]

4.3 Numerical Modeling of Concrete Properties

Reinforced concrete is one of the composite material having complex behavior, especially after cracking. The modeling of all the aspects of its behavior is extremely difficult yet it is one of the most important aspects of any realistic analysis.

Some numerical models of concrete are summarized here with some of the failure theories and criteria that have been employed.

4.3.1 Constitutive Relationships

Mathematical description of the mechanical properties of concrete is established by the constitutive equations. Several approaches have been proposed to model the observed stress-strain relationships under multiaxial stress state. These approaches can be classified into: Elasticity-based models, Plasticity-based models, and Endochronic models. Detailed discussion of these approaches is given in references [8,18]. In the following sections, the basic concepts and the limitations of these approaches will be briefly discussed.

4.3.1.1 Linear and Nonlinear Elasticity Models

These models are based on elasticity theory to represent the behavior of concrete under general types of loading. Linear elastic models have been used[8] in case where the cracking behavior is the most important factor of nonlinearity.

In general, two different approaches are employed in the formulation of nonlinear elastic models. These are the total (secant) and the incremental (tangent) formulations. In the total (secant) stress-strain models, the current state of stress is assumed to be uniquely determined as a function of the current state of strain. This type of formulation is path-independent which is not true for concrete in general. Therefore, the range of application of such models is only suitable for monotonic or proportional loading regimes. The total stress-strain models have been utilized in describing the nonlinear deformation behavior of concrete under biaxial and triaxial compressive stresses, mainly because of its simplicity.

The incremental stress-strain models are used to describe the behavior of materials in which the state of stress depends on the current state of strain and the stress path followed to reach that state. Due to path-dependent behavior,

incremental models provide more realistic description of concrete behavior under general loading conditions (non-monotonic and non-proportional loading regimes) than the total stress-strain formulation.

4.3.1.2 Perfect and Strain Hardening Plasticity Models

Nonlinear deformations of concrete under compressive stress are basically inelastic since upon unloading only a portion of the total strain can be recovered. Therefore, the stress-strain behavior of concrete materials may be separated into recoverable and irrecoverable components. The recoverable behavior is treated within the framework of elasticity theory, while the irrecoverable part is based on the theory of plasticity.

In triaxial compression regimes, concrete behaves as a ductile material on the yield of failure surface before reaching its crushing strain. To account for this plastic flow, various plasticity formulations are adopted as an elastic-perfectly material (perfect plasticity), or as an elastic-plastic-hardening (strain-hardening plasticity) behavior of concrete up to the ultimate strength.

In the perfect plastic model, the complete stress-strain relationship consists of three parts: before yielding, during plastic flow, and after fracture (failure). Concrete behavior before yielding is assumed to be elastic until the combined state of the stress reaches the yield surface. During plastic flow, the plastic stress-strain relations describe the behavior of concrete. Post fracture behavior is governed by the constitutive relations of fractured concrete (crushing under compressive stress state). After crushing, the concrete is assumed to lose its resistance completely against further deformations and the current stresses state drops suddenly to zero.

The formulation of the constitutive relations for a strain hardening plastic material is based on three fundamental assumptions. These assumptions are: shape of an initial yield surface, formulation of a suitable hardening rule that

describes the evolution of subsequent loading surfaces, and formulation of an appropriate flow rule that specifies the stress-strain relation in the plastic range.

The initial yield surface is required to mark the stress level at the onset of plastic deformations. The evaluation of subsequent loading surface during plastic deformation is described by specifying an appropriate hardening rule. Three types of hardening rules are frequently used in strain-hardening plasticity models. These are : isotropic, kinematic, and mixed hardening rule. In an isotropic hardening model, the initial yield surface is assumed to expand uniformly without distortion as plastic flow occurs. The kinematic hardening rule assumes that during plastic flow the loading surface translates as a rigid body in the stress space, maintaining the size and shape of the initial yield surface. In the mixed hardening rule, the loading surface experiences both translation and uniform expansion in all directions.

4.3.1.3 Endochronic Theory Models

The endochronic theory of viscoplasticilty was originally proposed by Valanis and has been applied to predict the mechanical response of metals under complex strain histories. Unlike the elasticity and plasticity models, the endochronic formulation is incremental nonlinear. The basic concept underlying the theory is that of intrinsic time. Intrinsic time is a non-decreasing scalar variable that depends on the increments of strains as well as time. The major difference of the endochronic theory from the plasticity, incremental and total elastic strain theory, is that it is incrementally nonlinear.

4.3.2 Modeling of Concrete Fracture

Generally, concrete fracture may be either a compression fracture (i.e. crushing of concrete) or a tension fracture (i.e. cracking of concrete).

The crushing failure occurs when the material can resist no further compressive loading while the tension failure of concrete is characterized by a gradual growth of cracks that join together and eventually disconnect larger parts of the structure. It is a usual assumption that formation of cracks is a brittle process and that the strength in the tension-loading direction abruptly goes to zero after such cracks have formed, Fig. (4.5a). But when reinforcement bars bridge the concrete cracks, the strength mechanism becomes more complex and the carrying strength of concrete between cracks can be safely exploited[19].

4.3.3 Methods of Crack Representation

In general, the models, which have been developed to represent cracking in connection with the finite element analysis of reinforced concrete members, are composed of three basic components, a criterion for crack initiation, a method of crack representation and a method for cracking propagation.

Two fracture criteria are commonly used, the maximum principal stress criterion and the maximum principal strain criteria. When a principal stress or strain exceeds its limiting value a crack is assumed to occur in a plane normal to the direction of the offending principal stress or strain, Figure (4.5b).

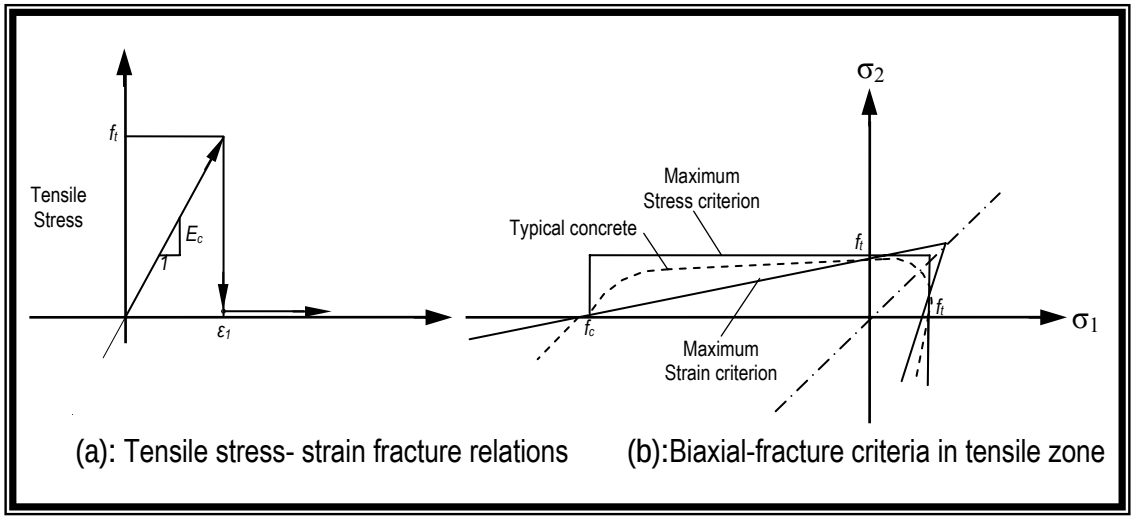

Figure (4.5): Cracking of Concrete .[19]

In finite element analysis of concrete structures, two approaches have been employed for crack modeling, these are the smeared cracking and the discrete cracking models. The particular cracking model to be selected depends upon the purpose of the analysis. If overall load-deflection behavior is desired, without regard to completely realistic crack patterns and local stresses, the smeared crack model is probably the best choice, while if detailed local behavior is of interest, adoption of the discrete cracking model is useful. The two approaches will be discussed in the following sections.

4.3.3.1 Smeared Cracking Model

In this approach, the cracked concrete is assumed to remain a continuum, i.e., the cracks are smeared out in a continuous fashion. It is assumed that the concrete becomes orthotropic or transversely isotropic after the first cracking has occurred, one of the material axis being oriented along the direction of cracking. In the smeared cracking model, a crack is not discrete but implies an infinite number of parallel fissures across that part of the finite element as shown in Figure (4.6).[12,19]

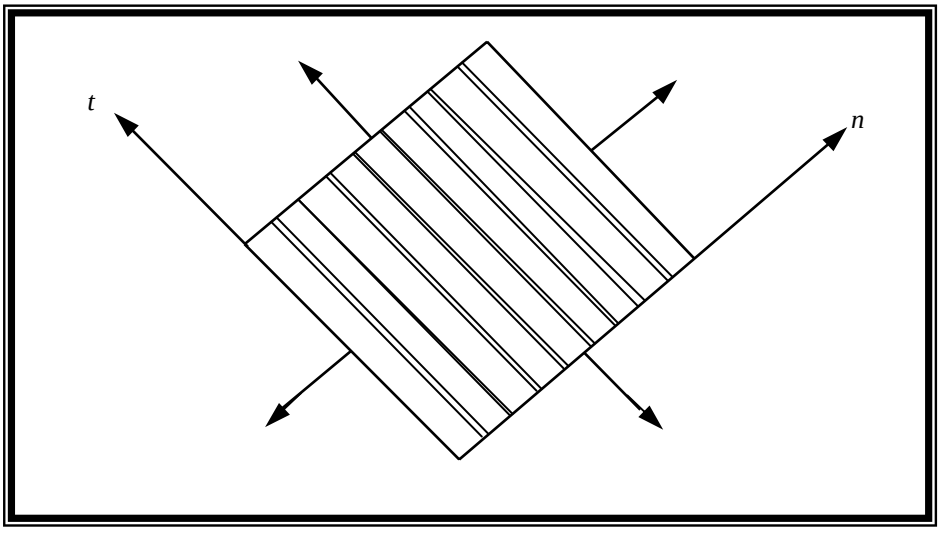

Figure (4.6): Smeared Cracked Model.[19]

Two different models are used for defining the crack direction. The first is the fixed orthogonal crack. In this approach, the direction of the crack is fixed normal to the direction of the first principal tensile stress that exceeds the cracking stress. By fixing the direction of the cracks, the subsequent rotation of the principal stress is ignored. The second model is the rotating or swinging crack model. In this approach, the crack direction is assumed to be normal to the principal tensile strain direction when the tensile strains reaches a specified limiting value. With further loading and changing of the principal strain direction, the crack is assumed to rotate and the orthotropic material axes are set in the new crack direction.

4.3.3.2 Discrete Cracking Model

An alternative to the continuous smeared cracking model is the introduction of discrete crack model. This is normally done by disconnecting the displacement at nodal points for adjoining elements as shown in Fig. (4.7). One obvious difficulty in such an approach is that the location and orientation of the cracks are not known in advance. Thus, geometrical restriction imposed by the reselected finite element mesh can hardly be avoided. This can be rectified to some extent by redefinition of element nodes. Such techniques are unfortunately extremely complex and time consuming[9]. In the present study, the smeared fixed-crack model has been adopted.

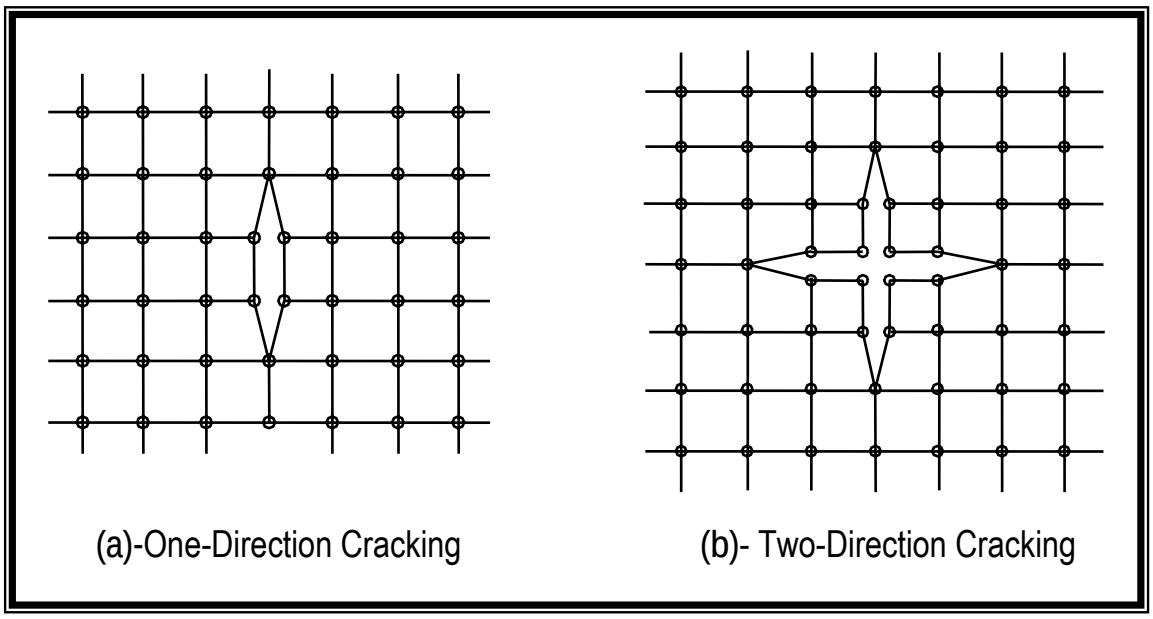

Figure (4.7): Discrete Crack Model.[19]

4.3.4 Post Cracking Behavior

In the plain and reinforced concrete structures, cracking is not a perfectly brittle phenomenon and experimental evidence shows that the tensile stresses normal to a cracking plane are gradually released as the crack width increases. This type of response is usually modeled in the finite element analysis by using either the tension stiffening or the strain softening concepts. For reinforced concrete structures where the behavior is characterized by the formation of closely spaced cracks, the first concept seems to be more suitable than the latter. The latter is found to be useful for analyzing plain concrete structures where the behavior is governed by the formation of a single micro crack or a few dominant cracks[19].

In the case where reinforcement exists, the nature of the stress release is further complicated by the restraining effect of the reinforcing steel. After cracking, the concrete stresses drop to zero and the steel carries the full load. The concrete between cracks, however, still carries some tensile stresses. This tensile stress drops as the load increases and the drop is associated primarily with bond deterioration between steel and concrete. This ability of concrete to

share the tensile load with the reinforcement is termed as ***tension stiffening*** phenomenon[19].

The tension stiffening effect of concrete has been studied in finite element analysis by using two procedures. First, the tension portion of the concrete stress-strain curve has been given a descending branch. Descending branches of many different shapes have been employed, linear, bilinear and curved shapes. The second is to increase the steel stiffness. The additional stress in the steel represents the total tensile force carried by both the steel and the concrete between the cracks[19].

4.3.5 Shear Transfer Across the Cracks

Several mechanisms exist by which shear is transferred across reinforced concrete sections. Among these mechanisms are the shear stiffness of uncracked portion of concrete, aggregate interlock in the crack surface (or interface shear transfer), dowel in the reinforcement bars action and the combined effect of tension in reinforcement and arching action.

For the shear transfer across the cracked concrete planes crossed by reinforcement, the two major mechanisms are the dowel action and the aggregate interlock. Shear transfer by these two mechanisms is accompanied by slippage or relative movement of crack faces. In the dowel action, shear forces are partially resisted by the stiffness of reinforcing bars because slippage imposes bearing forces of opposite direction on the bars. The aggregate inter-lock mechanism is of frictional nature. Slippage causes the irregular faces of the crack to separate slightly. Tensile stresses created in the steel bars by the separation of crack faces in turn develop same shear resistance[9] .

4.4 Concrete Models Adopted in The Analysis :

In this study, a plasticity-based present model is adopted for the nonlinear analysis of three-dimensional reinforced concrete structures under static loads. In compression, the behavior of concrete is simulated by an elastic-plastic work hardening model followed by a perfectly plastic response, which is terminated at the onset of crushing. The plasticity model in compression state of stress has the following characteristics[9]:

1. yield criterion
2. hardening rule
3. flow rule
4. crushing condition

In tension, linear elastic behavior prior to cracking is assumed. A smeared crack model with fixed orthogonal cracks is adopted to represent the fractured concrete. The model will be described in terms of the following:

1. cracking criterion
2. post-cracking formulation
3. shear retention model

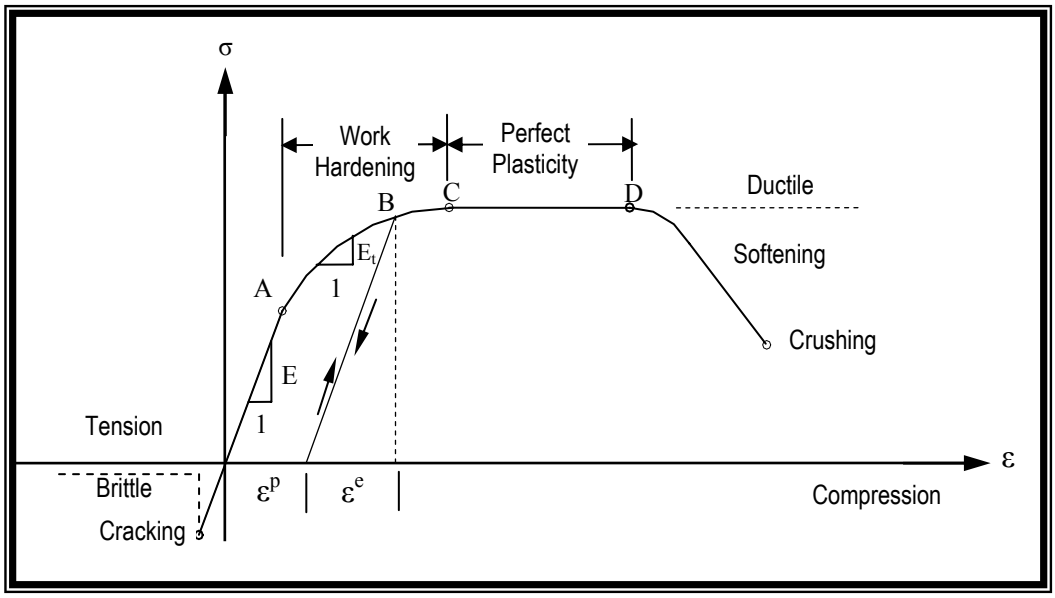

Figure (4.8): Uniaxial Stress-Strain Curve, Pre-and Post -Failure Regime.[19]

4.4.1 Modeling of Concrete in Compression:

4.4.1.1 The Yield Criterion :

Under a triaxial state of stress, the yield criterion for concrete is generally assumed to be dependent on three stress invariants. However, a yield criterion dependent on two stress invariants only has been proved to be adequate for most practical situations. The yield criterion incorporated in the present model is of such type and it has been successfully used in research. It can be expressed as[9]:

$$f(\sigma) = f(I_1, J_2) = \sqrt{(\alpha I_1 + 3\beta J_2)} = \sigma_\circ \qquad \ldots(4.2)$$

where (α) and (β) are material parameters, (I_1) is the first stress invariant given by:

$$I_1 = \sigma_x + \sigma_y + \sigma_z \qquad \ldots(4.3)$$

J_2 is the second deviatoric stress invariant given by:

$$J_2 = \frac{1}{3}\{(\sigma_x^2 + \sigma_y^2 + \sigma_z^2) - (\sigma_x\sigma_y + \sigma_y\sigma_z + \sigma_z\sigma_x)\} + \tau_{xy}^2 + \tau_{yz}^2 + \tau_{xz}^2 \quad \ldots(4.4)$$

and $\sigma_\circ \geq 0$ is the equivalent effective stress at the onset of plastic deformation, this $\sigma_\circ$ can be determined from the uniaxial compression test as:

$$\sigma_\circ = C_p \,.\, f'_c \quad \ldots(4.5)$$

where C_p is the plasticity coefficient,which has a variable between 0 and 1, this coefficient is used to mark the initiation of the plastic deformation.

The parameters (α) and (β) are determined by using the uniaxial and biaxial compression tests. Then for a uniaxial compression state, the yield stress is given by:

$$\sigma_x = -\sigma_\circ \quad \ldots(4.6)$$

and for the equal biaxial compression state, the yield stress is given by:

$$\sigma_x = \sigma_y = -\gamma\sigma_\circ \quad \ldots(4.7)$$

If the results obtained by **Kupfe**r for the failure envelope is employed for initial yield, the value of the constant (γ) is equal to (1.16). From Eq. (4.2) through Eq. (4.7), the material constants can be found to be:

$$\alpha = 0.35468\sigma_\circ \quad \text{and} \quad \beta = 1.35468 \quad \ldots(4.8)$$

writing $C = \frac{\alpha}{(2\sigma_\circ)} = 0.17734$

Therefore Eq. (4.2) can be written as:

$$f(\sigma) = (2C\sigma_\circ I_1 + 3\beta J_2)^{1/2} = \sigma_\circ \qquad \ldots(4.9)$$

this can be solved for $\sigma_\circ$ as:

$$f(\sigma) = C.I_1 + \{(C.I_1)^2 + 3\beta J_2\}^{1/2} = \sigma_\circ \qquad \ldots(4.10)$$

4.4.1.2 The Hardening Rule

The concept of plastic flow in work-hardening materials extends to the notion of perfectly plastic solids for which the yield or failure surface remains fixed in stress space. The hardening rule defines the motion of the subsequent loading surfaces during plastic loading. A number of hardening rules has been proposed to describe the growth of subsequent loading surface for work-hardening materials. Some of these rules are isotropic hardening, kinematic hardening and mixed hardening. The isotropic model applies mainly to proportional loading. For cyclic and reversed types of loading, the kinematic hardening rule is more appropriate. Combinations of isotropic and kinematic hardening are called mixed hardening rules[19].

An isotropic hardening rule is used in the present study. Therefore, from Eq. (4.10), the subsequent loading surface may be expressed as[9]:

$$f(\sigma) = \sqrt{C.I_1 + \{(C - I_1)^2 + 3\beta J_2\}} = \bar{\sigma} \qquad \ldots(4.11)$$

where $\bar{\sigma}$ represents the stress level at which further plastic deformation will occur and this is termed as the effective stress or equivalent uniaxial stress.

The incremental theory of plasticity implies a relationship between the effective stress and the effective plastic strain. The effective plastic strain increment $\delta\varepsilon_p$ that results from an incremental plastic work dw_p, may be determined by using the work-hardening hypothesis as:

$$\delta\varepsilon_P = \frac{d\, w_p}{\bar{\sigma}} = \frac{\{\sigma\} d\,\{\varepsilon_p\}}{\bar{\sigma}} \qquad \ldots(4.12)$$

where $d\varepsilon_p$ represents the effective accumulated plastic strain increment, along the strain path.

The effective plastic strain can be written as:

$$\varepsilon_p = \int d\varepsilon_p \qquad \ldots(4.13)$$

In the present model, a parabolic stress-strain curve is used for the equivalent uniaxial stress-strain relationship beyond the limit of elasticity, $(C_p\, f'_c)$. This relationship represents the work-hardening stage of behavior. When the peak compressive stress is reached, a perfectly plastic response is assumed to occur. Figure (4.1) shows the equivalent uniaxial stress-strain curve in the various stages of behavior. These are given by:

(a) During the elastic stage, when $\bar{\sigma} \le C_p . f'_c$

$$\bar{\sigma} = E . \varepsilon_c \qquad \ldots(4.14)$$

(b) After the initial yielding and up to the ultimate concrete compressive strength, when:- $C_p\ f'_c \le \bar{\sigma} \le f'_c$

$$\bar{\sigma} = C_p\, f'_c + E[\varepsilon_c - \frac{C_p.f'_c}{E}] - [\frac{E}{2\varepsilon_o}][\varepsilon_c - \frac{C_p f'_c}{E}]^2 \qquad \ldots(4.15)$$

c) for $\varepsilon_c \geq (2 - C_p) f'c / E$

$$\bar{\sigma} = f'c \qquad \ldots(4.16)$$

Where $\bar{\varepsilon_o}$ represents the total strain corresponding to the parabolic part of the curve that can be calculated from:

$$\bar{\varepsilon_o} = \frac{2(1 - C_p)}{E} f'c \qquad \ldots(4.17)$$

A value of ***0.3*** is assumed for the plasticity coefficient ***(Cp)*** in the present study and hence plastic yielding begins at a stress level equals to ***(0.3 f′c).***

The total effective strain ε_c is composed of two parts, elastic and plastic components:

$$\varepsilon_c = \varepsilon_e + \varepsilon_p \qquad \ldots(4.18)$$

The elastic strain ε_p is given by:

$$\varepsilon_e = \frac{\bar{\sigma}}{E} \qquad \ldots(4.19)$$

By substituting Eq. (4.18) and Eq. (4.19) into Eq. (4.15), the effective stress- plastic strain relation can be expressed as:

$$\bar{\sigma} = C_p\, f'c - E\, \varepsilon_p + (2E^2.\varepsilon_o \varepsilon_p)^{1/2} \qquad \ldots(4.20)$$

Differentiation of Eq. (4.20) with respect to the plastic strain leads to the slope of the tangent of the effective stress-plastic strain curve, which represents the hardening coefficient, H, that is needed in the formulation of the incremental stress-strain relation:

$$H' = \frac{d\,\bar{\sigma}}{d_{\varepsilon p}} = E\left(\sqrt{\frac{\varepsilon_0}{2\varepsilon_p} - 1}\right) \qquad \ldots(4.21)$$

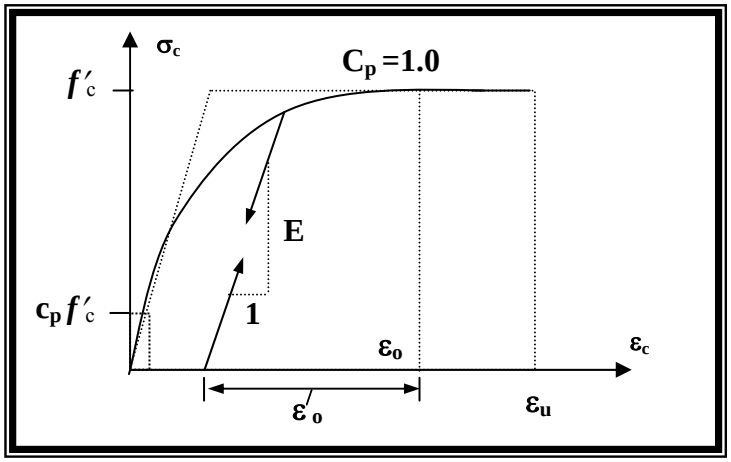

Figure (4.9): Uniaxial Stress-Strain Curve for Concrete.[9]

4.4.1.3 The Flow Rule

To construction the stress-strain relation in the plasticity range, the normality of the plastic strain increment vector to the yield surface is commonly employed as a flow rule (associated flow rule). The normality condition of the plastic strain vector, $d\{\varepsilon_p\}$, to the yield surface. F($\{\sigma\}$), can be expressed mathematically in the following form:

$$d(\varepsilon_p) = d\lambda \ \frac{\partial f(\sigma)}{\partial \sigma} \qquad \ldots(4.22)$$

The normal to the current loading surface $\frac{\partial f(\sigma)}{\partial \sigma}$ is termed as the flow vector. The yield function derivatives with respect to the stress component define the flow vector **{a}** as:

$$\{a\} = \left[\frac{\partial f}{\partial \sigma_x}, \frac{\partial f}{\partial \sigma_y}, \frac{\partial f}{\partial \sigma_z}, \frac{\partial f}{\partial \tau_{xy}}, \frac{\partial f}{\partial \tau_{yz}}, \frac{\partial f}{\partial \tau_{zx}} \right]^T \quad \ldots(4.23)$$

These derivatives are given in Appendix (B):

4.4.1.4 Incremental Stress-Strain Relationship:

During the plastic loading, both of the initial yield and the subsequent stress states must satisfy the yield condition. $\boldsymbol{F(\sigma, K) = 0}$. The yield function defined in Eq. (4.15), can be rewritten as,

$$F(\sigma, K) = f(\sigma) + f(k) = 0 \quad \ldots(4.24)$$

where k, is the hardening parameter, which governs the expansion of the yield-surface. By differentiating Eq. (4.24), then

$$dF = \frac{\partial F}{\partial \sigma} d\sigma + \frac{\partial F}{\partial K} dK = 0 \quad \ldots(4.25)$$

or

$$a^T d\sigma - A\, d\lambda = 0 \quad \ldots(4.26)$$

where

$$A = -\frac{1}{d\lambda} \frac{\partial F}{\partial k} dk \quad \ldots(4.27)$$

The total incremental strain vector can be rewritten as:

$$d\{\varepsilon)\} = d\{\varepsilon^e\} + d\,\lambda \frac{\partial F}{\partial \sigma} \qquad \ldots(4.28)$$

The elastic strain increment is related to the stress increment by the elastic constitutive relation which is given in:

$$d\,\{\sigma\} = [D]d\,\{\varepsilon_e\} \qquad \ldots(4.29)$$

where [D] is the elastic constitutive matrix given by

$$[D] = \frac{E}{(1+\nu)(1-2\nu)} \begin{bmatrix} 1-\nu & \nu & \nu & 0 & 0 & 0 \\ \nu & 1-\nu & \nu & 0 & 0 & 0 \\ \nu & \nu & 1-\nu & 0 & 0 & 0 \\ 0 & 0 & 0 & (1-2\nu)/2 & 0 & 0 \\ 0 & 0 & 0 & 0 & (1-2\nu)/2 & 0 \\ 0 & 0 & 0 & 0 & 0 & (1-2\nu)/2 \end{bmatrix} \qquad \ldots(4.30)$$

substitution of Eq. (4.29) into Eq. (4.28) yields

$$d\,\varepsilon = [D]^{-1}\, d\sigma + d\lambda\{a\} \qquad \ldots(4.31)$$

Pre-multiplying both sides of Eq. (4.31) by $\{a\}^T [D]$ and eliminating of $a^T . d\sigma$ by making use of Eq. (4.26), the following expression for the plastic multiplier $d\lambda$ is obtained,

$$d\,\lambda = \left[\frac{\{a\}^T [D]}{H' + \{a\}^T [D]\{a\}} \right] d\{\varepsilon\} \qquad \ldots(4.32)$$

By substituting Eq. (4.32), into Eq. (4.28), and pre-multiplying both sides by [D], the complete elastic incremental stress-strain relationship can be expressed as:

$$d\{\sigma\} = \left[[D] - \frac{[D]\{a\}\{a\}^T [D]}{H' + \{a\}^T [D]\{a\}} \right] d\{\varepsilon\} \quad \ldots(4.33)$$

where the second term in the brackets represents the stiffness degradation due to the plastic deformation.

4.4.1.5 The Crushing Condition:

The crushing type of concrete fracture is a strain controlled phenomenon. The lack of available experimental data on concrete ultimate deformation capacity under multiaxial stress states has resulted in the appropriate strain criterion being developed by simply covering the yield criterion described in terms of stresses directly into strain.

Thus,

$$c.I_1 + \{(c.I_1) + 3.\beta.J_2\}^{\frac{1}{2}} = \varepsilon_{cu} \quad \ldots(4.34)$$

where, I_1, is the first strain invariant, J_2, is the second deviatoric strain and, ε_{cu}, is the ultimate strain value that can be extrapolated from the uniaxial compression test. When, ε_{cu}, reaches the value specified as the ultimate strain, the material is assumed to lose all its characteristics of strength and rigidity.

4.4.2 Modeling of Concrete in Tension

The maximum tensile stress criterion is used in this research work to monitor cracking. For a previously uncracked sampling point, if the principal stress σ_1 exceeds the limiting value of tensile stress, a crack is assumed to form. The limiting tensile stress required to define the onset of cracking can be calculated

for states of triaxial tensile stress and for combination of tension and compression principal stresses as follows[12]:

a) For triaxial tension zone $(\sigma_1 \geq \sigma_2 \geq \sigma_3 \geq 0)$

$$\sigma_i = \sigma_{cu} = f_t \qquad i = 1,2,3 \qquad \ldots(4.35)$$

b) For the tension-tension-compression zone $(\sigma_1 \geq \sigma_2 \geq 0, \sigma_3 \leq 0)$

$$\sigma_i = \sigma_{cr} = f_t\left[1 + \frac{0.75\,\sigma_3}{f'_c}\right] \qquad i = 1,2 \qquad \ldots(4.36)$$

c) For the tension-compression-compression zone $(\sigma_1 \rangle 0, \sigma_3 \leq \sigma_2 \leq 0)$

$$\sigma_1 = \sigma_{cr} = f_t\left[1 + \frac{0.75\,\sigma_2}{f'_c}\right]\left[1 + \frac{0.75\,\sigma_3}{f'_c}\right] \qquad \ldots(4.37)$$

where σ_{cr} is the cracking stress and both f_t and f'_c are given positive values, equation (4.36) incorporates the fact that compression in one direction favors the cracking in the others and thus reduces the tensile capacity of the material.

When the major principal stress σ_1 violates the cracking criterion, planes of failure develop perpendicular to its direction. Concrete behavior is no longer isotropic; it becomes orthotropic with the direction of orthotropy coinciding with the direction of σ_1. Therefore, the normal and shear stresses across the plane of failure and the corresponding normal and shear stiffness are reduced, and the concrete is assumed to be transversely isotropic with axes of isotropy being perpendicular to the direction of σ_1 . Thus, the incremental stress-strain relationship in the local axes can be expressed as:

$$\begin{Bmatrix} \Delta\sigma_1 \\ \Delta\sigma_2 \\ \Delta\sigma_3 \\ \Delta\tau_{12} \\ \Delta\tau_{23} \\ \Delta\tau_{31} \end{Bmatrix} = \begin{bmatrix} E_1 & 0 & 0 & 0 & 0 & 0 \\ 0 & E/\left(1-\nu^2\right) & \nu E/\left(1-\nu^2\right) & 0 & 0 & 0 \\ 0 & \nu E/\left(1-\nu^2\right) & E/\left(1-\nu^2\right) & 0 & 0 & 0 \\ 0 & 0 & 0 & \beta_1 G & 0 & 0 \\ 0 & 0 & 0 & 0 & G & 0 \\ 0 & 0 & 0 & 0 & 0 & \beta_1 G \end{bmatrix} \begin{Bmatrix} \Delta\varepsilon_1 \\ \Delta\varepsilon_2 \\ \Delta\varepsilon_3 \\ \Delta\gamma_{12} \\ \Delta\gamma_{23} \\ \Delta\gamma_{31} \end{Bmatrix} \quad \ldots(4.38)$$

or in a condensed from:

$$\{\Delta\sigma\} = [D_{cr}]\{\Delta\varepsilon\} \quad \ldots(4.39)$$

Where E_1 is the reduced modulus of elasticity in the direction of σ_1, and $\beta_1 G$ is the reduced shear modulus across the failure plane.

$[D_{cr}]$ is the material stiffness in the local axes. The stress increments in the global axes (x, y, z) may be obtained by using the coordinate transformation matrix such that:

$$\{\Delta\sigma\} = [T]^T [D_{cr}][T]\{\Delta\varepsilon\} \quad \ldots (4.40)$$

where [T] is the transformation matrix expressed in terms of the direction cosines as:

$$[T] = \begin{bmatrix} l_1^2 & m_1^2 & n_1^2 & l_1 m_1 & m_1 n_1 & n_1 l_1 \\ l_2^2 & m_2^2 & n_2^2 & l_2 m_2 & m_1 n_1 & n_1 l_1 \\ l_3^2 & m_3^2 & n_3^2 & l_3 m_3 & m_1 n_1 & n_1 l_1 \\ 2l_1 l_2 & 2m_1 m_2 & 2n_1 n_2 & l_1 m_2 + l_2 m_1 & n_2 m_1 + n_1 m_2 & l_2 n_1 + l_1 n_2 \\ 2l_2 l_3 & 2m_2 m_3 & 2n_2 n_3 & l_2 m_3 + l_3 m_2 & n_3 m_2 + n_2 m_3 & l_3 n_2 + l_2 n_3 \\ 2l_3 l_1 & 2m_3 m_1 & 2n_3 n_1 & l_3 m_1 + l_1 m_3 & n_1 m_3 + n_3 m_1 & l_1 n_3 + l_3 n_1 \end{bmatrix} \quad \ldots (4.41)$$

where l_i, m_i and n_i represent the direction cosines of the local coordinate axes (x, y, z) direction respectively.

For the tension-tension-compression and the triaxial tension states of stress, the cracking criterion may be violated by the major principal stress σ_1, and the second principal stress σ_2, simultaneously. Thus, two sets of orthogonal cracked planes may develop and the constitutive matrix in the local material axes become diagonal:

$$[D]_{cr} = \begin{bmatrix} E_1 & 0 & 0 & 0 & 0 & 0 \\ 0 & E_2 & 0 & 0 & 0 & 0 \\ 0 & 0 & E_3 & 0 & 0 & 0 \\ 0 & 0 & 0 & \beta_1 G & 0 & 0 \\ 0 & 0 & 0 & 0 & \beta_2 G & 0 \\ 0 & 0 & 0 & 0 & 0 & \beta_1 G \end{bmatrix} \quad \ldots(4.42)$$

In the current model, a maximum of three sets of cracking is allowed to form at each sampling point.

4.4.2.2 Post-Cracking Models

4.4.2.2.1 Tension-Stiffening Model

The tensile stresses normal to the cracked planes are gradually released, and represented by an average stress-strain curve. In the present study such a relationship may be obtained by using the tension-stiffening model. This is specified by a linear descending stress-strain curve similar to that shown in Fig. (4.10) and this is given by[12]:

a) For $\varepsilon_{cr} \le \varepsilon_n \le \alpha_1 \varepsilon_{cr}$

$$\sigma_n = \alpha_2 \sigma_{cr} \left[\frac{\alpha_1 - \frac{\varepsilon_n}{\varepsilon_{cr}}}{\alpha_1 - 1.0} \right] \quad \ldots(4.43)$$

b) For $\varepsilon_n \rangle \alpha_1 \varepsilon_{cr}$

$$\sigma_n = 0.0 \qquad \ldots(4.44)$$

where σ_n and ε_n are the stress and strain normal to the cracked plane, ε_{cr} is the cracking strain associated with the cracking stress σ_{cr} and α_1, and α_2 are the tension-stiffening parameters. α_1 represents the rate of stress release as the crack widens, while α_2 represents the sudden loss of stress at the instant of cracking.

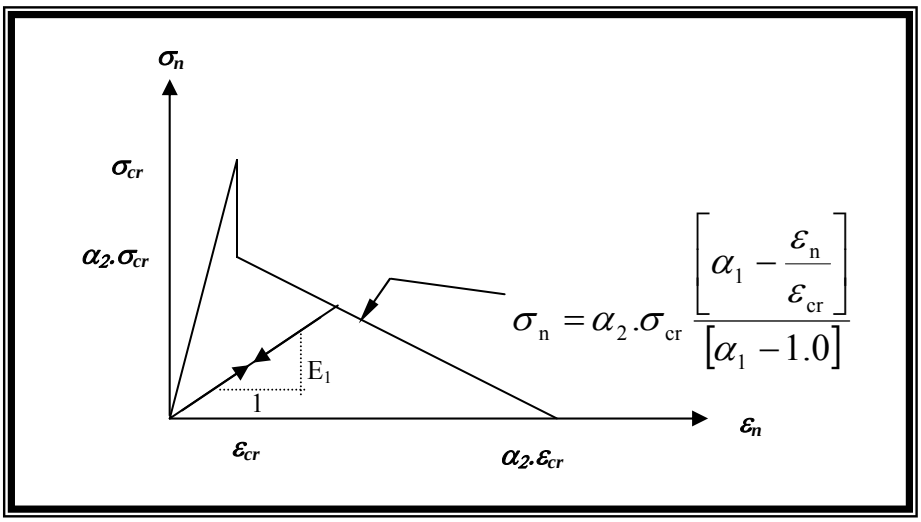

Figure (4.10): Post Cracking Model for Concrete.[9]

4.4.2.2.2 Shear Retention Model

At a cracked sampling point, the shear stiffness across the cracked plane becomes progressively smaller as the crack widens. A reduced shear modulus βG, has been used across the cracked plane. The value of β depends on the stage of loading and it is given by:

a) For $\varepsilon_n \leq \varepsilon_{cr}$

$$\beta = 1 \qquad \ldots(4.45)$$

b) For $\varepsilon_{cr} \le \varepsilon_n \le \gamma_1 \varepsilon_{cr}$

$$\beta = \frac{\gamma_2 - \gamma_3}{\gamma_1 - 1}\left[\gamma_1 - \frac{\varepsilon_n}{\varepsilon_{cr}}\right] + \gamma_3 \qquad \ldots(4.46)$$

c) For $\varepsilon_n \rangle \gamma_1 \varepsilon_{cr}$

$$\beta = \gamma_3 \qquad \ldots(4.47)$$

Figure (4.11) shows schematically the value of *(β)* for different stages. γ_1, γ_2, γ_3 are shear retention parameters. γ_1 represents the rate of decay of shear stiffness as the crack widens, γ_2 is the sudden loss in shear stiffness at the instant of cracking and γ_3 is the residual shear stiffness due to the dowel action.

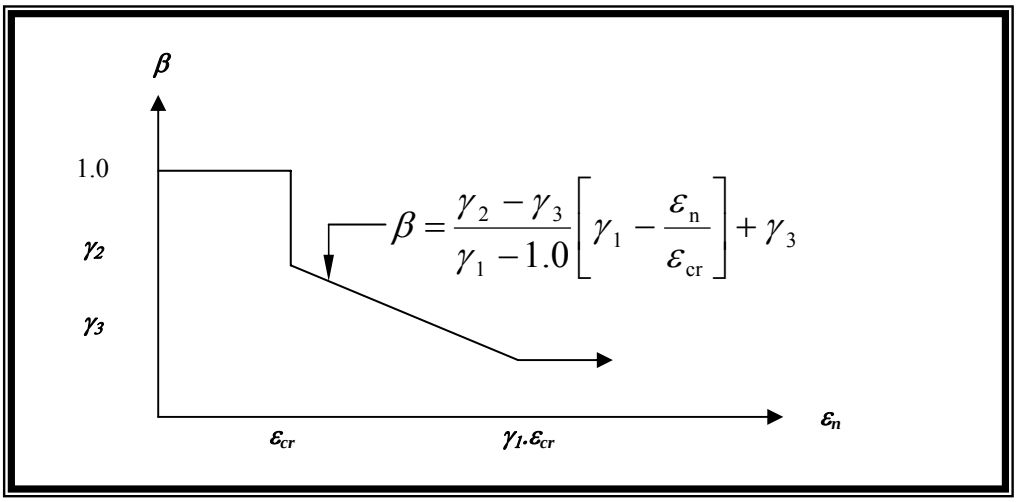

Figure (4.11): Shear Retention for Concrete.[9]

4.5 Modeling of Reinforcement

Compared to concrete, steel is a much simpler material to represent. Its stress-strain behavior can be assumed to be identical in tension and compression. In reinforced concrete members, reinforcing bars are normally long and relatively

slender and therefore they can be assumed to be capable of transmitting axial forces only. In the current study, the uniaxial stress-strain behavior of reinforcement is simulated by an elastic-linear work hardening model, as shown in Fig. (4.12).

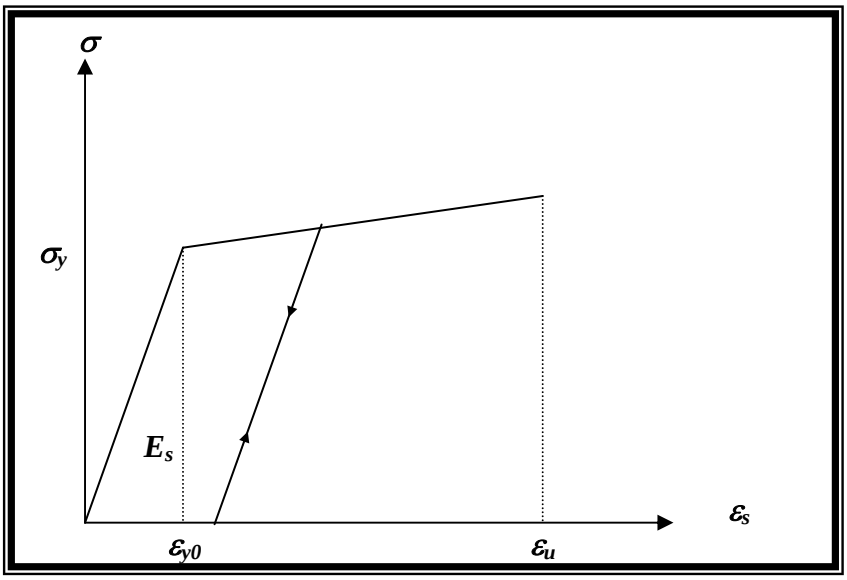

Figure (4.12): Stress-Strain Relationship of Steel Bars Used in the Analysis.[2]

CHAPTER FIVE
NUMERICAL APPLICATIONS AND PARAMETRIC STUDY

5.1 Introduction

This chapter deals with chosen examples reanalyzed numerically by the present computer program ***3DCBEFA*** (Analysis of three-dimensional curved beam on elastic foundation). These examples can be classified into two main groups. The first group contains verification examples used to prove the numerical models that simulate the behavior of concrete, steel, and the elastic foundation. The verification is achieved by comparing the finite element results obtained from ***3DCBEFA*** with the available experimental results. The second group contain application of the program on reinforced concrete curved beam in horizontal plane resting on elastic foundations.

Most of the numerical examples considered in this chapter were previously tested experimentally. The main results obtained through this study is the load-defflection response and crack progration through the elastic, inelastic and ultimate ranges up to failure.

5.2 Numerical Applications

5.2.1 Simply Supported Reinforced Concrete straight Beam(ExampleNo. 1)

A simply support reinforced concrete beam is analyzed using computer program (***3DCBEFA***). A beam was tested by **Scordlis** and **Bresler**[15]. The beam has a total length (3.64 m) with cross-sectional dimensions (552.45 mm × 228.6 mm). It has no web reinforcement and the longitudinal reinforcement consists of four bars with a total area of 4 in^2. The beam subjected to concentrated load at midspan, as shown in Fig.(5-1a).

Taking the advantage of symmetry of the geometry and loading, only half of the beam is modeled by (18) brick elements of 20-noded.

Fig.(5-1b) shows the details of the finite element mesh for the half of the beam. The Material properties of concrete and steel are given in Table (5-1).

The load-deflection response at midspan of the beam is shown in Fig.(5-2). The computed deflection and load failure show good agreement with the experimental results for most loading levels.

Scordelis and **Bresler**[15] solved this example using finite element method. They used 20-node brick element to represented the concrete and the steel bars are represented by axial element.

Fig.(5-2) shows also a comparison of the calculate deflection with the previous study of **[Scordelis** and **Bresler]**[15]. The crack patterns of front face of the beam at failure stage is shown in Fig.(5-3).

Note: all dimensions are in mm

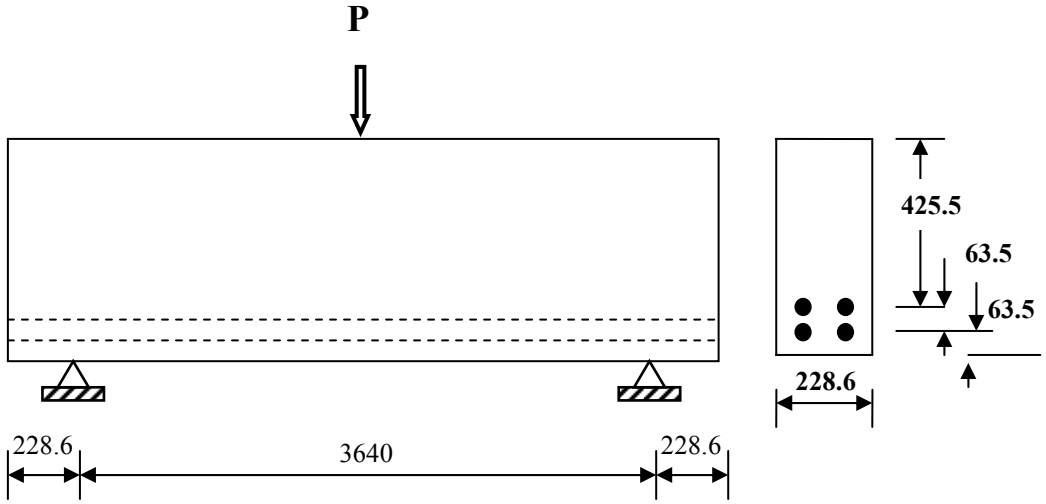

(a) beam geometry, loading arrangement and reinforcement details.

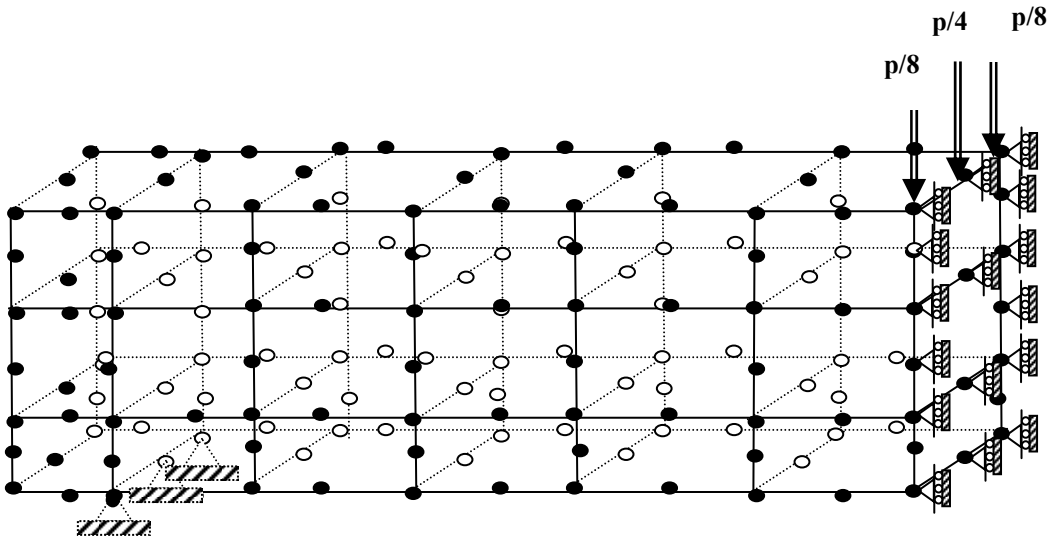

(b): finite element idealization of one half of the beam.

Figure (5.1): simply supported reinforced concrete straight beam

Table (5-1): Material Properties and Additional Paramerters of Simply Supported Reiforced Concrete Beam

	Material properties and material parameters	Symbol	value
Concrete	Young's modulus	$E_c(N/mm^2)$	22000
	Compressive strength	$Fc(N/mm^2)$	30.000
	Tensile strength *	$F_t(N/mm^2)$	2.7
	Poisson's ratio	ν	0.15
	Uniaxial crashing strain **	ε_{cu}	0.003
Steel	Young's modulus	$E_s(N/mm^2)$	191.50
	Yield stress	$F_y(N/mm^2)$	4134
	Hardening parameter	H'	0.0
Tension stiffening parameter	Rate of stress release **	α_1	25
	Sudden loss of tension stiffness at the instant of cracking **	α_2	0.5
Shear retention parameters	Rate of decay of shear stiffness **	γ_1	10.0
	Sudden loss of shear stiffness at the instant of cracking **	γ_2	0.5
	Residual shear stiffness due to the ** dowel action	γ_3	0.1

* Assumed by Scordlis and Bresler

** Assumed in the present study.

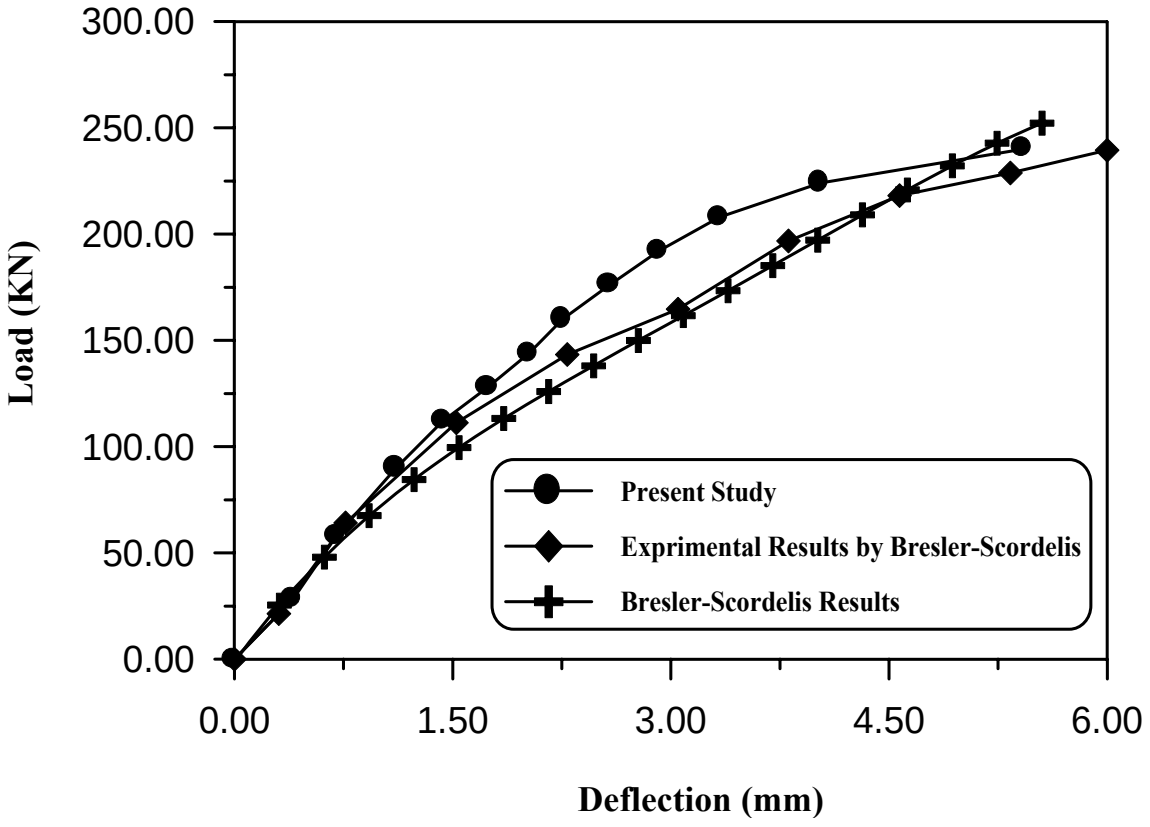

Figure(5-2): Load-deflection curves at midspan of simply supported straight beam(Example No. 1)

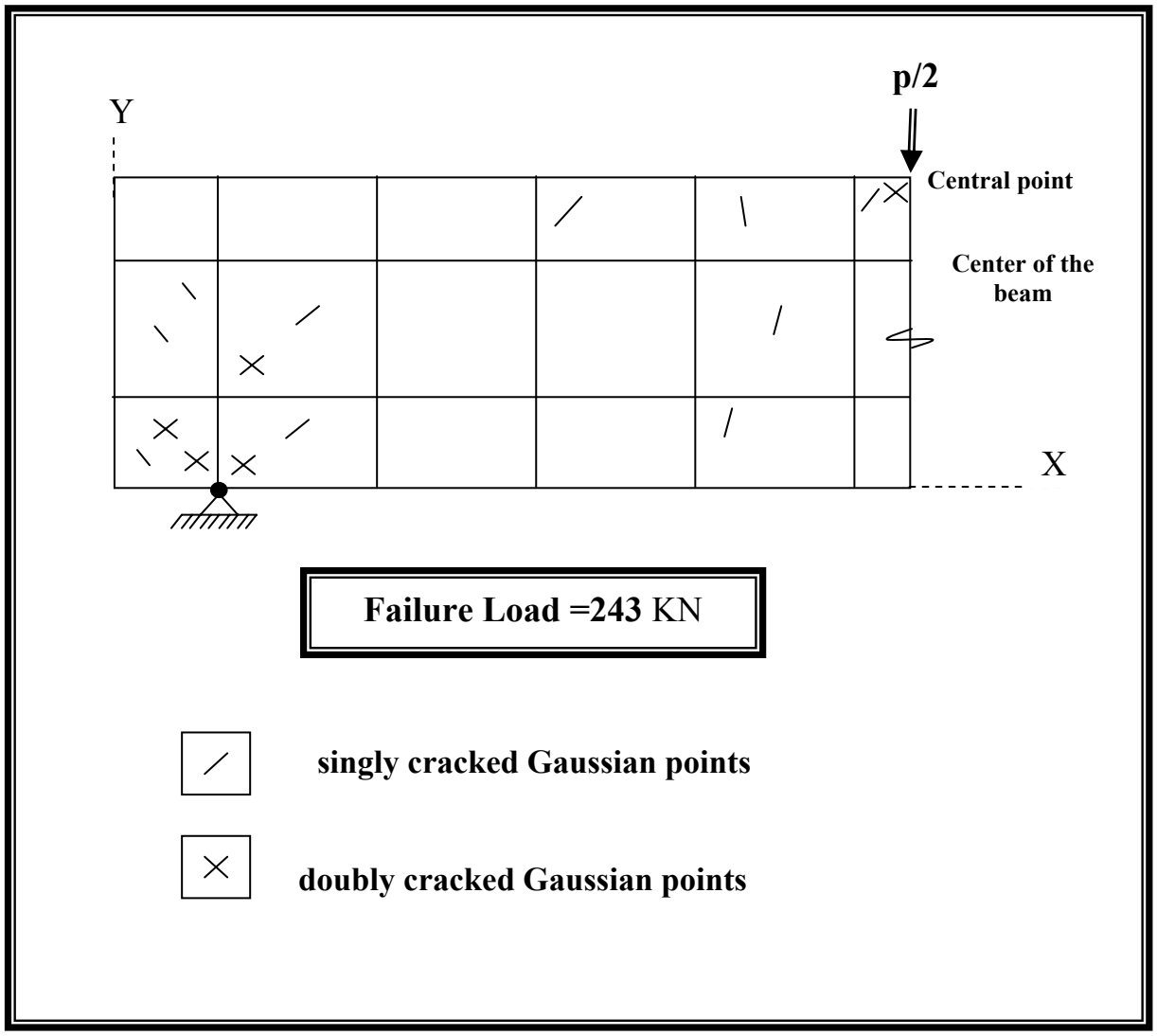

Figure (5-3): crack pattern for front view of simply support straight beam(Example No.1)

5.2.2 Fixed Supported Reinforced Concrete Curved Beams With Subtended Angle 86° (Example No. 2)

A fixed reinforced concrete curved beam has a cross section of (150 mm × 310 mm) was tested under a concentrated load by **Jordaan et. al**.[33] (1974). The reinforcement details are provided in Fig.(5-4). That figure shows also the details of the beam geometry. Concrete and steel properties and additional

material parameters are given in Table (5-2). Fig.(5-4) also shows the details of the finite element mesh for all the fixed supported reinforced concrete curved beam. The load-deflection curves of the beam under concentrated load are shown in Fig.(5-5). Results of the finite element analysis give good agreement with the experimental results of **Jordaan et. al**.[34] Fig.(5-6) is shown the deflection along the beam for three stages of loading (50% , 75% , and 100% of the ailure load). The crack patterns of the beam is shown in Fig.(5-7).

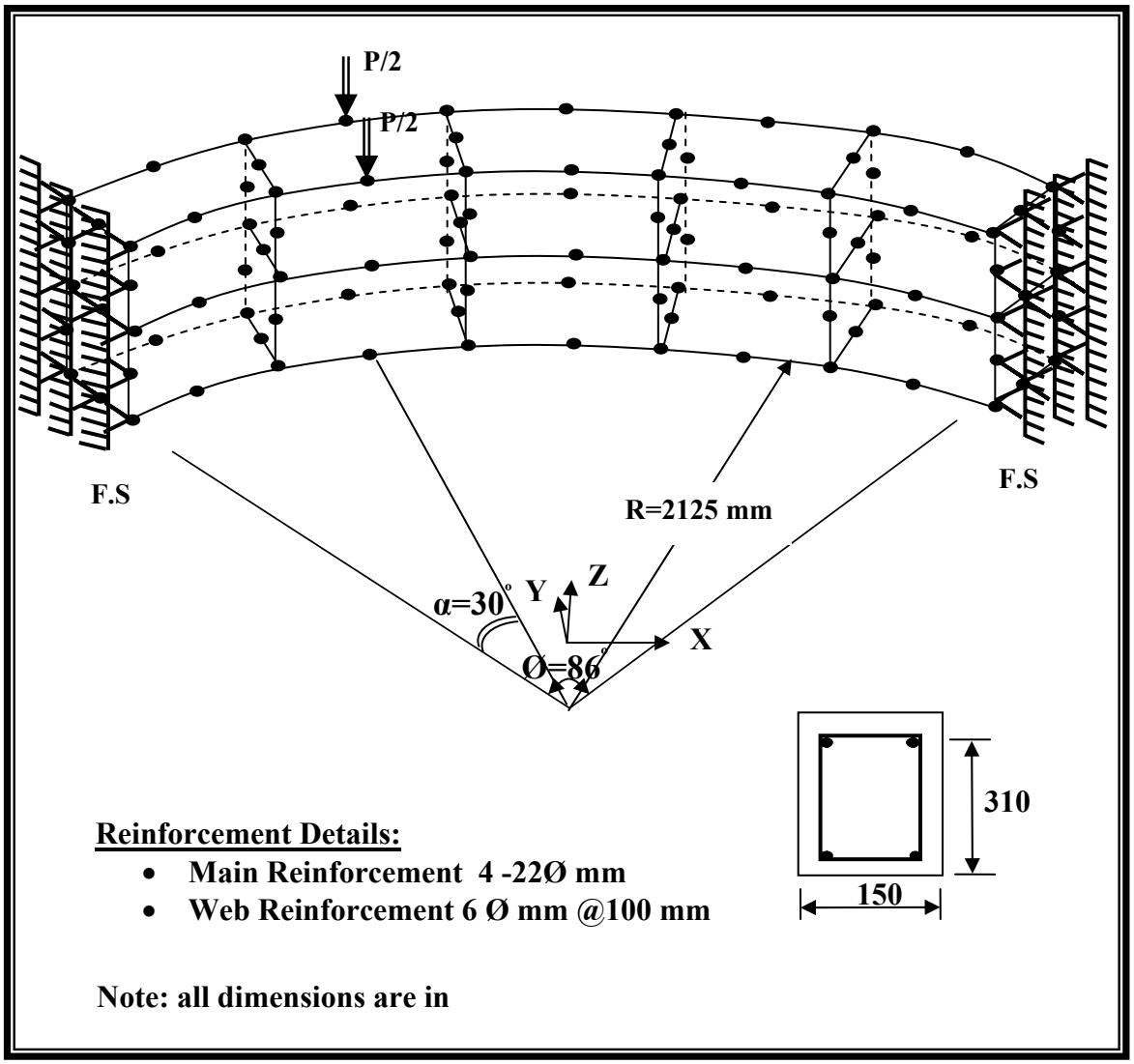

Figure (5-4): geometry and finite element idealization for fixed supported curved beam with subtended angle 86°.

Table(5-2): Material Properties and Additional Paramerters of Fixed Supported Reiforced Concrete Curved Beam with Subtended Angle 86°

	Material properties and material parameters	Symbol	value
Concrete	Young's modulus	$E_c(N/mm^2)$	30000
	Compressive strength	$Fc(N/mm^2)$	42.000
	Tensile strength *	$F_t(N/mm^2)$	2.8
	Poisson's ratio	ν	0.15
	Uniaxial crashing strain **	ε_{cu}	0.003
Steel	Young's modulus	$E_s(N/mm^2)$	200000
	Yield stress for main reinforcement Yield stress for web reinforcement	$F_y(N/mm^2)$ $F_y(N/mm^2)$	384 240
	Hardening parameter	H'	0.0
Tension stiffening parameter	Rate of stress release **	α_1	25
	Sudden loss of tension stiffness at the instant of cracking **	α_2	0.5
Shear retention parameters	Rate of decay of shear stiffness **	γ_1	10.0
	Sudden loss of shear stiffness at the instant of cracking **	γ_2	0.5
	Residual shear stiffness due to the ** dowel action	γ_3	0.1

* Assumed by Jordaan et al.

** Assumed in the present study.

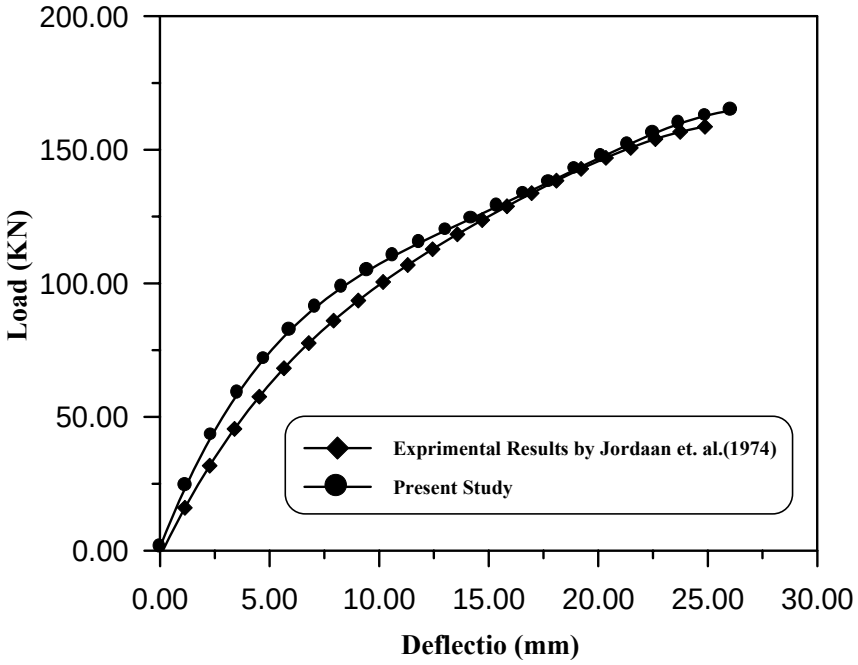

Figure(5-5): Load-deflection curves under point load of fixed supported curved beam with subtended angle 86° (Example No.2)

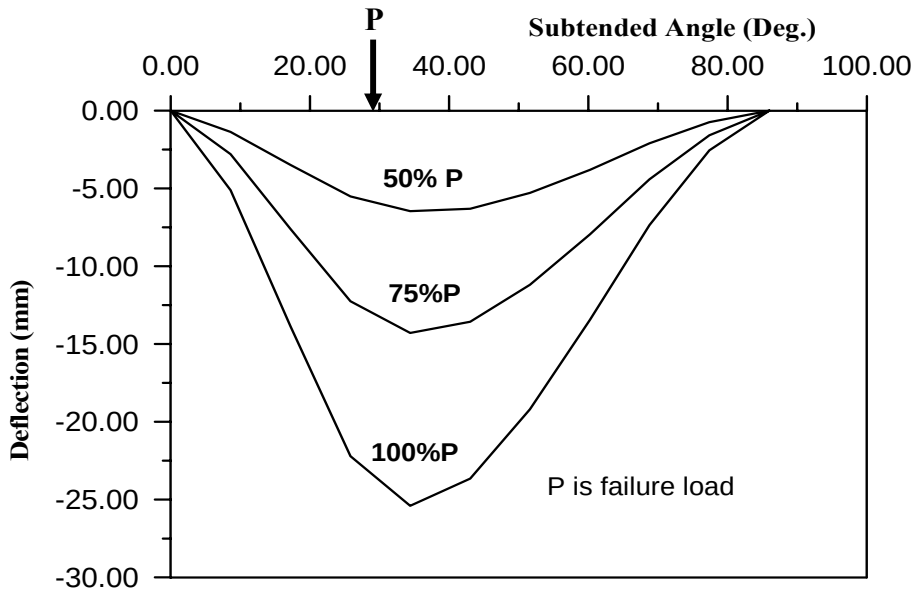

Figure(5-6): Load-deflection curves along the fixed supported curved beam with subtended angle 86° (Example No.2)

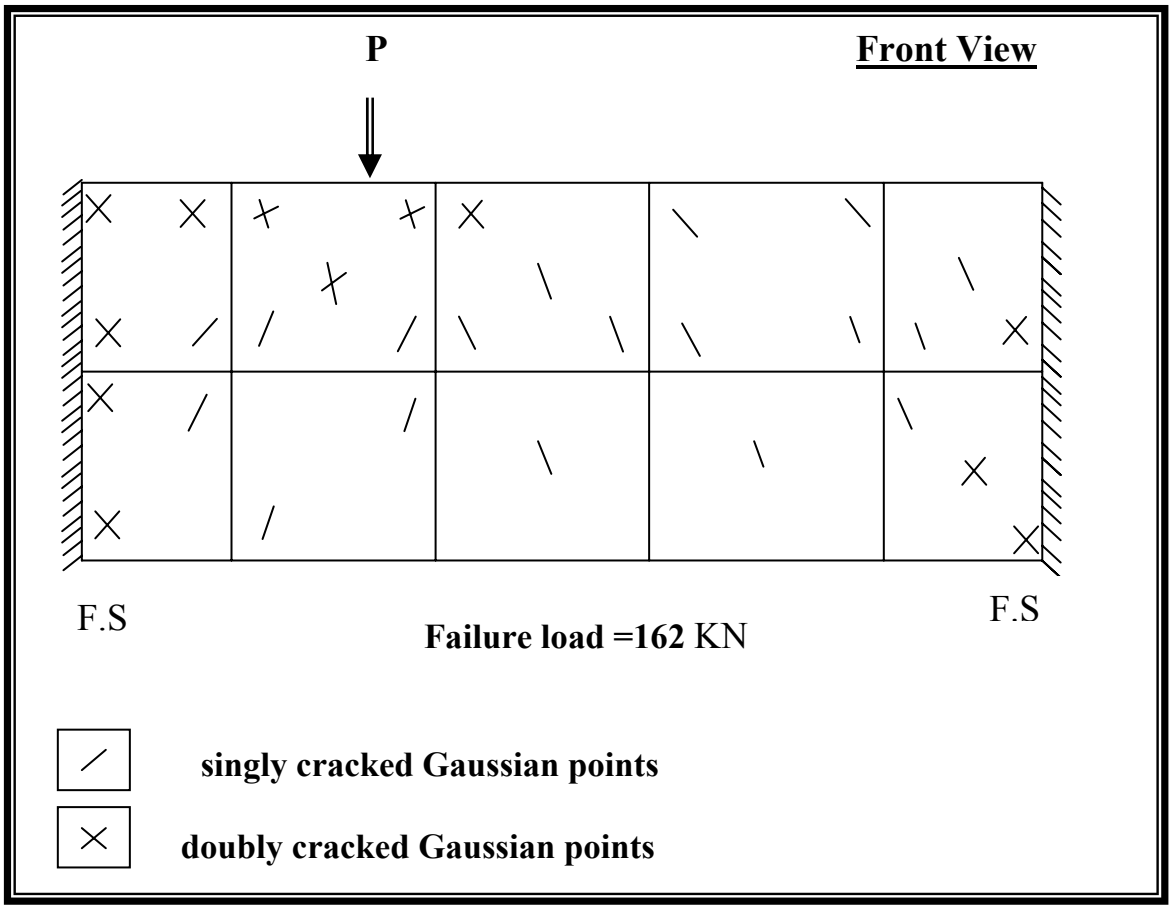

Figure (5-7): crack pattern at front face of reinforced concrete curved beam(example 2)

5.2.3 Fixed Supported Reinforced Concrete Curved Beams With Subtended Angle 75°(Example No. 3)

A fixed reinforced concrete curved beam has a cross section of (152 mm × 305 mm) was tested under a concentrated load by **Badawy et. al**.[10] (1977). The reinforcement details are provided in Fig.(5-8). That figure shows also the details of the beam geometry. Concrete and steel properties and additional material parameters are given in Table (5-3).

Fig.(5-8) shows also the details of the finite element mesh for all the fixed supported reinforced concrete curved beam.

The load-deflection curves of the beam under concentrated load are shown in Fig.(5-9). Results of the finite element analysis give good agreement with the experimental results of **Badawy et al**.[10]

Fig.(5-10), shows the crack patterns of the front face of the beam at failure stage. At a load stage of about 97.8 % of the available experimental ultimate load, the numerical model used in the present study indicates crushing in a Gaussian point located in the top of front surface beneath the concentrated load. The crushing occurred when the compressive strain of the Gaussian point exceeds the ultimate strain value, then its stiffness deteriorated to zero and the finite element analysis was terminated.

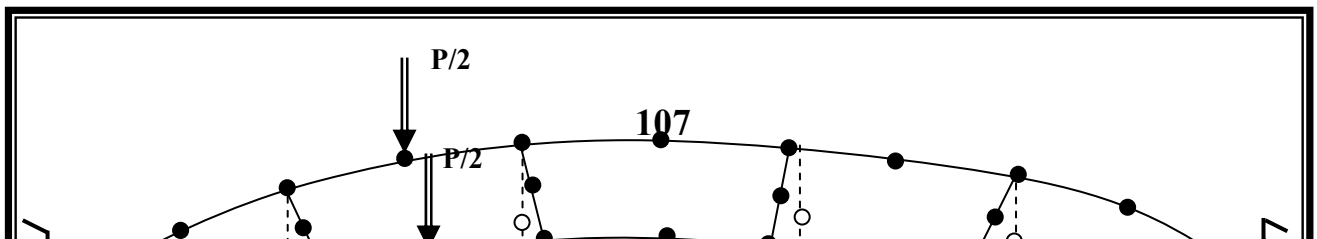

Table (5-3): Material Properties and Additional Paramerters of Fixed Supported Reiforced Concrete Curved Beam with Subtended Angle 75^{o}

	Material properties and material parameters	Symbol	value
Concrete	Young's modulus	$E_c(N/mm^2)$	23000
	Compressive strength	$Fc(N/mm^2)$	30.000
	Tensile strength *	$F_t(N/mm^2)$	2.7
	Poisson's ratio	ν	0.15
	Uniaxial crashing strain **	ε_{cu}	0.003
Steel	Young's modulus	$E_s(N/mm^2)$	200000
	Yield stress for main reinforcement Yield stress for web reinforcement	$F_y(N/mm^2)$ $F_y(N/mm^2)$	475 3003
	Hardening parameter	H'	0.0
Tension stiffening parameter	Rate of stress release **	α_1	25
	Sudden loss of tension stiffness at the instant of cracking **	α_2	0.65
Shear retention parameters	Rate of decay of shear stiffness **	γ_1	10.0
	Sudden loss of shear stiffness at the instant of cracking **	γ_2	0.35
	Residual shear stiffness due to the ** dowel action	γ_3	0.1

* Assumed by **Badawy et. al.**(10)

** Assumed in the present study.

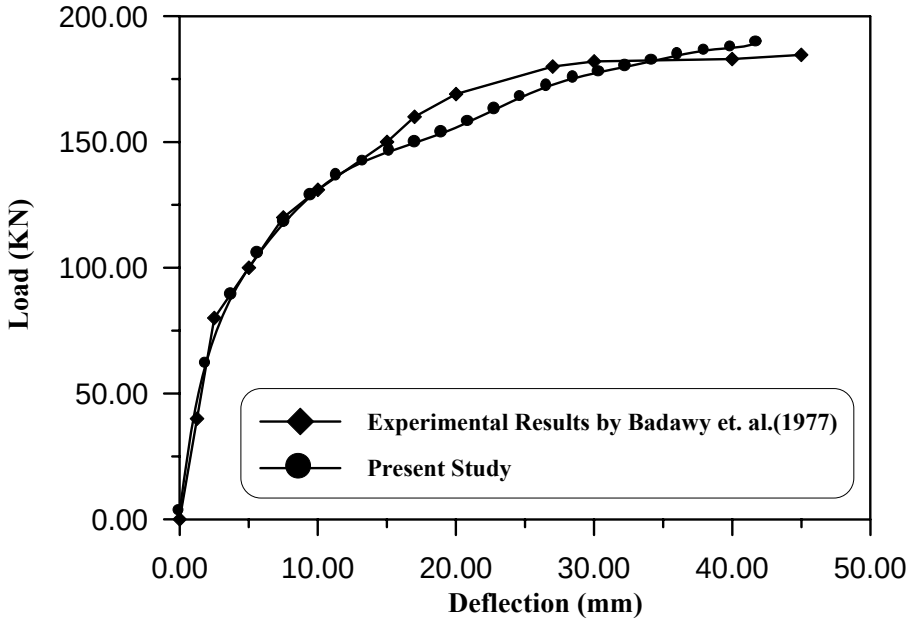

Figure(5-9): Load-deflection curves under point load of fixed supported curved beam with subtended angle 75°(Example No. 2)

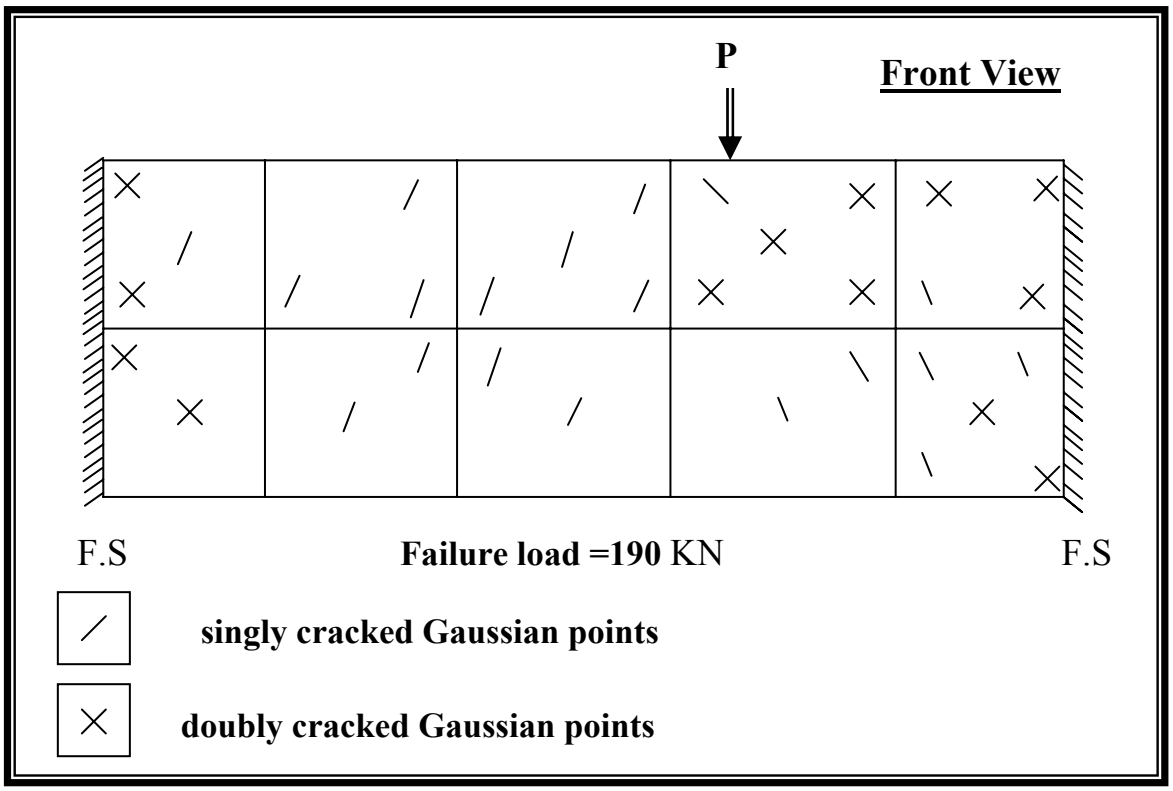

Figure (5-10): crack pattern at front face of curved beam(Example No. 3)

5.2.4 Simply-Fixed Supported Reinforced Concrete Curved Beams With Subtended Angle 75°(Example No. 4)

A simply-fixed reinforced concrete curved beam has a cross section of (152 mm × 305 mm) was tested under a concentrated load by **Badawy et. al**.[10] (1977). The reinforcement details are provided in Fig.(5-11). That Figure shows also the details of the beam geometry. Concrete and steel properties and additional material parameters are given in Table (5-4).

Fig.(5-11) shown also the details of the finite element mesh for all the fixed supported reinforced concrete curved beam.

The load-deflection curves of the beam under concentrated load are shown in Fig.(5-12). Results of the finite element analysis give good agreement with the experimental results of **Badawy et. al**.[10]

The crack patterns of front face of the beam at failure stage is shown in Fig.(5-13).

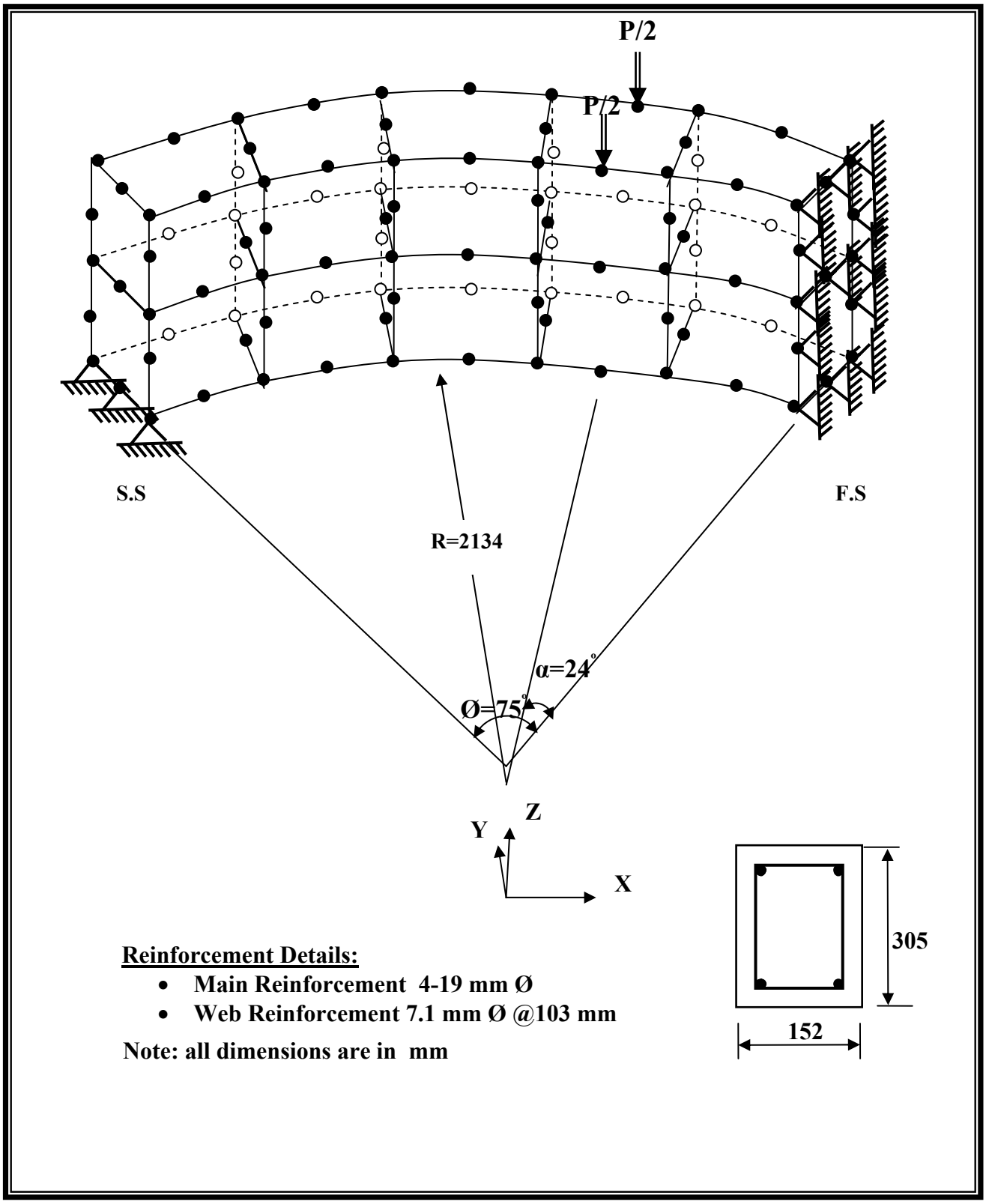

Figure (5-11): geometry and finite element idealization for simply-fixed supported reinforced concrete curved beam with subtended angle 75° (Example No. 2)

Table (5-4): Material Properties and Additional Paramerters of Simply-Fixed Supported Reiforced Concrete Curved Beam with Subtended Angle 75^{o}

	Material properties and material parameters	Symbol	value
Concrete	Young's modulus	$E_c(N/mm^2)$	23000
	Compressive strength	$Fc(N/mm^2)$	30.000
	Tensile strength *	$F_t(N/mm^2)$	2.7
	Poisson's ratio	ν	0.15
	Uniaxial crashing strain **	ε_{cu}	0.003
Steel	Young's modulus	$E_s(N/mm^2)$	200000
	Yield stress for main reinforcement Yield stress for web reinforcement	$F_y(N/mm^2)$ $F_y(N/mm^2)$	475 3003
	Hardening parameter	H'	0.0
Tension stiffening parameter	Rate of stress release **	α_1	25
	Sudden loss of tension stiffness at the instant of cracking **	α_2	0.65
Shear retention parameters	Rate of decay of shear stiffness **	γ_1	10.0
	Sudden loss of shear stiffness at the instant of cracking **	γ_2	0.4
	Residual shear stiffness due to the ** dowel action	γ_3	0.1

* Assumed by **Badawy et. al**.(10)

** Assumed in the present study.

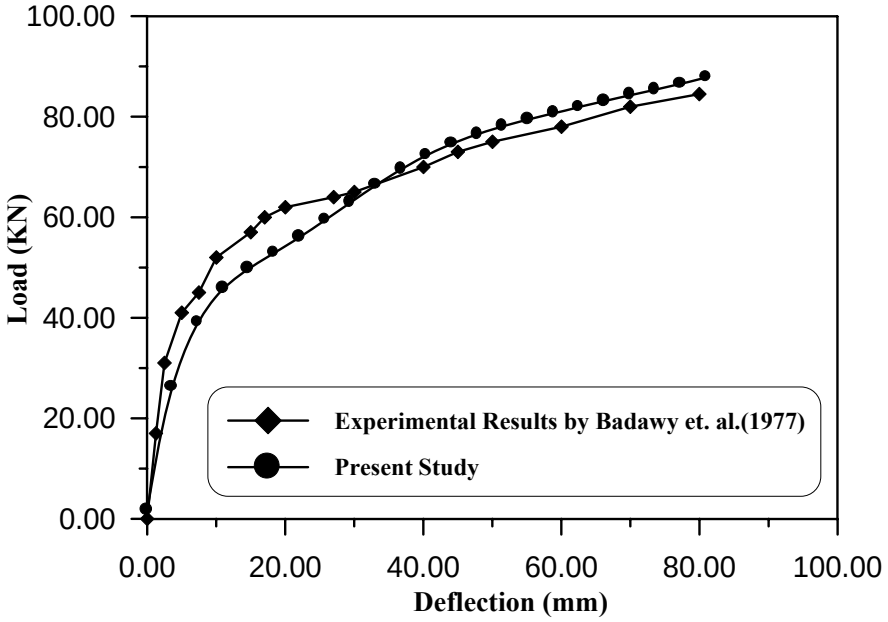

Figure(5-12): Load-deflection curves under point load of simply-fixed supported curved beam with subtended angle 75° (Example No.4)

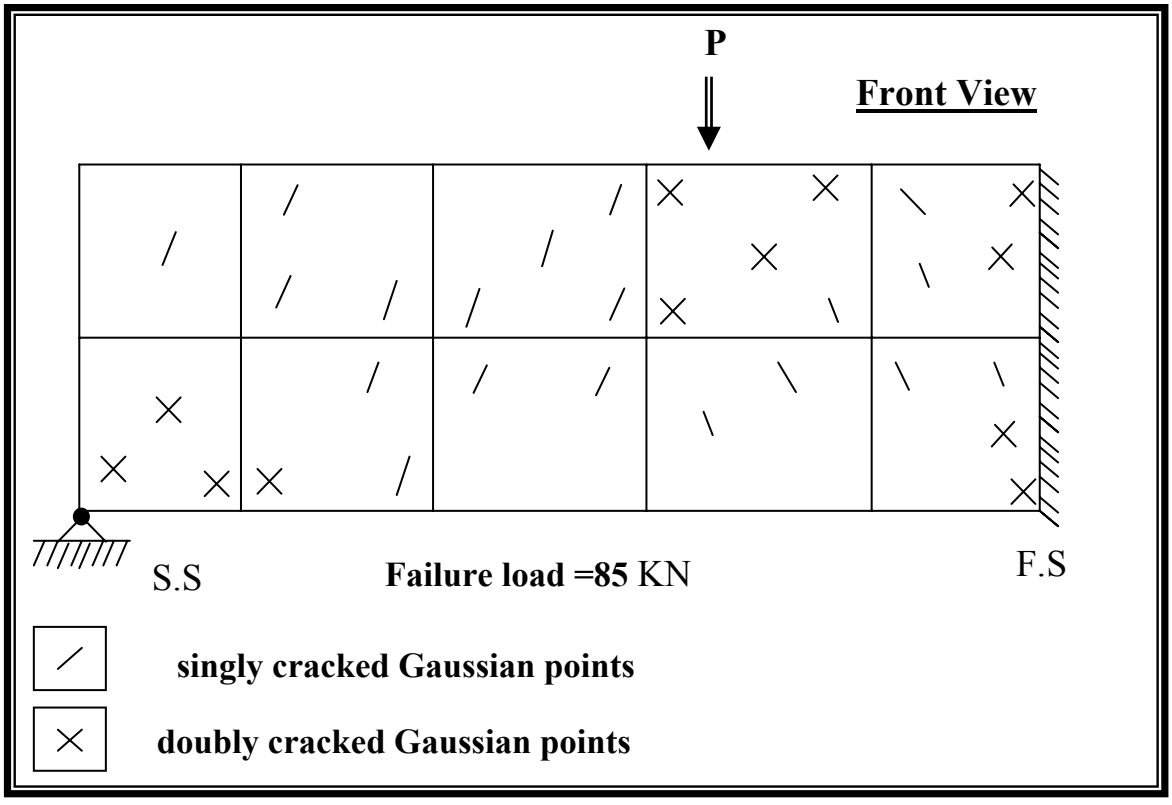

Figure (5-13): crack pattern at front face of reinforced concrete curved beam(Example No.4)

5.2.5 Fixed Supported Reinforced Concrete Curved Beams on Elastic Foundation (Example No.5)

A fixed reinforced concrete curved beam has a cross section of (152 mm × 305 mm) as shown in Fig.(5-14) is considered to study the influence of some parameters on the behavior of reinforced concrete curved beam resting on elastic foundation. The beam is subjected to concentrated load as shown in Fig.(5-14). The geometry of this problem and reinforcement details are provided in Fig.(5-14). Concrete and steel properties and additional material parameters are given in Table (5-5).

A twenty-node isoparametric brick element used to model the concrete. The reinforcement bars are modeled as axial member imbedded within the brick element. Soil is represented by normal subgrade reaction and horizontal subgrade reaction, the normal component is represented by Winkler, Kondner, and Polynomial models, while the horizontal component is represented by Winkler model.

Fig.(5-14) shown also the details of the finite element mesh for one half of the fixed supported reinforced concrete curved beam.

For Winkler model the value of normal subgrade reaction is (30×10^6 N /mm^3) , for Kondner model the value of ***a*** is (384.34 mm^3/ KN) and ***b*** is (0.176 mm^2/ KN), for Polynomial model the value of normal subgrade reaction is depended on the load test for the soil as shown in Fig.(5-21) to Fig.(5-224) for different type of soil. Fig.(5-14) shows also the details of the finite element mesh for all the fixed supported reinforced concrete curved beam.

The load-deflection curves of the beam under concentrated load are shown in Fig.(5-15). The crack patterns of front face of the beam at failure stage is shown in Fig.(5-16).

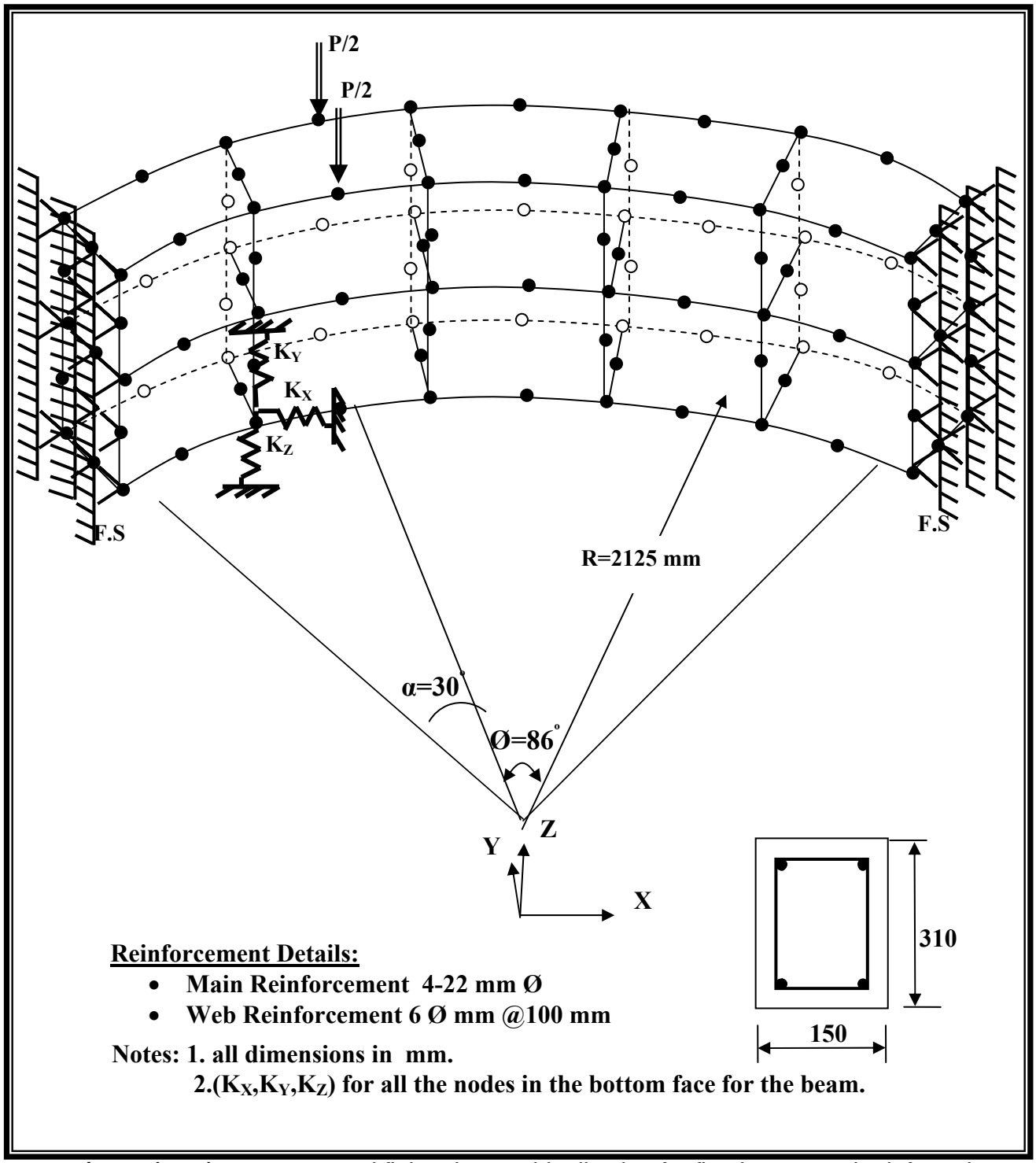

Figure (5-14): geometry and finite element idealization for fixed supported reinforced concrete curved beam on elstic foundation with subtended angle 86°(Example No.5)

Table (5-5): Material Properties and Additional Paramerters of Fixed-Fixed Supported Reiforced Concrete Curved Beam with Subtended Angle 86°

	Material properties and material parameters	Symbol	value
Concrete	Young's modulus	$E_c(N/mm^2)$	23000
	Compressive strength	$Fc(N/mm^2)$	30.000
	Tensile strength *	$F_t(N/mm^2)$	2.7
	Poisson's ratio	ν	0.15
	Uniaxial crashing strain *	ε_{cu}	0.003
Steel	Young's modulus	$E_s(N/mm^2)$	200000
	Yield stress for main reinforcement Yield stress for web reinforcement	$F_y(N/mm^2)$ $F_y(N/mm^2)$	475 3003
	Hardening parameter	H'	0.0
Tension stiffening parameter	Rate of stress release *	α_1	25
	Sudden loss of tension stiffness at the instant of cracking *	α_2	0.65
Shear retention parameters	Rate of decay of shear stiffness *	γ_1	10.0
	Sudden loss of shear stiffness at the instant of cracking *	γ_2	0.3
	Residual shear stiffness due to the * dowel action	γ_3	0.1

* Assumed in the present study.

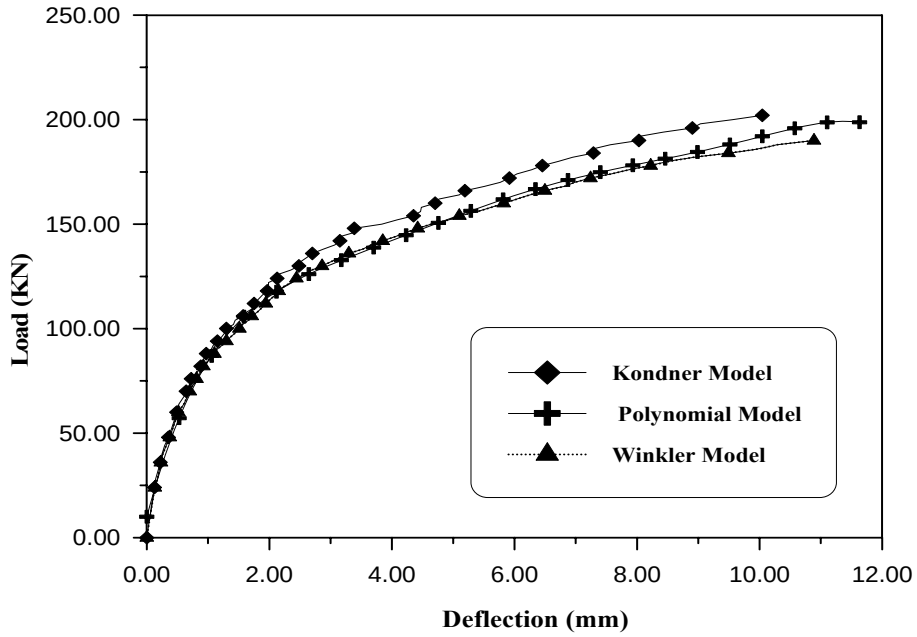

Figure(5-15): Load-deflection curves under point load of fixed supported curved beam with subtended angle 86° for different soil models

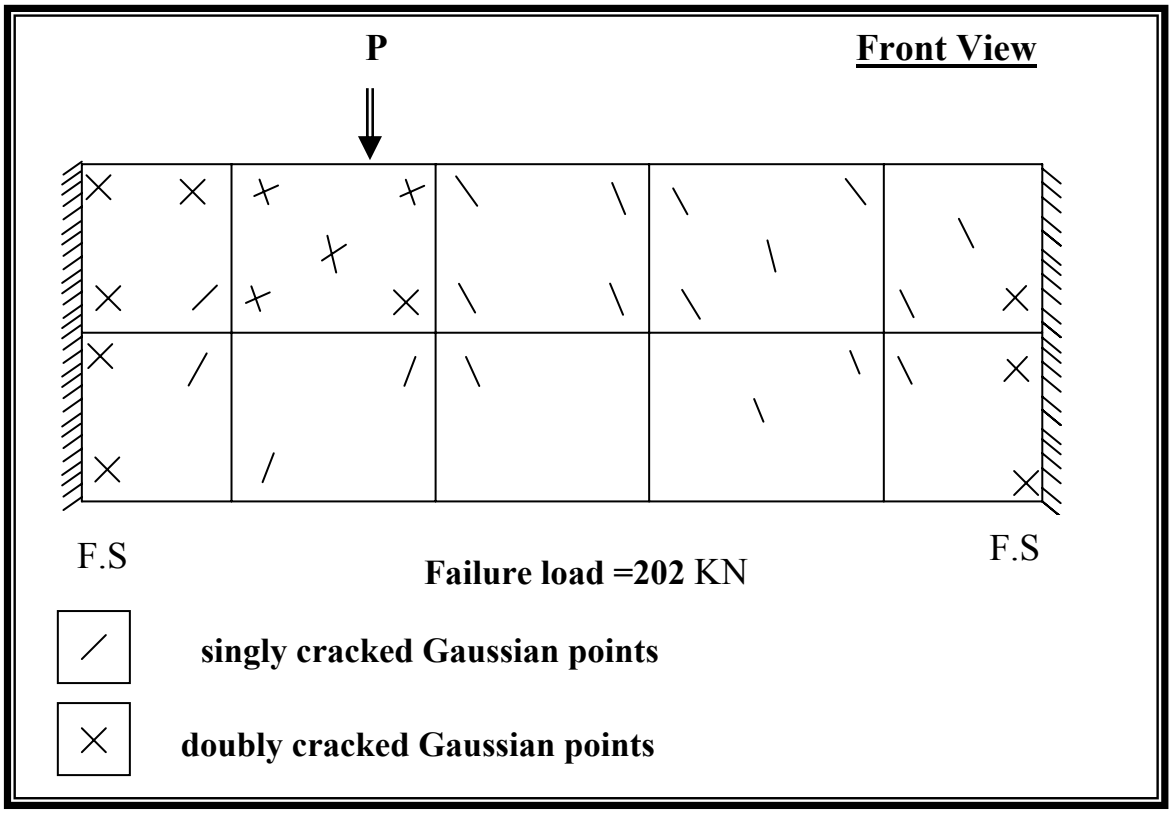

Figure (5-16): crack pattern at front face of reinforced concrete curved beam on elastic foundation(example 5)

5.3 Parametric Study

Example No.5 is chosen to study the influence of some parameters that affect the behavior of reinforced concrete curved beam on elastic foundation under static load. These parameters include the effect of radius to span-length ratio, effect of boundary conditions, effect (α_2) [the sudden loss of stress at the instant of cracking], effect of type of soil, and effect of reinforcement bars)

20-node brick element are employed to model the concrete, and steel bars are modeled as axial element embedded within brick concrete element. Kondner model used to modeled the normal subgrade reaction of soil. Tangential subgrade reaction for soil modeled by winkler model.

5.3.1 Effect of radius To Span-length Ratio (R/L)

To investigate the effect of radius to span-length ratio, four reinforced concrete curved beams were analyzed numerically. Figure (5-17) shows the load deflection curve for those reinforced concrete curved beams which have different (R/L) ratio (R/L approach to ∞, R/L=5,3, and 1). From this figure, it can noticed that the ultimate load decreases when the decreases of (R/L) ratio, while the central deflection is inversely proportional to the (R/L) ratio, little increases accur with decreases (R/L). When the (R/L) is decreases, the subteneded angle for curved beams is increases due to increasing in subtended angle the ultimate load is decreases. This is accur with constant span length of the curved beam. Predicated ultimate loads for these four curved beams are also given in Table (5-6).

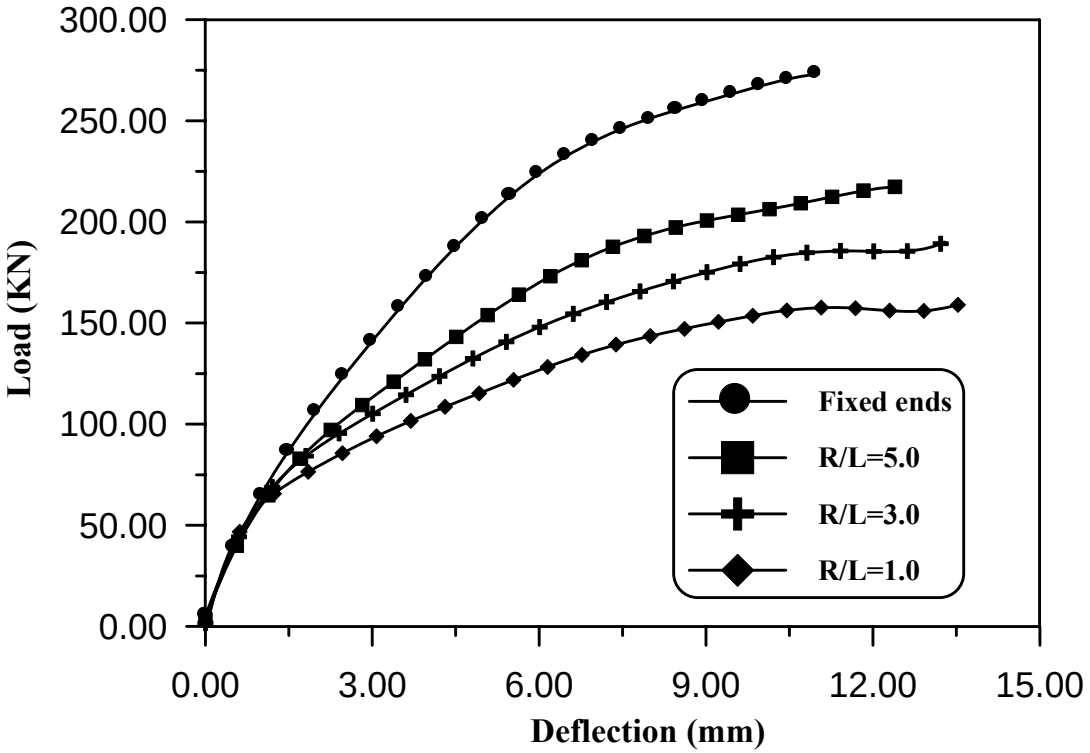

Figure(5-17): Load-deflection under point load for curved beam with various radius to span-length ratio(R/L).

Table (5-6): Value of Predicted Ultimate Load for the Reinforced concrete Curved Beam on Elastic Foundation

R/L	Predicted ultimate load(KN)	Load factor
∞	273	1.00 (Reference)
5	219	0.802
3	191	0.700
1	160	0.586

5.3.2 Effect of Boundary Condition

To investigate the effect of boundary conditions on behavior of the reinforced concrete curved beams, two reinforced concrete curved beams with different boundary conditions were analyzed numerically.

Figure (5-18) shows the load-deflection curves at the point under the load for four reinforced concrete curved beams (simply-fixed, , and fixed supported beam). From this figure, it can see that the collapse load for fixed support beam greater than other beam (simply-fixed supported) and the deflection for simply-fixed supported beam is grater than fixed supported beam.

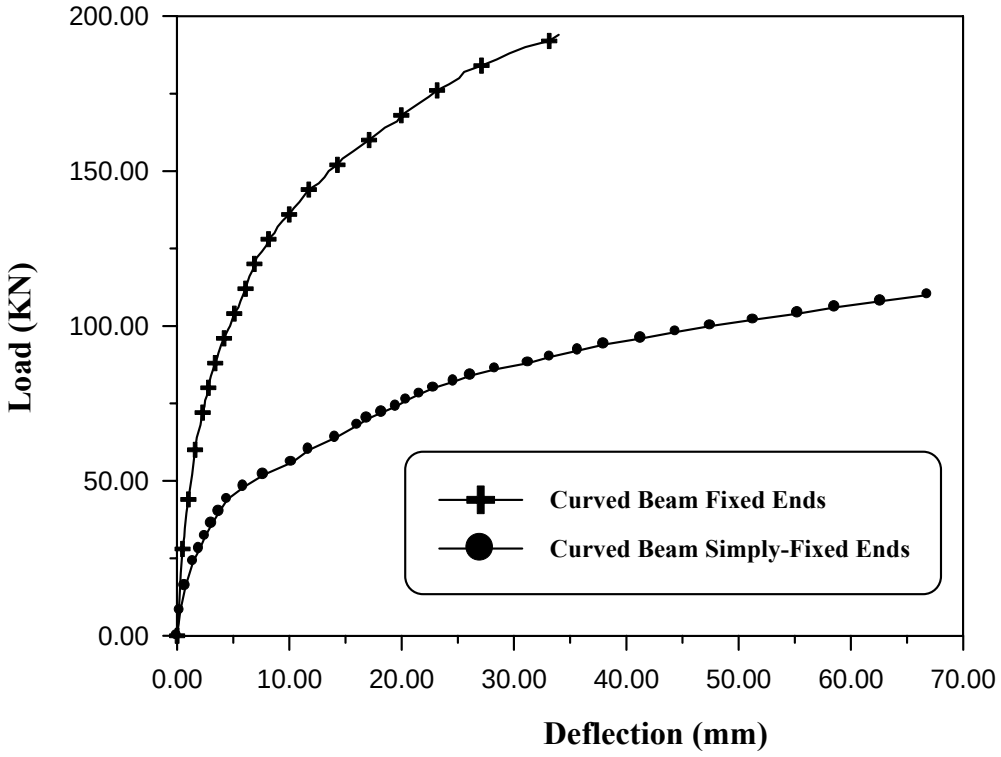

Figure(5-18): Load-deflection under point load for curved beam with various boundary conditions.

5.3.3 Effect of (α_1) [The rate of stress release as the crack widens]

Figure (5-19) shows the influence of (α_1) on the behavior of reinforced concrete curved beam on elasrtic foundation. Four curved beams on elastic foundation with different values for (α_1) (15.0, 20.0, 25.0, and 30.0)were analyzed numerically. Figure (5-19) indicates that the increase value of (α_1) has significant effect on the behavior of the curved beam on elastic foundation. It can be noticed that increase value of (α_1) increases the ultimate load and decreases the ultimate deflection of the curved beams by a little amout. Predicated ultimate loads for these four curved beams are also given in Table (5-7).

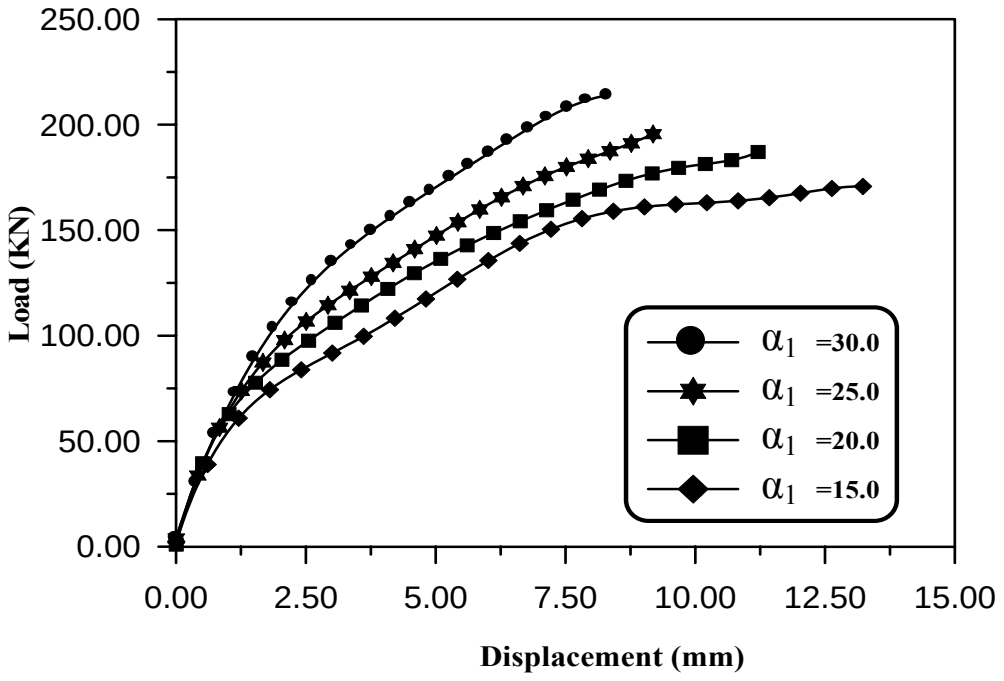

Figure(5-19): Load-deflection under point load for curved beam with various (α_1).

Table (5-7): Value of Predicted Ultimate Load for the Reinforced concrete Curved Beam on Elastic Foundation

α_1	**Predicted ultimate load(KN)**	**Load factor**
15	**171**	**1.00 (Reference)**
20	**182**	**1.065**
25	**196**	**1.140**
30	**220**	**1.286**

5.3.4 Effect of (α_2) [The sudden loss of stress at instant of cracking]

To study the effect of (α_2) on the behavior of reinforced concrete curved beams resting on elastic foundation. Four curved beams on elastic foundation with different value of (α_2) (0.45, 0.60, 0.75, and 0.90) were analyzed numerically. Figure (5-20) indicates that the increase of value (α_2) has significant effect on the behavior of curved beam.

Figure (5-20) shows that when value of (α_2) increases from 0.45 to 0.90, the ultimate load will increases about 83.33% , because th sudden loss ratio in normal stress at instant cracking will decreases, this decreasing causes increases in ultimate load . Predicated ultimate loads for these four curved beams are also given in Table (5-8).

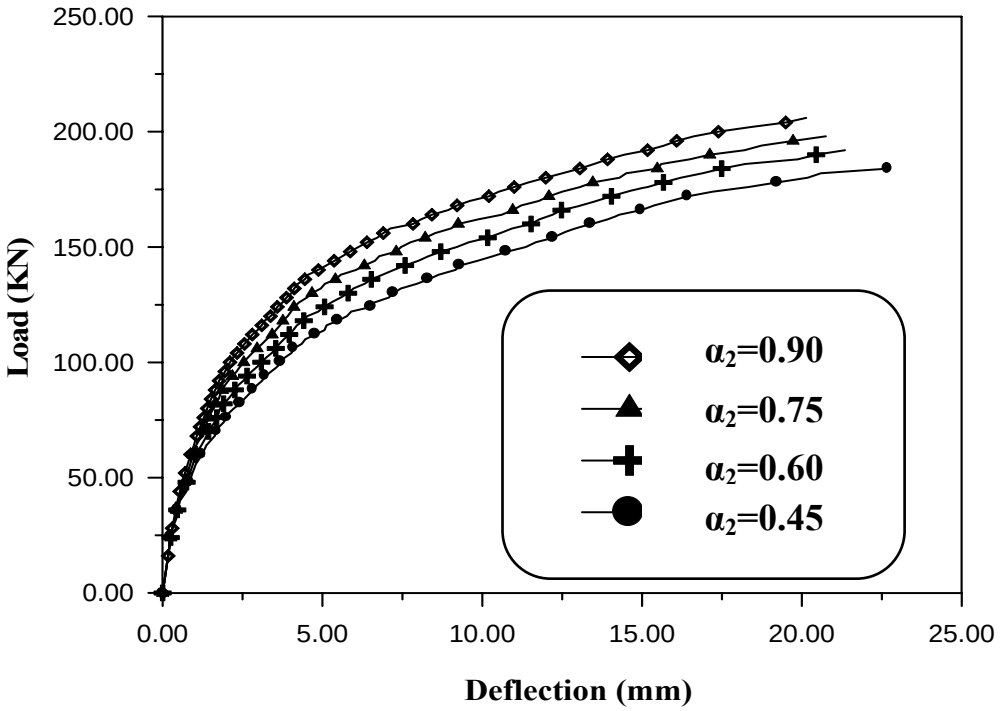

Figure(5-20): Load-deflection under point load for curved beam with various (α_2).

Table (5-8): Value of Predicted Ultimate Load for the Reinforced concrete Curved Beam on Elastic Foundation

α_2	Predicted ultimate load(KN)	Load factor
0.45	184	1.00 (Reference)
0.60	192	1.043
0.75	198	1.076
0.90	206	1.120

5.3.5 Effect of Type of Soil

To investigate the effect of type of soil on behavior of the reinforced concrete curved beams, four reinforced concrete curved beams resting on different types of soil (dense sand, medium sand, losse sand, and soft clay) were analyzed numerically.

Figure (5-25) shows the load-deflection curves at the point under the load for four reinforced concrete curved . From that figure, it can be seen that the deflection of the beam increases when the density of soil decreases. The ultimate load for beam on dense sand is greater than ultimate load for beam on medium, loose and soft clay.

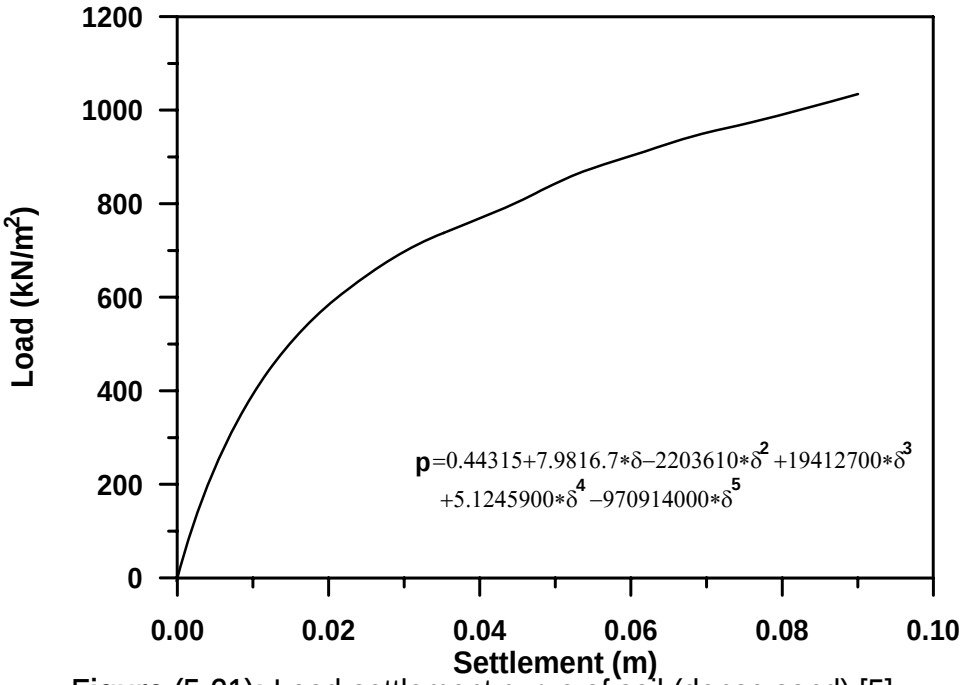

Figure (5-21): Load-settlement curve of soil (dense sand).[5]

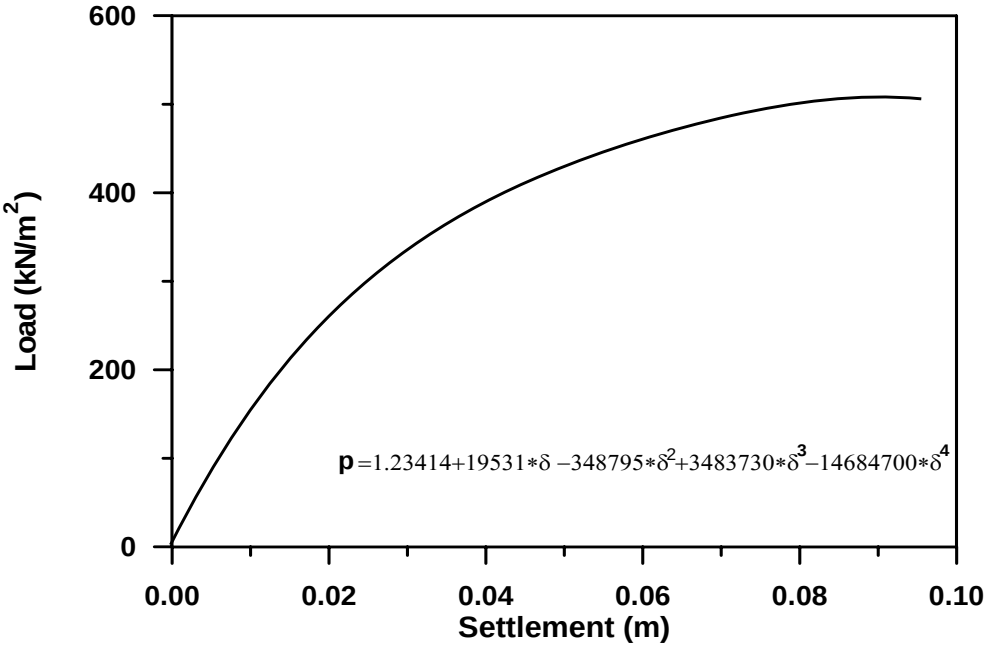

Figure (5-22): Load-settlement curve of soil (medium dense sand) .[5]

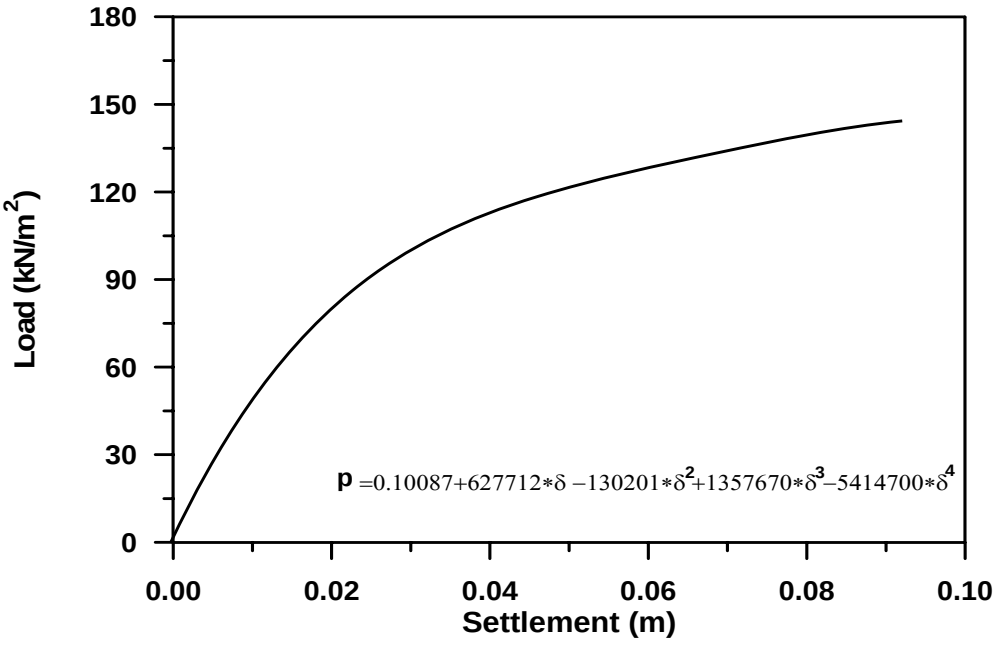

Figure (5-23):Load-settlement curve of soil (loose sand) .[5]

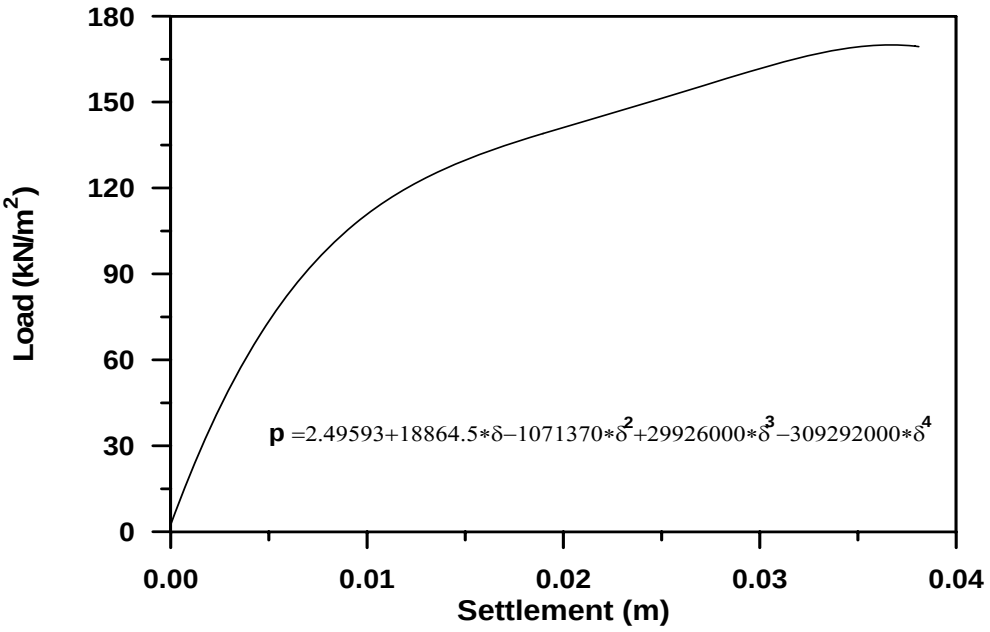

Figure (5-24): Load-settlement curve of soil (soft clay).[5]

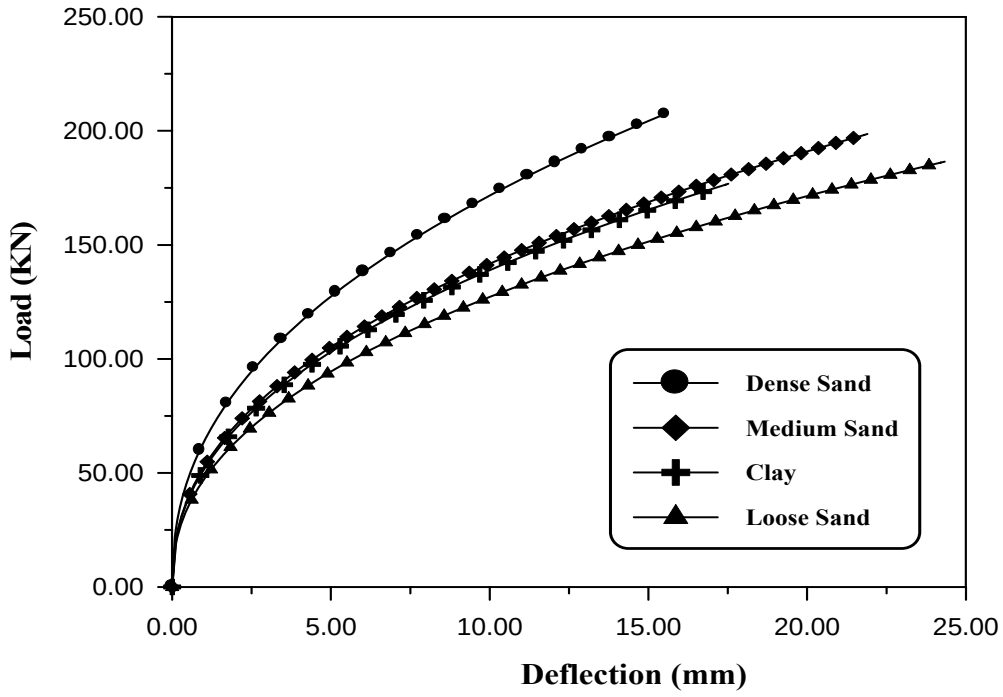

Figure(5-25): Load-deflection under point load for curved beam with various types of Soil.

5.3.6 Effect of Reinforcement Bars

To study the effect of reinforcement bars on behavior of reinforced concrete curved beam on elastic foundation, three fixed supported curved beams on elastic foundation were analyzed. The first beam has both main and web reinforcement bars. But the second beam has main reinforcement bars only. Finaly, the third beam was plane concrete . Figure(5-26) shows that, the ultimate load decreses about (50 %) if the web reinforcement bars are removed. This is lead to importance of the web reinforcement bars (its including shear and torsion reinforcement bars).

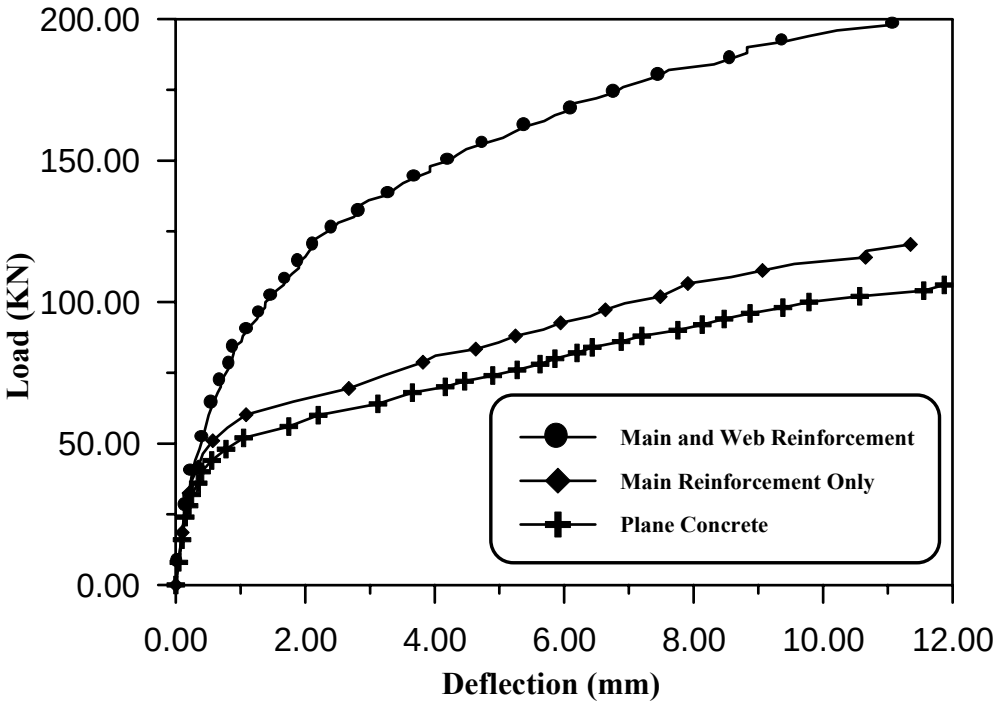

Figure(5-26): effect of reinforcement stee bars on load-deflection of curved beams on elastic foundation.

CHAPTER SIX
CONCLUSIONS AND RECOMMENDATIONS

6.1 Conclusions

Based on the results obtained from the present finite element procedure, and comparison with other avalible results, the following conclusions can be drawn:

1. The results obtained from the present finite element method show that the computational model adopted in this study is suitable for the prediction of load-deflection behavior of reinforced concrete curved beam on elastic foundations under static loading. The comparison between the numerical and the available experimental results gave good agreement with a difference of not more than about 5 % in the predicted ultimate load and about 8 % in the deflection .
2. In the problem of reinforced concrete curved beam on elastic foundation, various models can be suggested to represent both compressive and frictional resistance. The normal component can be represented by Winkler, Kondner, Ploynomial models, while the horizontal component can be represented by Winkler model.
3. The ultimate load for fixed supported curved beam is gearter than the ultimate load for simply-fixed supported curved beam by about 1.78% .
4. The effect of the radius to span-length ratio (R/L) was noticed to have most pronounced effect on the load-deflection behavior of curved beam on elastic foundation. It is found that the increases of the radius to span-length ratio increase the ultimate load and decrease in the ultimate deflection [when (R/L) increases from 1.0 to 5.0 the ultimate load increase of about 41%].
5. The shear reinforcement has pronounced effect on the behavior of reinforced concrete curved beam. It was found that the removing of the shear reinforcement bars leads to decreasing the ultimate load of about 51 % .

6. From the parametric studies carried out on curved beam resting on elastic foundation, it can be conclused that the increase of (α_1) [the rate of the stress release as the crack widens] leads to the increase of the ultimate load.

6.2 Recommendations For Future Works

The following topics are suggested for future research:

1. Investigating the behavior of reinforced concrete curved beam on elastic foundation experimentally, and analysing the soil by using twenty-node brick elements and for interface between the reinforced concrete curved beam and the elastic foundation.
2. Investigating the behavior of curved beam on elastic foundation under cyclic and daynamic loads experimentally and theoretically by the finite elements method.
3. Investigating the behavior of curved beam on elastic foundation with taking into account the bond slip between the concrete and reinforcement steel bars.
4. Extending of the present work to include the geometrically nonlinearity.
5. Investigate the behavior of curved beam on elastic foundation with taking into account time dependent effects of the creep and shrinkage of concrete.

APPENDIX B

Evaluation of the Flow Vector

The flow vector {a}, is defined as the derivative of the yield function with respect to the stress components, and given by:

$$\{a\} = \left[\frac{\partial f}{\partial \sigma_x}, \frac{\partial f}{\partial \sigma_y}, \frac{\partial f}{\partial \sigma_z}, \frac{\partial f}{\partial \tau_{xy}}, \frac{\partial f}{\partial \tau_{yz}}, \frac{\partial f}{\partial \tau_{zx}} \right] \tag{B-1}$$

where,

$$\left.\begin{aligned}
a_1 &= \frac{\partial f}{\partial \sigma_x} = c + \left[2\left(c^2 + \beta\right)\sigma_x + \left(2c^2 - \beta\right)\left(\sigma_y - \sigma_z\right) \right] / Q \\
a_2 &= \frac{\partial f}{\partial \sigma_y} = c + \left[2\left(c^2 + \beta\right)\sigma_y + \left(2c^2 - \beta\right)\left(\sigma_x - \sigma_z\right) \right] / Q \\
a_3 &= \frac{\partial f}{\partial \sigma_z} = c + \left[2\left(c^2 + \beta\right)\sigma_z + \left(2c^2 - \beta\right)\left(\sigma_x - \sigma_z\right) \right] / Q \\
a_4 &= \frac{\partial f}{\partial \sigma_x} = 6.\beta.\tau_{xy} / Q \\
a_5 &= \frac{\partial f}{\partial \sigma_y} = 6.\beta.\tau_{yz} / Q \\
a_6 &= \frac{\partial f}{\partial \sigma_z} = 6.\beta.\tau_{zx} / Q
\end{aligned}\right\} \tag{B-2}$$

where c and β, are the material constants, and Q is given by:

$$Q = 2\left[\begin{matrix} \left(c^2 + \beta\right)\left(\sigma_x^2 + \sigma_y^2 + \sigma_z^2\right) + \left(2c^2 - \beta\right)\left(\sigma_x\sigma_y + \sigma_y\sigma_z + \sigma_z\sigma_x\right) \\ 3\beta\left(\tau_{xy}^2 + \tau_{yz}^2 + \tau_{zx}^2\right) \end{matrix} \right]^{1/2} \tag{B-3}$$

APPENDIX A

Table (A-1) Weights and Locations of Sampling Points in The 27 and 15 Integration Rules

Points	27 Integration Rule				15a,15b, 14 Integration Rule			
	ξ	η	ζ	Weight	ξ	η	ζ	Weight
1	+A	–A	–A	W1	0.0	0.0	0.0	W1
2	0.0	–A	–A	W2	0.0	–B	0.0	W2
3	–A	–A	–A	W1	0.0	+B	0.0	W2
4	–A	0	–A	W2	0.0	0.0	–B	W2
5	–A	+A	–A	W1	0.0	0.0	+B	W2
6	0	+A	–A	W2	1.0	0.0	0.0	W2
7	+A	+A	–A	W1	–B	0.0	0.0	W2
8	+A	0.0	–A	W2	+C	-C	-C	W3
9	0.0	0.0	-A	W3	+C	+C	-C	W3
10	+A	-A	0.0	W2	+C	-C	+C	W3
11	0.0	-A	0.0	W3	+C	+C	+C	W3
12	-A	-A	0.0	W2	-C	-C	-C	W3
13	-A	0.0	0.0	W3	-C	+C	-C	W3
14	-A	+A	0.0	W2	-C	-C	+C	W3
15	0.0	A	0.0	W3	-C	+C	+C	W3
16	+A	+A	0.0	W2				
17	+A	0.0	0.0	W3				
18	0.0	0.0	0.0	W4				
19	+A	-A	+A	W1				
20	0.0	-A	+A	W2				
21	-A	-A	+A	W1				
22	-A	0.0	+A	W2				
23	-A	+A	+A	W1				
24	0.0	+A	+A	W2				
25	+A	+A	+A	W1				
26	+A	0.0	+A	W2				
27	0.0	0.0	+A	W3				

where

Symbol	Integration Rule			
	27	15a	15b	14
A	0.77459	-	-	-
B		1.0	0.84842	0.79582
C		0.6741	0.72766	0.75878
W1	0.171468	1.5644	0.712137	0
W2	0.27435	0.3556	0.686227	0.886427
W3	0.4389575	0.53778	0.396312	0.33518
W4	0.702332	-	-	-

NOTATIONS

SYMBOL	*DESCRIPTION*
[A]	Matrix which contains the differential operators.
As	Cross-sectional area of the bar.
$\{a\}^e$	Nodal displacements.
B	Body forces.
[B]	Strain-displacement matrix.
[B']	Strain-displacement matrix of the bar element.
C_p	Plasticity coefficient.
D_{cr}	Cracked material stiffness in the local axis.
[D]	Constitutive matrix.
[D']	Constitutive matrix of the bar element.
E_1	Reduced modulus of elasticity.
f'c	Ultimate compressive strength of concrete.
f_t	Maximum tensile strength of concrete.
{f}	Element assemblage external nodal force vector.
G	Shear modulus of elasticity.
H'	Hardening parameter.
I_1	First stress invariant.
$\bar{I}_1$	First strain invariant.
[J]	Jacobian matrix.
$\bar{J}_1$	Second deviatoric strain.
J_2	Second deviatoric stress invariant.
K	Hardening parameter which governs the expansion of the yield surface.
[k]	Stiffness matrix.
[k']	Stiffness matrix of the bar element.
l	Directional cosines in the x direction.
m	Directional cosines in the y direction.
n	Directional cosines in the z direction.
N_i	Shape function at the ith node.
[N]	Matrix containing interpolation functions.
S	Part of the surface of the body where external traction are prescribed.
T	Surface traction.
u	Displacement components in x direction.
$\{u\}^e$	Displacement vector at any point within the element.

V	Volume.
v	Displacement components in y direction.
w	Displacement components in x direction.
W_i	Weight of the sampling point.
W_{int}	Internal work.
W_{ext}	External work.
x, y, z	Global or cartisian coordinates.
x_i, y_i, z_I	Global coordinates of ith node.
$\{\varepsilon\}$	Strain vector.
ε	Strain.
ε_{cr}	Cracking strain.
ε_n	Strain normal to the cracked plane.
ε_{cu}	Ultimate concrete strain.
ε_c	Total effective strain of concrete.
ε_e	Elastic component of total effective strain of concrete.
ε_p	Plastic component of total effective strain of concrete.
$\{\varepsilon_p\}$	Effective accumulated plastic strain vector.
$\{\varepsilon'\}$	Strain vector of bar element.
ε'_o	Total strain corresponding to the parabolic part of the curve.
σ	Stress.
σ_n	Stress normal to the cracked plane.
σ_{cr}	Cracking stress of concrete.
σ_o	Equivalent effective stress at the onset of plastic deformation.
$\overline{\sigma}$	Equivalent uniaxial stress.
$\{\sigma\}$	Stress vector.
α_1	The rate of stress release as the crack widens.
α_2	Sudden loss of stress at instant of cracking.
α, β	Material parameters.
β_1	Reduction factor.
γ_1	Rate of decay of shear stiffness as the crack widens.
γ_2	Sudden loss in shear stiffness at the instant of cracking.
γ_3	Residual shear stiffness due to the dowel action.
ξ, η, ζ	Natural coordinate system.
λ	Compression reduction factor.
$\lambda_1, \lambda_2, \lambda_3$	Participation factors.

Note: **Any other symbol will be explained where it appears in the text.**

References /

REFERENCES

1. **Abul Mansur, M.,** and **Vijaya Rangan, B.** " Study of design Methods For Reinforced Concrete Curved Beams " ACI Journal, Title No. 78-21, May-June 1981.

2. **Abdul-Kareem, I.M.,**" Nonlinear Analysis of Reinforced Concrete Thick Plate Foundation On Cohesive Soil " .M.Sc.Thesis, University of Babylon, Hilla, Iraq, 2003.

3. **Ahmad, A. M.,** and **Jaafer, R.** "Natural Frequencies of Continuous Curved Beams on Winkler-Pasternak Foundations". Engineerin Technology, Vol. 11, No. 12 1992.

4. **Al-Hassaini, M.M.F.** " Graphic And Tables For The Analysis and Design Of Curved Concrete Beams " M.Sc. Thesis submitted to the Graduate Paculty of the Virginia Polytechnic Institute in Candidacy, in 1962.

5. **Al-Khafaji, A.G.A.** " Large Displacement and Post-Buckling Analysis of Plane Steel Structures with Non-Prismatic Members resting on Elastic Foundation".M.Sc.Thesis, University of Babylon, Hilla, Iraq, 2002.

6. **Al-Mahdi, A.R.N.,** " Thick Orthotropic Rectangular Plates On Elastic Foundations ". M.Sc. Thesis, Al-Nahreen University, Baghdad, Iraq, 1992.

7. **Al-Rubai, Q.K.,** (2001) " Larg Displacement Elastic Stability Analysis of Plane Structure Under Static Loads and Resting On Nonlinear WinklerFoundation " M.Sc. Thesis, University of Technology, Baghdad, Iraq.

8. **Al-Shaarabaf, I.A.S,** and **Mohammed, A.Z.,**(1999) " Nonlinear Analysis of Reinforced Concrete Cylindrical Shell Using Two and Three Dimensional Finite Element Models ", Engineering and Technology. Vol. 21, No. 8, pp. 1-10.

9. **Al-Shaarabaf, I.A.S,** (1990), " Three-Dimensional Nonlinear Finite Element Analysis of Reinforced Concrete Beams in Torsion ", Ph.D. Thesis,University of Bradford, England.

References /

10. **Badawy, H.E.I., McMullen, A.E.** and **Jordaan, I.J.,** (1977), "Experimental Investigation of The Collapse of Reinforced Concrete Curved Beams ". Magazine of Concrete Research. Vol. 29, No. 99, pp.59-69.

11. **Badawy, H.E.I., Jordaan, I.J.,** and **McMullen, A.E.** (1977), "Effect of Shear on Collapse of Curved beams ". Proceedings of the AmericanSociety of Civil Engineers. Vol. 103, No. ST9. September 1977.

12. **Bathe,K.J., Ramaswamy, S.,** (1979), " On Three-Dimensional Nonlinear Analysis of Concrete Structures " Nuclear Engineering and Design, Vol. 52, pp.385-409

13. **Bechert, H.,** "Zur Berechnung der kreisring-fundamente auf elastisher Unterlage"Beton-and Stahlbetonau, Vol. 53, No. 6. West Germany, pp.156-158**,** June 1958**.[**Mentioned in Panayotounakos, D.E., ASCE, A.M., and Theocaris, P.S. , 1979].

14. **Bell, L.C.,** and **Heins, C. P.,** " Analysis of Curved Girder Bridges ". Journal of the Structural Division, August. 1970.

15. **Bowels, J.E. ,** (1996), " Foundation Analysis and Design " . McGraw- Hill International Edition, 5th Edition.

16. **Cervera, M., Hinton, E.,** and **Hussan, O.,** (1987). " Nonlinear Analysis of Reinforced Concrete Plate and Shell Structures Using 20-Node Isoparametric Brick Elements ". Computers and Structures, Vol. 25, No.6, pp. 845-869.

17. **Carreiva, D.J.,** and **Kuang-Hanchu.** " Stress-Strain Relationship For Reinforced Concrete in Tension ". ACI Journal, January-February 1986.

18. **Chakraborty, M.,**" Ultimate Torque of Reinfored Rectangular Beams "Journal of the Structural Division, 1979.

19. **Chen,W.F.,** (1982), "Plasticity in Reinforced Concrete ", McGraw-Hill, Inc., New York.

References /

20.Cheung, Y.K., and **Nag, D.K.,** (1968), " Plates and Beams on Elastic Foundations Linear and Nonlinear Behavior ", Geotechnique, Vol. 18, pp. 250-260.

21.Cook, R. D., (1974), "Concept and Applicatio of Finite Element Analysis" Johnwilely and Sons. inc., New York.

22.Darwin, D. R., "Reinforced Concrete In: Finite Element Analysis of Reinforced Concrete II" ASCE Journal 1993, PP. 203-32.

23.Dawoud, R.H., Hanna, M.M., and **Fareed, A.** " Flexural Stresses in Rectangular Reinforced Concrete Curved Members ". ACI Journal, March 1970.

24.Dow, J.O., Cabiness, H.D., and **Ho, T.H.** " Linear Strain Element with Curved Edges "Journal of Structural Engineering, Vol. 112, No. 4, April, 1986.

25.Fatehi, T.T., Vreden, W., and **Author.** " Circularly Curved Beams Transversely Loaded ". ACI Journal, Proceedings, Vol. 60, No. 10, Oct.1963, pp. 1457.

26.Henry, F.D.C., "The Design and Construction of Engineering Foundations" Chapman and hall Publication Company, London 1986.

27.Hus, T.T.C., Inan, M, and **Fonticiella, A.L**. "Behavior of Reinforced Concrete Horizontally Curved Beams", ACI Journal, Title No. 75-15 April 1978.

28.Husain, A. H. "Static Analysis of Concrete Shell Foundation By Finite Elements". M.Sc. Thesis, University of Kufa, Najaf, Iraq, 2002.

29.Imegwn, E.O., " Ultimate Strength of Plane Curved Girders", The Structural Engineering, London, England, Vol. 42, No. 4 , pp. 129-134, April 1964.

30.Jackson, N.,"The Automatic Calculation of Collapse loadsFor Circulare-Arc Beams". Structural Engineers Journal,December 1965.No. 12,Vol. 43.

References /

31. **James, M., Duncan,** and **Chang, C.Y.**"Nonlinear Analysis of Stress and Strain In Soils" Journal of The Soil Mechanics and Foundations Division, Vol. 96, No. SM5, Sep. 1970.

32. **Johansen, K.W.,** and **Hansen, P.Lange.** " Studies On The Load Carrying Capacity of Steel Structures ". Technical University of Denmark, Copenhagen, Denmark, 1954.

33. **Jordaan, I.J.** "Ultimate Loads and Modes of Failure For Circular-Arc Bow Girders ". M. Sc. Thesis, University of Witwatersrand, Johannesburg, South Africa, 1964 .[Mentioned in Jordaan, I.J. Journal of ASCE 1974].

34. **Jordaan, I.J., Khalifa, M.M.A.,** and **McMullen, A.E.**"Coolapse of Curved Reinforced Concrete Beams",Journal of Structures Division , Vol. 100, No. ST11, pp. 2255-2268, Nov.1974.

35. **Kassam, S.A.**"Lateral Vibration of Cantilever On Viscoelastic Foundations"Armed Forces Science Research Journal XVII(39), pp.34-41.

36. **Kerr, A.D.,**"Elastic and Viscoelastic Foundations Models" Journal of Applied Mechanics, Trans. ASME., Vol. 31, Series E., No. 3 1964.[Mentioned in **Al-Mahdi** 1992].

37. **Kwon, M.,** and **Spacone, E.** "Three-dimensional Finite Element Analysis of Reinforced Concrete Coloumns". Computers and Strucures, No. 80 , pp. 199-212, 2002.

38. **Khalifa, M.M.A.,** " Collapse of Reinforced Concrete Beams Curved in Plan ".M.Sc. Thesis, University of Calgary, Calgary, Alberta, Canada, 1972.

39. **Lambe, T.W.** and **Whitman, R.V.,** (1984),"Soil Mechanics, SI Version " , 2th EditionWiley Eastran Limited.

40. **Mansur, M.A.,** and **Rangan, B.V.,** " Study of Design methods For Reinforced Concrete Curved Beams ", ACI Journal, May-June 1981 pp.226-231.

References /

41. **Moorman, R.B.B.**"A semi-Grapgical Method of Analysis for Horizontally Curved Beams" Bulletin, University of Missouri, No. 29, 1938.[Mentioned in **Al-Hassaini** 1962].

42. **Oravas, G.** "Beitrag Zur Berechung des kreisringes auf Elastisher Unterlage" Der Bauing enieur, Vol. 31, No. 5, West Germany, 1956 pp.177-180. **.[Mentioned in Panayotounakos, D.E., ASCE, A.M.,** and **Theocaris, P.S.** , 1979].

43. **Osterbloom, I.**"Bending and Torsion in Horizontally Curved Beam", Proceedings, ACI , Vol. 28, pp. 597-606, 1932.[Mentioned in **Al-Hassaini** 1962].

44. **Panayotounakos, D.E., ASCE, A.M.,** and **Theocaris, P.S.** " Circular Beam On Elastic Foundation ", Journal of the Engineerin Mechanics Division. October 1979, pp. 839-853.

45. **Petersen, C.** "Die Ubterrangungs matrix des kreisformig gekrummten Tragers auf Elastisher Unterlage" Die Bautechnik, Vol. 8, West Germany, Aug. 1967 pp.289-294. **.[**Mentioned in **Panayotounakos, D.E., ASCE, A.M.,** and **Theocaris, P.S.** , 1979].

46. **Phillips, D.V.,** and **Zienkiewicz, O.C. (1976)**, " Finite Element Nonlinear Analysis of Concrete Structures ", Proceedings of Institute of Civil Engineering, Vol. 61, part 2, pp. 59-88.

47. **Pippard** and **Baker,** " The Analysis of Eingineering Structures" Edward Arnold and Company, and Edition, London, pp. 411-428, 1943.[Mentioned in **Al-Hassaini** 1962].

48. **Raju, N.K.,**"Advanced Reinforced Concrete Design". CBS publishers 1986.

49. **Sayegh, A.F.,** and **tso, F.K.,** " Finite Element Analysis of 3-D Beams-Column On A Nonlinear Foundation ", Computers and Structures. Vol.28, No.6, pp. 699-415.

References /

50.Safarian, S.S., "Design a Circular Concrete Ring-Beam and Column System Supporting a Silo Hopper". ACI Journal, Februray 1969 pp. 103-110

51.Selvadurai, A.P.S.," Elastic Analysis of Soil-Foundation Interaction" Elsevier Scientific Publishing Company, 1979.

52.Shalash, Q.T., (1974), " Soil-Structure Interaction By Finite element Method ", M.Sc. Thesis, Baghdad University, Baghdad, Iraq.

53.Shanmugam, N.E., Fellow, ASCE. Thevendran, V., Richard Liew, J. Y, Member, ASCE, and **Tan, L. O.** "Experimental Study On Stel Beams Curved In Plan ", Journal of Structural Engineering, Vol. 121, No. 2, February, 1995.

54.Volterra, E."Bending of Circular Beams Resting on an Elastic Foundation" Journal of Applied Mechancs, American Society of Mechanical Engineers, Series E., Vol. 19(74), No. 1, Mar. 1952, pp. 1-4. **.[**Mentioned in **Panayotounakos, D.E., ASCE, A.M.,** and **Theocaris, P.S. ,** 1979].

55.Volterra, E."Deflection of Circular Beams Resting on an Elastic Foundation Obtained By The Methods of Harmonic Analysis" Journal of Applied Mechancs, American Society of Mechanical Engineers, Series E., Vol. 20(75), No. 2, June 1953, pp. 227-232. **.[**Mentioned in **Panayotounakos, D.E., ASCE, A.M.,** and **Theocaris, P.S.** , 1979].

56.Volutini, Becla "Analysis of Continuous Circular Curved Beam". ACI Journal, Vol. 22, pp. 217-28, Nov. 1950.[Mentioned in **Al-Hassaini** 1962].

57.Wang, T.M. and **Stephens, J.E.**"Natural Frequences of Timoshenko Beams on Pasternak Foundations". Journal of Sound and Vibration, No.51, pp. 149-155, 1977.

58.Wang, T.M., and **Gagnon, L.W.**"Vibration of Continuous Timoshenko Beams on Pasternak Foundatios". Journal of Sound and Vibration, No.59, pp. 211-220, 1978 .

59.Zeinkiewcz, O.C., (1977) , " The Finite Element Method " , 3th Edition, McGraw-Hill Book Company, New York.

Republic of Iraq

Ministry of Higher Education

and Scientific Research

NONLINEAR ANALYSIS OF REINFORCED CONCRETE HORIZONTALLY CURVED BEAMS ON ELASTIC FOUNDATIONS

A Thesis

Submitted to the College of Engineering of the University of Babylon in Fulfillment of Partial Requirements for the Degree of Master of Science in Civil Engineering (Structural Engineering)

By

Moslem Abdul-Ameer Khudhair Al-Temeemi

B.Sc.

October , 2005

ABSTRACT

This research deals with the analysis of reinforced concrete horizontally curved beams on elastic foundations by the finite elements method. The material nonlinearity was taken into account for concrete and steel. A twenty-nod isoparametric brick element with sixty degrees of freedom is employed to model the concrete. The reinforcing bars are modeled as axial members embedded within the brick element.

Soil is represented by normal and horizontal subgrade reactions. The normal component is represented by Winkler, Kondner, Polynomial models, while the horizontal component is represented by Winkler model.

The present finite element and the available experimental and numerical results have shown good agreement.

Parametric studies have been carried out to examine the influence of some selected parameters (like radius to span-length ratio (R/L), boundary conditions, α_1(the rate of stress release as the crack widens), α_2 (the sudden loss of stress at instant of cracking), and the type of soil on the overall hehavior of reinforced concrete curved beam on elastic foundations. From the results obtained according the consider examples, it was found that the ultimate load of curved beam on elastic foundation could be increased with increasing the radius to span-length ratio (R/L)[when (R/L) increases from 1 to 5, the ultimate load increases about 40%]. The shear reinforcement bars have a significant effect on decreasing the ultimate load, it was found that the ultimate load decreasing about 51 % when the shear reinforcement was removed.